
The Impact of Star Cluster Environments on Planet Formation

Rhana Bethany Nicholson

*A thesis submitted in partial fulfilment of the requirements of Liverpool
John Moores University for the degree of Doctor of Philosophy*

June 2019

Declaration of Authorship

I, Rhana Bethany Nicholson, declare that this thesis titled, “The Impact of Star Cluster Environments on Planet Formation” and the work presented in it are my own. I confirm that:

- This work was done wholly or mainly while in candidature for a research degree at this University.
- Where any part of this thesis has previously been submitted for a degree or any other qualification at this University or any other institution, this has been clearly stated.
- Where I have consulted the published work of others, this is always clearly attributed.
- Where I have quoted from the work of others, the source is always given. With the exception of such quotations, this thesis is entirely my own work.
- I have acknowledged all main sources of help.
- Where the thesis is based on work done by myself jointly with others, I have made clear exactly what was done by others and what I have contributed myself.

Signed:

Date:

To Mum and Dad, for making me do Kumon...

“For all the tenure of humans on Earth, the night sky has been a companion and an inspiration... At the very moment that humans discovered the scale of the Universe and found that their most unconstrained fancies were in fact dwarfed by the true dimensions of even the Milky Way Galaxy, they took steps that ensured that their descendants would be unable to see the stars at all...”

- Carl Sagan, Contact



Acknowledgements

Firstly I must begin by thanking my supervisor, Richard Parker, without whom this thesis would most definitely not exist. Thank you for supervising me through everything, for always fighting for change and acceptance, for teaching me to write, and for some truly excellent drinking sessions (of which there is no evidence, thankfully!).

I would like to thank my director of studies, Stacey Habergham-Mawson (and bump), for believing in me and supporting me throughout. I'd also like to thank the entire NSO staff for providing a community in which I was always welcome and for reminding me of how awesome space is when I became too focused on the tiny details.

Thanks to Phil James, for inspiring my love of astronomy throughout my undergraduate degree. Observing on Tenerife with you and Daniel Harman was one of the best experiences of my PhD, and I will never forget that music video.

Thanks to the Fellowship of Ni (and honorary members), Naura's Posse, and the crew of White Lightning, for supporting me and helping me save worlds, imaginary and real.

Special thanks to Arwen and Elara, my fellow witches and partners in crime. To Mum and Dad, for teaching me that science and magic can be one and for helping me pursue my dreams of discovering mermaids (on this planet or others). Thanks to Albus, Riki, and Cery for reminding me that simply being is enough.

And finally to my partner Sam, the best bean that has ever been. I could not have done this without you...

Abstract

Faculty of Engineering and Technology
Astrophysics Research Institute

Doctor of Philosophy

The Impact of Star Cluster Environments on Planet Formation

by Rhana Bethany Nicholson

It is thought that most stars, including our Sun, form within clusters alongside many other stars. Planet formation and star formation occur simultaneously, and therefore the birth environment of stars will shape the formation of planets. Properties of the present day Solar System hint to a past in which the Sun formed in the presence of many other stars. There is an intrinsic interest in knowing the birthplace of the only known planetary system hosting life within the Universe and whether conditions of the birth environment are common or atypical. Understanding the origin of the Solar System could provide important constraints on star and planet formation.

Observations of the present day Solar System have revealed a conflict between the need for a large cluster containing massive stars so that disc enrichment can occur and to explain the orbits and enrichment levels of some objects within the Solar System, and the need for a low-mass, quiescent cluster where dynamical and radiative effects will not disrupt or disperse planet forming discs. Low-mass clusters containing massive stars may present a solution to this problem. The presence of massive stars within star-forming regions will affect planet forming discs to varying degrees, depending on the initial conditions of the region. How the initial conditions of star-forming regions change the relationship between massive stars and protoplanetary discs is unknown.

This thesis focuses on how the birth environment of stars can shape planet formation. The processes behind star formation, planet formation, and the impacts that star-forming regions can have on the formation of planets are reviewed. This thesis reviews what is currently known about the birth environment of the Sun based on evidence found within the Solar System and what this tells us.

In this thesis, I show that low-mass star-forming regions containing one or two massive stars are viable environments for creating enriched planet forming discs that resemble the levels of enrichment found in the Solar System. These unusual clusters enrich planet forming discs at a similar rate to more massive ($>1000 M_{\odot}$) clusters. Based on the percentage of stars enriched by Supernovae within low-mass clusters, and the percentage of low-mass clusters containing massive stars in comparison to more massive clusters, it is possible that a significant number of unperturbed, enriched stars have been produced within these star-forming environments. However, the UV radiation produced by massive stars within low-mass clusters is still strong enough to cause protoplanetary discs to disperse on short timescales, potentially inhibiting planet formation.

I find that the rate at which protoplanetary discs are dispersed depends on the initial conditions of the cluster and the location of the massive stars. The mass of the cluster, if massive stars are present, does not significantly alter the rate at which planet forming discs are dispersed. The initial density of the cluster is the most important aspect to consider. The background UV field produced by star-forming regions also varies depending on the initial spatial stellar profile. Planet forming discs within simulations that represent the initial conditions of nearby star-forming regions show that planet forming discs are dispersed on short ($\sim 1-3$ Myr) time-scales. This means one of three things; either the majority of planets form in low-mass star-forming regions, giant planet formation must occur on very short timescales, or the current calculations of mass-loss in discs due to external photoevaporation severely overestimate the detrimental effects of EUV and FUV radiation.

By calculating the UV background field in star-forming regions, I find that the initial spatial distribution of stars greatly affects the amount of UV radiation that stars receive. Delaying the effects of UV radiation by 0.5 Myr, to replicate the effects of delaying massive star formation, still results in vastly different UV field strengths. The types of stars that produce UV radiation are not limited to massive ($\geq 15 M_{\odot}$) stars, and lower mass ($3 < M < 15 M_{\odot}$) stars contribute large enough UV fields to potentially affect protoplanetary discs.

This thesis has shown that the environment in which protoplanetary discs are born can dictate and strongly shape their evolution. The constraints on the birth environment of the Solar System have been relaxed, and the importance of considering the initial conditions of the star-forming region have been highlighted.

Contents

Declaration of Authorship	i
Acknowledgements	iv
Summary	vi
1 Introduction	1
1.1 Motivation for study	1
1.2 Planets	2
1.2.1 History of planetary observations	2
1.2.2 The Solar System	4
1.2.3 Previous theories of planet formation	6
1.2.4 Exoplanets	8
1.2.5 Planet formation	11
1.2.6 Protoplanetary disc	15
1.2.7 Disc disruption, mass loss, and destruction	17
1.3 Star clusters	20
1.3.1 Star formation	20
Previous theories	20
Modern theories	21
1.3.2 Initial Mass Function	22
1.3.3 Low mass star formation	24
1.3.4 High mass star formation	25
1.3.5 Star-forming regions and stellar groups	26
1.3.6 Cluster Mass Function	27
1.3.7 Cluster dynamics	31
1.3.8 Protoplanetary disc disruption and clearing in clusters	34
Stellar winds	34
Stellar flybys	34
Photoevaporation	36

1.4	Formation of the Solar System	42
1.4.1	Short-lived radioisotopes in chondrites	43
1.4.2	Birth environment of the Solar System	45
1.5	Aims	47
2	Methods	49
2.1	Creating clusters	49
2.2	Simulation set-up	52
2.3	<i>N</i> -body simulations	55
2.3.1	Software packages	57
2.4	Protoplanetary discs	58
2.4.1	Photoevaporation	59
2.5	UV radiation fields	62
3	Supernova enrichment of planetary systems in low-mass clusters	66
3.1	Introduction	67
3.2	Methods	68
3.2.1	Creating low-mass clusters	68
3.2.2	<i>N</i> -body simulations	69
3.3	Results	70
3.3.1	Cluster evolution and supernova enrichment	71
3.3.2	Dynamical histories of polluted stars	72
3.3.3	Other initial conditions	72
3.3.4	Low mass clusters containing one massive star	75
3.4	Discussion	76
3.5	Conclusions	80
4	Rapid destruction of protoplanetary discs due to external photoevaporation	81
4.1	Introduction	82
4.2	Method	83
4.3	Results	86
4.3.1	Substructure in star-forming regions	86
4.3.2	Virial ratio	90
4.3.3	Disc radii	92
4.3.4	Disc masses	95
4.3.5	Mass of star-forming regions	95
4.4	Discussion	99

4.4.1	Changing the initial conditions of star-forming regions . . .	100
4.4.2	Caveats	102
4.5	Conclusions	106
5	UV background fields in clusters	108
5.1	Introduction	109
5.2	Method	111
5.3	Results	113
5.3.1	FUV and EUV fluxes	113
5.3.2	Feedback	115
5.3.3	Mass of stars	116
5.4	Discussion	117
5.5	Conclusions	122
6	Conclusions	124
6.1	Main results	124
6.1.1	Supernova enrichment of planetary systems in low-mass clusters	124
6.1.2	Rapid destruction of protoplanetary discs due to external photoevaporation	125
6.1.3	UV background fields in clusters	126
7	Future work	127

List of Figures

1.1	The Solar System	4
1.2	Laplace's theory of planet formation	7
1.3	Distribution of exoplanets with regards to mass	10
1.4	ALMA image of HL Tau	16
1.5	Initial Mass Function	23
1.6	Cluster Mass Function	28
1.7	The Orion Nebula	30
1.8	Observed protoplanetary discs in clusters (Haisch et al., 2001)	33
1.9	Stellar flybys	35
1.10	Protoplanetary disc evolution	38
1.11	Protoplanetary discs within the ONC	41
2.1	Star cluster mass functions for clusters containing different numbers of massive stars. Stars with masses $>20 M_{\odot}$ were specifically selected because of their exceptionally short lives, exploding as SN within a few Myr, which allows for enrichment to take place while planet formation is still occurring.	50
2.2	Initial spatial distribution of clusters	54
2.3	Block time stepping scheme diagram	58
2.4	Protoplanetary disc mass loss with distance due to massive stars within the ONC	60
2.5	Φ_i values of massive stars	63
2.6	EUV and FUV luminosity of stars with mass	64
3.1	The sampled cluster mass function	69
3.2	First SN event snapshot	73
3.3	Enrichment of stars by first SN event	73
3.4	Second SN event snapshot	74
3.5	Enrichment of stars by second SN event	75
3.6	Stellar interaction history	76

3.7	Density of cluster with time	77
4.1	Photoevaporation of discs in clusters where f_D is varied	88
4.2	Photoevaporation of discs in clusters where α_{vir} is varied	91
4.3	Photoevaporation of discs in clusters where r_{disc} is varied	94
4.4	Photoevaporation of discs in clusters where m_{disc} is varied	96
4.5	Photoevaporation of discs within low-mass clusters	99
5.1	FUV and EUV fluxes	114
5.2	FUV and EUV fluxes from O-type and B-type stars	118

List of Tables

2.1	Parameter space of simulations	55
2.2	SeBa stellar evolution	59
3.1	Initial conditions of simulations	70
4.1	Disc photoevaporation rates in clusters with varying D	89
4.2	Percentage of discs surviving in clusters with varying D	89
4.3	Disc photoevaporation rates in clusters with varying α_{vir}	92
4.4	Percentage of discs surviving in clusters with varying α_{vir}	92
4.5	Disc photoevaporation rates in clusters with varying r_{disc}	97
4.6	Percentage of discs surviving in clusters with varying r_{disc}	98
5.1	FUV and EUV fluxes	115
5.2	FUV and EUV fluxes produced by O-type stars	117
5.3	FUV and EUV fluxes produced by B-type stars	119
5.4	The percentage of FUV and EUV flux from B-type stars in comparison to O-type stars	119

List of Abbreviations

CAIs	Calcium Aluminium Inclusions
CMF	Cluster Mass Function
EUV	Extreme Ultra Violet
FUV	Far Ultra Violet
GMC	Giant Molecular Cloud
IMF	Initial Mass Function
LMC	Large Magellanic Cloud
MMSN	Minimum Mass Solar Nebula
Myr	Million years
ONC	Orion Nebula Cluster
Proplyd	Protoplanetary disc
SN	SuperNova
SNe	SuperNovae
YSO	Young Stellar Object

Physical Constants

Solar Mass $M_{\odot} = 1.989 \times 10^{30} \text{ kg}$

Earth Mass $M_{\oplus} = 5.972 \times 10^{24} \text{ kg}$

Jupiter Mass $M_J = 1.898 \times 10^{27} \text{ kg}$

Chapter 1

Introduction

1.1 Motivation for study

Some of the foundational questions in astrophysics relate to our origins; from the creation of the Universe, to our own life hosting planet. The question of the origin of our Solar System and other planetary systems intricately links physical processes that range in scale from atomic to galactic, and links other fields, such as biology, with planet and star formation. The impacts of star-forming environments on planets are vast; from sometimes making planet formation impossible, to providing the necessary ingredients for life cycles on Earth. It also deeply links the questions about our origins and the universality of life.

With the discovery of vast numbers of exoplanets, planet formation has become regarded as a standard outcome of star formation. However, the diversity of exoplanets suggests that their formation processes are anything but standardised. As the majority of stars form in groups, the conditions that stars are subjected to will also impact their forming planets. Studying the links between planet formation and star forming regions can help us understand what conditions are conducive (or hostile) to the creation of planets, and how common these conditions are in the Universe.

One of the outstanding challenges in star and planet formation is to characterise the type of star formation event which formed the Sun, and hence the birth environment of the Solar System (e.g. [Adams, 2010](#); [Pfalzner et al., 2015](#); [Portegies Zwart, 2009](#)). Understanding the environment and processes that formed and shaped the Solar System will help us understand where to search for potential life-hosting planetary systems. If our Solar System formed in unique conditions, this paints a bleak view for the potential for other life in our galaxy. However, if the Solar System formed in a 'typical' star forming region, then this could indicate that our planetary system is not unique with regards to how it formed,

and that the environment in which planets form needn't be a major factor when considering the reason as to why we have yet to detect other life. To answer this question, we need to understand how our planetary system was formed before we can begin to understand how unique we are among the stars (Nicholson and Forgan, 2013).

1.2 Planets

1.2.1 History of planetary observations

The study of planets is one of the oldest branches of astronomy, with observations of the Solar System dating back millenia. Most ancient cultures throughout the world recognised the existence of at most seven celestial bodies, which were called 'planets'; the Sun, the Moon, Mercury, Venus, Mars, Jupiter, and Saturn (Pedersen and Jones, 2011).

The first observations of the Solar System were limited to the brightest planet, Venus, and date back to the Sumerians, with records as early as 2000 BC (Evans, 1998). Recorded observations of Mars were first made by ancient Egyptian astronomers, and Chinese records of the motion of Mars date to 1045 BC. Records of Jupiter and Saturn are similarly found from civilisations across the globe dating back to these ancient times.

The study of celestial bodies in ancient Greece led to many discoveries, and was a major phase in the field of astronomy. Anaxagoras explained the principles behind eclipses, described the Sun as a large fiery mass, and hypothesised that stars were other bodies like the Sun much further away (Curd, 2015). Aristarchus of Samos was the first astronomer to propose the heliocentric model, placing the Sun at the centre of the known Universe, with the planets orbiting the Sun. This theory was forgotten for nearly 2000 years before Copernicus, Galileo and Kepler later came to the same conclusion (Hannam, 2011). This new context resulted in the Sun and Moon being removed from the category of 'planet', with the Earth added to it. The Solar System became simultaneously simpler and more complex.

The advent of telescopes advanced our understanding of the Solar System further. During the 1600s, Galileo discovered individual features of celestial bodies such as Sun spots, Jupiter's moons, and the rings around Saturn. Uranus, having previously been observed on many occasions (potentially as early as 128 BC, Bourtembourg, 2013) but mistaken for a star, was classified as a planet in 1781 owing to the advancement in the quality of telescopes (Herschel and Watson,

1781). Neptune was discovered by Adams (1846), and Pluto in 1930 by Clyde Tombaugh (Esclançon et al., 1930).

In 1801, a tiny object was discovered orbiting at the radii of a predicted planet, and was named Ceres (Piazzi, 1801). More objects were discovered in this vicinity, appearing indistinguishable from stars at the time, gaining them the greek name *asteroeides*, meaning “star-like”. By the 1850s, this region was known as the asteroid belt. After the discovery of Pluto in 1930, many astronomers suspected that Pluto was not alone and hypothesised that a secondary ‘asteroid’ belt existed within the Solar System, which later became known as the Kuiper belt. In 1992, the first Kuiper belt object (KBO) since Pluto and Charon was discovered (Jewitt and Luu, 1993), named Albion. Since the discovery of Albion, more than one thousand KBOs have been discovered.

Leuschner (1907) suggested that comets, then considered to have parabolic orbits that made single visits into the Solar System, were in fact objects with very large, elliptical orbits and would therefore return in time. Opik (1932) first considered the idea that there was a reservoir of these objects within a cloud at the outer edges of the Solar System, which was later taken up by Jan Oort (Oort, 1950). This theoretical region, thought to comprise of a disc and spherical cloud, is challenging current observational limits due to the small and non-reflective nature of comets, and the great distances involved.

Within our Solar System, discoveries are still being made to this day that change our understanding of the Solar System and how it was formed. Sedna and Eris, with their unusually large and eccentric orbits, are some of the latest such discoveries. 2012 VP₁₁₃, also known as Biden, is another trans-Neptunian object that was discovered in 2014 and has the longest known perihelion in the Solar System. 2018 VG₁₈ is the most distant natural object observed within the Solar System at the time of writing (~100 AU).

The peculiarity of Sedna’s orbit, along with its similarity to other extreme trans-Neptunian objects such as 2012 VP₁₁₃, has led to the implication that there is an undiscovered object in the outer Solar System shepherding objects into these orbits. The gravitational potential necessary means that Planet 9, as this object is known, is predicted to have a mass $\geq 10 M_{\oplus}$, a diameter two to four times that of Earth, and an elongated orbital period lasting 10,000-20,000 years (Brown and Batygin, 2016). Such a large planet at such great distances opens many questions as to the origin and formation of this potential planet.

From these observations throughout history, a picture of the Solar System and its various inhabitants has been built.

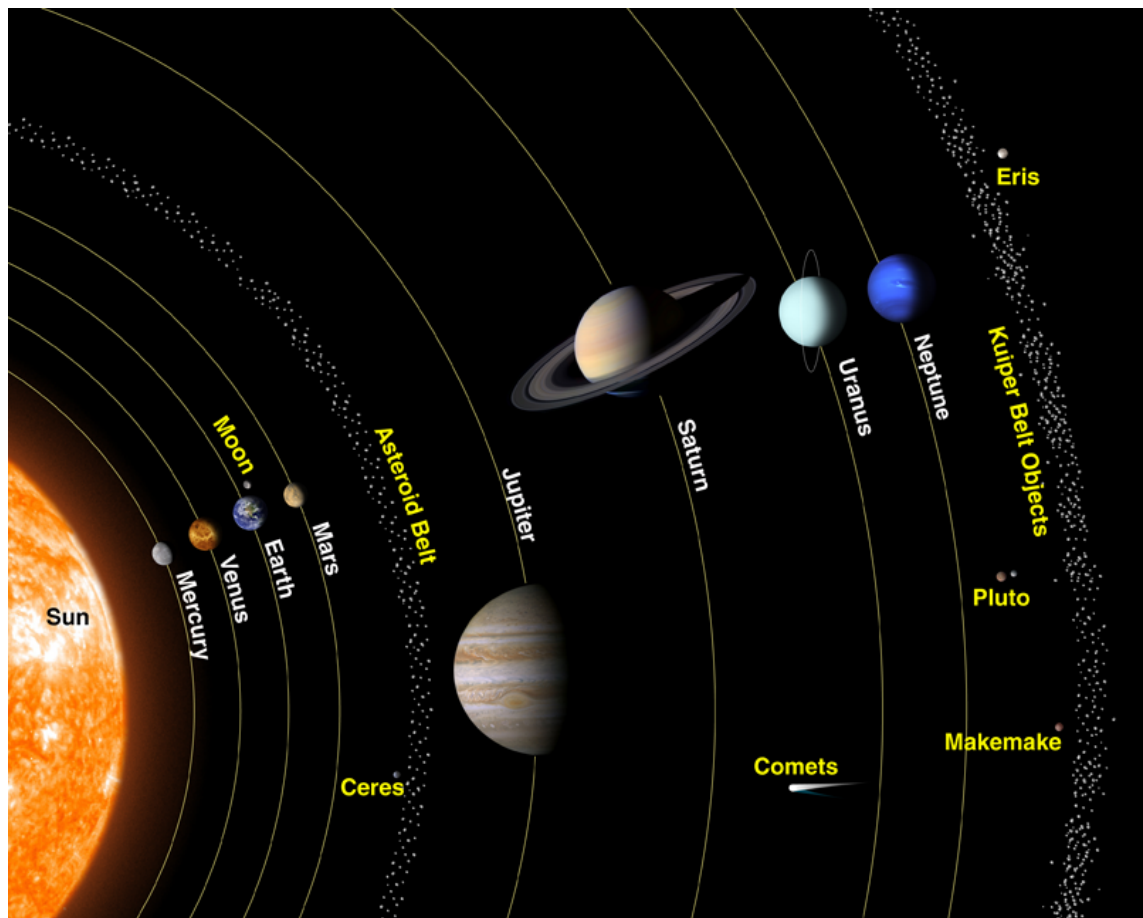


FIGURE 1.1: The Solar System with all the terrestrial, giant and a few major dwarf planets. Sizes of planets and Sun, and distances to the Sun are not to scale. From NASA.

1.2.2 The Solar System

Our Sun lies at the centre of the Solar System. It is a G-type main sequence star and is ~ 4.6 billion years old. It is a Population I star, meaning it is rich in heavy elements (Asplund et al., 2009). These heavy elements likely came from a massive star born in the vicinity of the region where the Sun formed, which exploded as a supernova after a few Myr, enriching the surrounding material, from which the Sun then formed.

Closest to the Sun are the terrestrial planets; Mercury, Venus, Earth, and Mars. These planets are all comprised primarily of rock, with solid surfaces and central metallic cores that are surrounded by silicate mantles (Anderson and Kovach, 1967; Baraffe et al., 2014). Other bodies within the Solar System also have this internal structure, such as the Moon, Io, and Titan, although their metallic cores are much smaller than their planetary counterparts (Ross et al., 1990; Tobie et al.,

2005; Lucey, 2006; Wieczorek, 2006).

These terrestrial planets vary greatly with regards to mass, surface conditions, and atmospheric compositions. Mercury, the smallest planet in the Solar System, has a thin atmosphere, resulting in the surface of the planet being subjected to temperatures varying from blistering (~ 700 K) to freezing (100 K). The surface is covered in deep craters, as well as some ice (within shaded regions) and evidence of organics has been discovered (Delitsky et al., 2017). Venus, a planet approximately the same size as Earth, has a surface that is marked by volcanoes, lava and canyons (Phillips et al., 1992). Earth, the planet we inhabit, is covered mostly in water, has solid land, and ice covering its polar regions. It is also currently the only known astronomical body to harbour life. Mars, which is approximately a third of the mass of Earth, has a cratered and mountainous surface, polar ice caps, and evidence of organics (Freissinet et al., 2015).

After the terrestrial planets is the asteroid belt, a circumstellar disc populated by numerous asteroids and objects large enough to be considered minor planets (such as Ceres). The objects within the asteroid belt are the remnants of planet formation and formed from the primordial solar nebula. They have not undergone the constant melting and resurfacing that the Earth has, and so they still reflect the composition of the solar nebula at the time that planet formation was occurring.

The giant planets lie past the asteroid belt; Jupiter, Saturn, Uranus, and Neptune. These planets can be separated into the two categories of gas giants and ice giants. Jupiter and Saturn are classified as gas giants and are primarily composed of hydrogen and helium (Niemann et al., 1998; Atreya et al., 1999). Gas giant is somewhat of a misnomer however, as due to the pressure within the atmospheric layers of these planets, there is no distinction between gaseous and liquid material as it is all above the critical point where they can coexist. It is thought that the gas giants have a molten, rocky core (Fortney and Nettelmann, 2010). The core is surrounded by a thick atmosphere that is separated into layers. Uranus and Neptune are ice giants. Ice giant planets are mainly composed of elements heavier than hydrogen and helium that were incorporated as solids either directly or in ice during planet formation (Ali-Dib et al., 2014). Little of the water in the planets is now ice, and instead it exists as a super critical fluid due to the pressure and temperature within the planet. Uranus and Neptune have similar compositions to Jupiter and Saturn, but deep within their atmospheres they are significantly more enriched in ice grains. Their interiors are composed of mostly ice and rock (Hubbard and Macfarlane, 1980).

The Kuiper belt is a circumstellar disc that resides outside the major planets. It extends from ~ 30 AU, approximately the orbit of Neptune, to 50 AU from the Sun. It is similar in composition to the asteroid belt, however is more than 20 times wider and contains a great deal more mass (Gomes, 2009; Pitjeva and Pitjev, 2018). Within the Kuiper belt there are 100–10000 of objects that are thought to be primarily composed of frozen volatiles and some rock (Brown, 2012). Some of the objects within this region are thought to have been scattered by the gas giants during formation and are continuously perturbed by Neptune.

Due to the distance from the Sun and planets, KBOs are thought to have remained relatively unaffected by processes that have affected other Solar System bodies. Therefore the composition of KBOs is likely to provide vital information about the conditions and makeup of the earliest stages of planet formation within the Solar System (Luu and Jewitt, 2002). Three officially recognised dwarf planets inhabit this region (Pluto, Haumea and Makemake), and are primarily made of rock and ice (Schaller, 2010; Stern et al., 2015; Grundy et al., 2016).

At the very edge of the Solar System lies the theoretical Oort cloud. The Oort cloud is thought to exist at a distance of 1,000 – 200,000 AU and be comprised of icy objects (Hills, 1981; Weissman, 1996; Dones et al., 2004). Due to the distance of the Oort cloud from the Sun, it is only loosely gravitationally bound to the Solar System, and so is affected by passing stars and the Galactic tide. This causes comets to become dislodged from their orbits and sent into the inner Solar System. It is thought that the icy objects within the Oort cloud formed in the earliest stages of planet formation, and were originally closer to the Sun, but were scattered great distances by the giant planets not long after they formed (Morbidelli, 2005).

1.2.3 Previous theories of planet formation

Traditionally the study of planets has been restricted to what is within our Solar System and, until recently, has defined our understanding of planet formation and evolution.

The formation theory developed in 1755 was called the "nebular hypothesis" (see Fig. 1.2, Woolfson, 1993). Laplace suggested that a spinning cloud of gas collapsed. As it collapsed and contracted inwards, it flattened along the axis of rotation. As the core contracted, it left behind a series of rings, in which the material coalesced to form a single planet within each ring. This built the groundwork for understanding the near circular orbits of the planets and their alignment along a

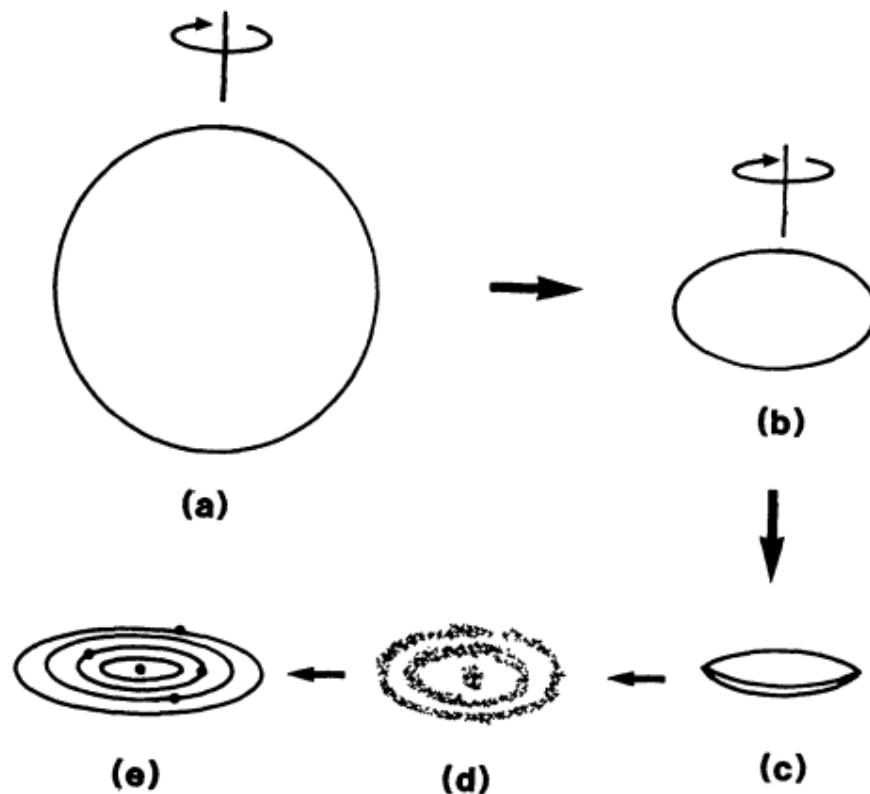


FIGURE 1.2: Diagram from [Woolfson \(1993\)](#) showing Laplace's theory on the formation of the Solar System: a) a rotating cloud of gas; b) the cloud collapsing and flattening along its rotation axis; c) formation of a lenticular disc; d) a series of rings left behind from a contracting core; e) one residual planet left inhabiting each ring

central plane. Questions about the distribution of angular momentum within the Solar System cast doubt on this theory, given that the Sun contains the majority of the mass of the Solar System, but ≤ 1 per cent of the total angular momentum ([Jeans, 1919](#)).

Due to the issues with the nebula hypothesis, it was abandoned in favour of models where a pre-existing, slowly rotating Sun periodically erupted, causing large amounts of material to be flung from the surface into the surrounding environment, from which planets then formed ([Chamberlin, 1901](#); [Moulton, 1905](#)). The Laplacian model was rejected for decades whilst these other theories took precedence ([Woolfson, 1993](#)).

However, in the 1960s the solar nebula disc model (SNDM) emerged, a theory that is more similar to the Laplacian model. This theory explained the presence of discs around young stellar objects (YSOs) and demonstrated that material within these discs can accrete to form Earth-sized objects. It also addressed many of the

issues with previous planet formation theories (Safronov, 1972).

According to the SNDM, stars form from massive, dense molecular clouds with discs, from which planets subsequently form, making planet formation a natural result of star formation. Material within the disc is able to accumulate and accrete mass, growing in size through various mechanisms until the rocky objects are terrestrial planetary masses (see Section 1.2.5). Giant planets form from either these objects, or directly from the gas around the star. Ice grains can form within the disc past the snow line, the particular radius from the central protostar where temperatures are cold enough that volatiles can freeze. These solid ice grains provide more material for giant planets to accrete, resulting in large planets. This line exists at the asteroid belt, explaining the distribution of terrestrial and giant planets within the Solar System.

1.2.4 Exoplanets

Within the past 20 years, the field of planetary physics has radically changed with the detection of planets outside our Solar System. In 1988, the first such planet was detected (Campbell et al., 1988) and in 1992 the first confirmed exoplanet was discovered (Wolszczan and Frail, 1992). However, the first unknowingly detected evidence of the existence of an exoplanet was in 1917, when spectroscopic data of the nearest white dwarf to Earth was polluted with heavy elements (van Maanen, 1917; Zuckerman, 2015). As heavy elements sink into the centre of the star and therefore should not be present in spectra, these heavy elements indicate that asteroids and comets have been knocked from their orbits and recently accreted onto the white dwarf by a substantial object, which is most likely a planet.

Since the discovery of the first confirmed exoplanet, there have been nearly 4,000 confirmed exoplanets and more than 600 multiple planetary system detections (Schneider et al., 2011). Exoplanets and planetary systems range vastly in size and architectural structure, far more than previous planet theories allow for. Variations within exoplanet systems range in; distance from their host star, motion, orbital inclination and eccentricity, composition of the planets, arrangement of the planets, number, density, temperature, and even number of stars. Exoplanets of all masses have been found; from slightly larger than the Moon (Kepler-37b, Barclay et al., 2013), to nearly 30 times the mass of Jupiter (HR 2562 b; although this is likely a brown dwarf forming around a star, Konopacky et al., 2016), raising questions as to whether all planets form via the same process. Orbital periods of exoplanets have been found to be as short as few hours (such as K2-137b, with

an orbital period of ~ 4.31 hours, [Smith et al., 2018](#)), to hundreds of thousands of years (2MASS J2126-8140, with the largest known orbital radius at $\sim 4,500$ AU, [Deacon et al., 2016](#)), challenging planet formation models to answer how these massively wide orbit planets form.

Planets have been found that are orbiting against the rotational direction of their star (WASP-17b [Anderson et al., 2010](#)), are ancient in comparison to our own planetary system (such as PSR B1620-26 b, an exoplanet found in a globular cluster with an age of ~ 12.7 billion years; [Sigurdsson et al., 2003](#)), and even orbiting pulsars (PSR J1719-1438 B). Planets are found orbiting binary and even triple star systems ([Kostov et al., 2013](#); [Schwarz et al., 2017](#)), systems which in fact may be more hospitable to life ([Wootton and Parker, 2019](#)). The diversity of the detected planets and planetary systems defies previous formation hypotheses, with some planets being considered physically impossible until they were detected, and still is reshaping our current theories of planet formation ([Manara et al., 2018](#)).

[Fig. 1.3](#) shows masses and orbital radii for the majority of the exoplanets that have been confirmed to date, most of which were detected by the *Kepler* satellite ([Burke et al., 2014](#); [Coughlin et al., 2016](#); [Thompson et al., 2018](#)). Various methods, such as micro lensing ([Refsdal, 1964](#); [Cassan et al., 2012](#)), direct imaging ([Marois et al., 2008](#)), radial velocity ([Charbonneau et al., 2000](#); [Agol et al., 2005](#)), and transit ([Agol and Fabrycky, 2018](#)) are used to detect exoplanets. Each method has ranges of planetary masses and separations that it is particularly well suited for sampling, for example the transit method is good at picking up large planets that have small separations from their host star. The lack of Earth-mass planets at ~ 1 AU which can be seen in [Fig. 1.3](#), shows that due to the current technological limits, this is likely not to be a complete sampling of planets. Future missions, such as the James Webb Space Telescope (JWST) will help search for lower mass planets with larger separations.

Planets are now defined as large bodies that are in orbit around at least one star ([Winn and Fabrycky, 2015](#)). There can be one or many planets in orbit around single or multiple stars. There are also free floating planets ([Sumi et al., 2011](#)), planets that have either been liberated from their initial planetary systems or have potentially formed by themselves. Due to the extraordinary diversity and abundance of exoplanets, it is now commonly considered that the majority of stars host planets, with at least an average of one planet per star ([Cassan et al., 2012](#)), rather than planet-hosting stars being the exception.

The number of planets within the Solar System, as well as the large collection of moons, dwarf planets, asteroids, and the range of exoplanets that have been

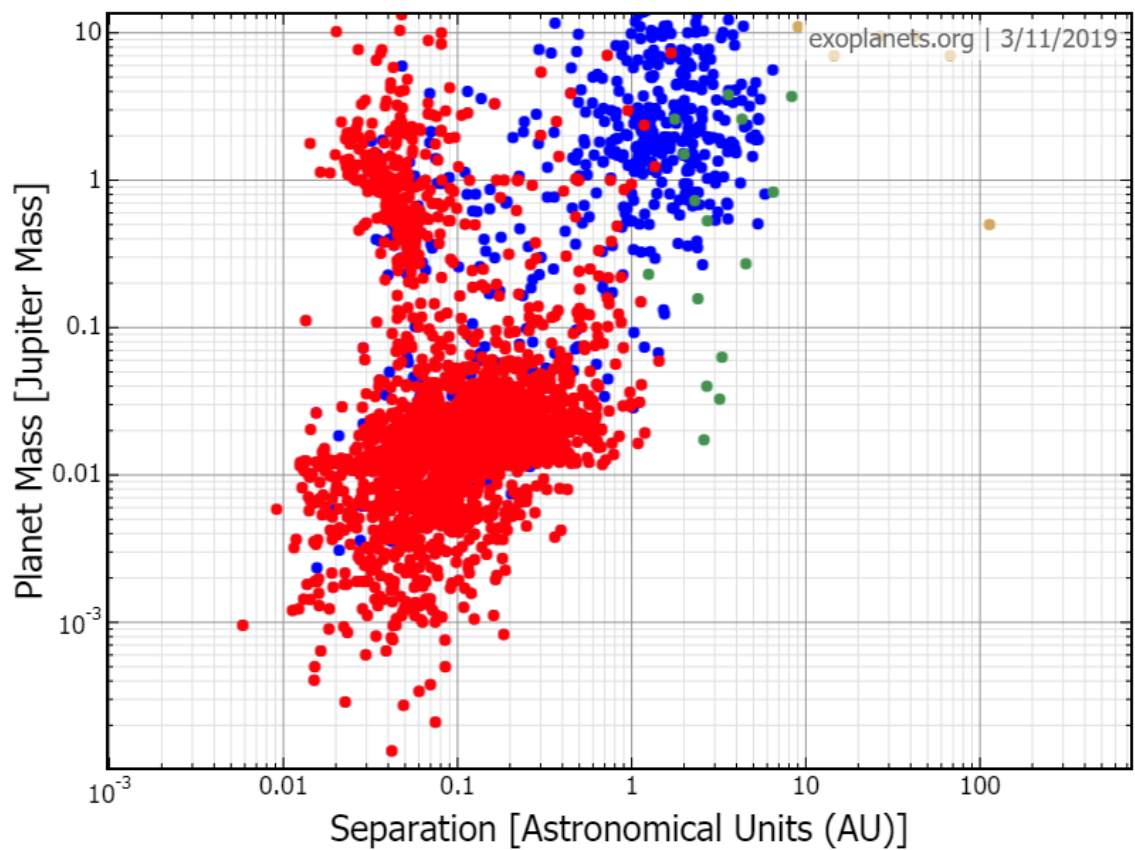


FIGURE 1.3: Distribution of planets with regards to mass ($M_{Jupiter}$) and separation distance (AU), courtesy of exoplanets.org. Each colour indicates the method used to detect each planet; Red points are detected using transit, blue using radial velocity, green using microlensing, and yellow using direct imaging.

detected, indicates that planet formation occurs relatively easily. With the diversity of detected exoplanets, a universal formation process is hard to pin down.

1.2.5 Planet formation

Planets coalesce from the disc of material that remains after a protostar has formed. The dust and gas within the disc coalesce to form objects from small pebble sized planetesimals to terrestrial and giant planets. The evolution of micron sized particles to terrestrial planets requires a growth through a minimum of at least 12 orders of magnitude. Conceptually, planet formation can be broken down into three main processes; planetesimal formation, terrestrial planet formation, and giant planet formation. Each growth stage has complications and as the full process of planet formation has never been observed, it is still theoretical.

Planetesimal formation is the first processes (Johansen et al., 2014). The growth of these particles is an important process as they are the first step of assembly for a planetary system. The word planetesimal refers to bodies of a range of sizes whose orbital evolution is dominated by mutual gravitational interactions between bodies. The process starts on the smallest scale, with dust and ice grains that are floating within a gas disc. In the formation of planetesimals, the coupling of solid particles and gas in the disc is very important in the initial stages. The gas within the disc is supported vertically due to pressure, therefore it does not collapse. However, in a simple model, the dust grains are not supported by this pressure gradient and therefore settles vertically to form a thin, central disc within the larger gas disc.

At these microscopic scales, chemical bonds and van der Waals forces enable grains to stick together. The collisions of particles occasionally results in particles sticking together, forming larger bodies. Larger particles start to gain higher collisional speeds and eventually decouple from the small eddies of the gas component of the disc (Johansen and Lambrechts, 2017). This process continues until particles become large enough to decouple from the gas of the disc, and growth through sticking occurs until objects that are tens to hundreds of kilometers in diameter are formed.

The coalescing of planetesimals to sizes where runaway growth is possible is extremely difficult to achieve. Grain surfaces are insufficiently sticky and therefore particles bounce off one another. However, run-away growth is achieved (Blum and Wurm, 2000) and rapidly (Kleine et al., 2004; Baker et al., 2005). For regions that are under normal turbulent conditions, planetesimals must reach

sizes of 1000 km to begin the process of runaway growth into planets (Ida et al., 2008). Evidence found in asteroids shows that large planetesimals formed in the solar nebula within a couple of Myr, meaning that the process for forming large planetesimals is faster than regular turbulence allows. In regions that are less turbulent, this size limit may be reduced to between 1 - 10 km for runaway growth to occur (Gressel et al., 2012), reducing the time to produce planetary building blocks.

Terrestrial planet formation can occur once there is a substantial population of planetesimals that have formed within the disc that are large enough that their evolution is now being dominated by gravitational interactions (Morbidelli et al., 2012; Raymond et al., 2014). During this phase, larger bodies grow more quickly than smaller bodies, leading to runaway growth. The runaway phase happens throughout the disc, and the timescale of this depends on the planetesimal size, the local density of the planetesimals and the local dynamical time. The density in the disc will also determine the maximum size of the planetesimal embryos when the runaway growth phase ends. Depending on different factors, this phase can form objects the sizes of moons and Mars around 1 AU radii within $10^5 - 10^6$ yr.

The collisional evolution of the planetesimals leads to the growth of a new population of objects that are planet embryos, the stage between planetesimals and planets. These objects coalesce to form terrestrial planets and the cores of giant planets, bodies that are held together by self-gravity, rather than the strength of the material they are formed from (Benz, 2000). This formation phase, out of all three, is the most well defined and understood phase of planet formation, however it remains a difficult process due to the sheer number of planetesimals necessary; to form the terrestrial planets within the Solar System, over 500 million planetesimals that are ~ 10 km in radius are needed (Armitage, 2010).

For the formation of giant planets, there are two theories: core accretion and formation via gravitational fragmentation of an unstable disc (Helled et al., 2014).

In the core accretion model, giant planet formation is the final planetary formation phase (Helled et al., 2014). Core accretion is similar to terrestrial planet formation, however once the core of ice and rock has formed, it accretes an envelope of gas (Bodenheimer and Pollack, 1986; Lissauer, 1993). This occurs once planets have grown to become approximately one Earth mass and begin to couple to the gas in the disc once again and alter its orbit, however it is due to gravity rather than aerodynamics this time. If the planet is significantly large ($\sim 10 M_{\oplus}$), the planet can begin to capture an envelope of gas from the disc. The mass of the planet at this stage is dominated by the core, with only a small envelope. This

phase is brief (~ 0.5 Myr), and ends once the mass of the core has reached its isolation mass, the mass at which it has cleared its orbit of planetesimals.

The time to form planets via the core accretion method is $\sim 2 - 3$ Myr (Lissauer and Stevenson, 2007). However, the time depends on the core formation speed, the rate at which gas within the protoplanetary disc (proplyd) can cool and be accreted onto the core, and the density of planetesimals within the disc. Past the snow line, many more solid grains are available for accretion to take place, however disc density is likely to decrease with radius. The density of planetesimals within discs can greatly affect outcomes of simulations (Dodson-Robinson et al., 2009b). The snow line within the Solar System (~ 3 AU) separates the terrestrial planets from the giant planets. Classic core accretion states that giant planets are able to grow more quickly than terrestrial planets due to the accretion of ices. However, these timescales are still exceedingly long, and increase with distance from the central star (Dodson-Robinson et al., 2009a; Rafikov, 2011).

In the disc instability growth theory, it is thought giant planets form via gravitational fragmentation of an unstable protoplanetary disc. Perturbations within the planet forming disc grow and cause densities in certain regions to be enhanced. These density enhanced regions can become destabilised once self-gravity, rather than disc pressure and shear, becomes the most important effect on the gas. These non-axisymmetric perturbations in the disc cause the redistribution of mass and angular momentum, disc torques, shocks, and a source of heating in gravitationally unstable regions. Spiral arms can act to stabilise the protoplanetary disc. These spiral arms can experience collapses in regions, creating bound, self-gravitating clumps, which may then be able to form into giant gas planets. The time taken for giant planets to form via disc instabilities is quicker than in core accretion (Boss, 1997). However, it becomes increasingly difficult at larger radii for gas to clump and form planets (Kratte et al., 2010), and at smaller radii gas cannot cool quickly enough to form bound clumps from spiral arms (Matzner and Levin, 2005; Rafikov, 2005), making planet formation via disc instability difficult.

As previously mentioned, observations of exoplanets are finding a vast range of planets that are constantly challenging current understanding of planet formation and evolution. The diversity of exoplanets can be explained in part by planet formation processes, such as the separation of giant planets from terrestrial planets within the Solar System. However, core accretion models struggle to explain the existence of planets such as hot Jupiters, the presence of massive planets beyond 15 AU, planets with retrograde orbits, and water on terrestrial planets due to terrestrial planets forming within the snow line.

Considering the protoplanetary disc and the interactions that can occur between the disc and forming planets, some of these observations can be explained by planetary migration (Mulders et al., 2015). The three types of migrations depend on the mass of the planet, as the more massive a planet, the greater effect there will be on the disc (Armitage and Rice, 2005).

Type I migration applies to planets that are roughly an Earth mass (terrestrial planets). These planets interact with the disc, however they are not massive enough to affect the disc's density profile. Whilst the planet is orbiting around the star, it causes spiral density waves within the disc, also known as Linblad torques. The inner edge of the density wave can accelerate the planet, and the outer edge acts to slow the planet. Based on the balance of these torques, they can send a planet inwards or outwards, changing the orbit of the planet, but usually the outer wave slows the planet, causing it to spiral inwards.

More massive planets ($\sim 5 M_{\oplus}$), can be affected by type II migration. Planets of these masses can significantly affect the density profile of discs. The planet will create density variations in the disc, similar to type I migration only more significant, whilst continuing to accrete material. This accretion will open a gap within the disc at the location of the planet (potentially observed in HL Tau, Fig. 1.4); type II migration is therefore sometimes known as 'gap opening'.

Type II migration allows for type III migration to occur. Once a gap is cleared, the planet will continue to accrete material with low angular momentum, causing the giant planet to migrate inwards. Type III migration applies exclusively to giant planets that have opened and sustained a gap within the protoplanetary disc.

Planets can also interact with one another, causing them to become misaligned with the spin direction of the star, have eccentric orbits, and even have orbits that are counter to the spin of the star (Naoz et al., 2011). Irregularities within the Solar System show that there was a period where planets were dynamically interacting with one another. Uranus's axis of rotation is approximately parallel with the rotation plane of the Solar System. The reason for this axis tilt is unknown, however it is thought that an Earth-sized object crashed into Uranus during planet formation (Slattery et al., 1992). Planetary migration, combined with planets becoming trapped in resonances and interacting with one another, can explain some observations within the Solar System and exoplanetary systems, but not all.

1.2.6 Protoplanetary disc

Flattened, rotating discs of gas and dust are found around almost all low mass stars after their birth (Williams and Cieza, 2011). Due to the universality of planets, these discs can be considered protoplanetary discs, and observations have provided overwhelming evidence that planets form within them (e.g. Kraus and Ireland, 2012; Quanz et al., 2015; Keppler et al., 2018).

Protoplanetary discs (see Fig. 1.4) form simultaneously with their host protostar. Gravitational collapse of molecular clouds form stars, and from the remaining material forms planets. When a molecular cloud is collapsing, it is initially collapsing radially. This gas is diffuse and has too much angular momentum to collapse straight into the density of a star. Circumstellar discs are an inevitable consequence of angular momentum conservation during the formation of a star through gravitational collapse, and survive as well-defined structures that are in semi equilibrium. Material from larger radii with higher angular momentum falls inwards, causing the material surrounding the protostar to flatten and form a disc. As the material flattens into a disc, the radius of the disc increases to 100s of AU. Some of the material within the disc is driven onto the star due to the viscosity of the disc causing material to lose angular momentum.

Protoplanetary discs are composed of gas and dust, with the majority of discs being composed of gas, and ~ 1 per cent of the disc composed of dust. The material within the disc is well mixed together, and planets form from this. Observations of protoplanetary discs have shown a typical radius of 100 – 200 AU, however models and some observations have shown that discs could be anywhere between 50 and 1000 AU, and have masses ranging from smaller than $0.001 M_{\odot}$ to $0.1 M_{\odot}$ and larger (Andrews et al., 2013; Ansdell et al., 2016; Segura-Cox et al., 2016; Yen et al., 2017; Ansdell et al., 2018). The masses and sizes of protoplanetary discs will greatly depend on various properties, such as the infall time of material and the angular velocity.

Observations of protoplanetary discs show that there are different stages of protoplanetary evolution. Lada and Wilking (1984), when observing 32 members of the young star forming region Ophiucus, discovered three distinct classes of stellar objects based on their emission wavelengths, with the majority being pre-main sequence objects. Four objects appeared to be protostellar in nature, with the evolution of these objects potentially being dominated by accretion. Eight of stellar objects had previously been classified as T Tauri stars, stars are classed as

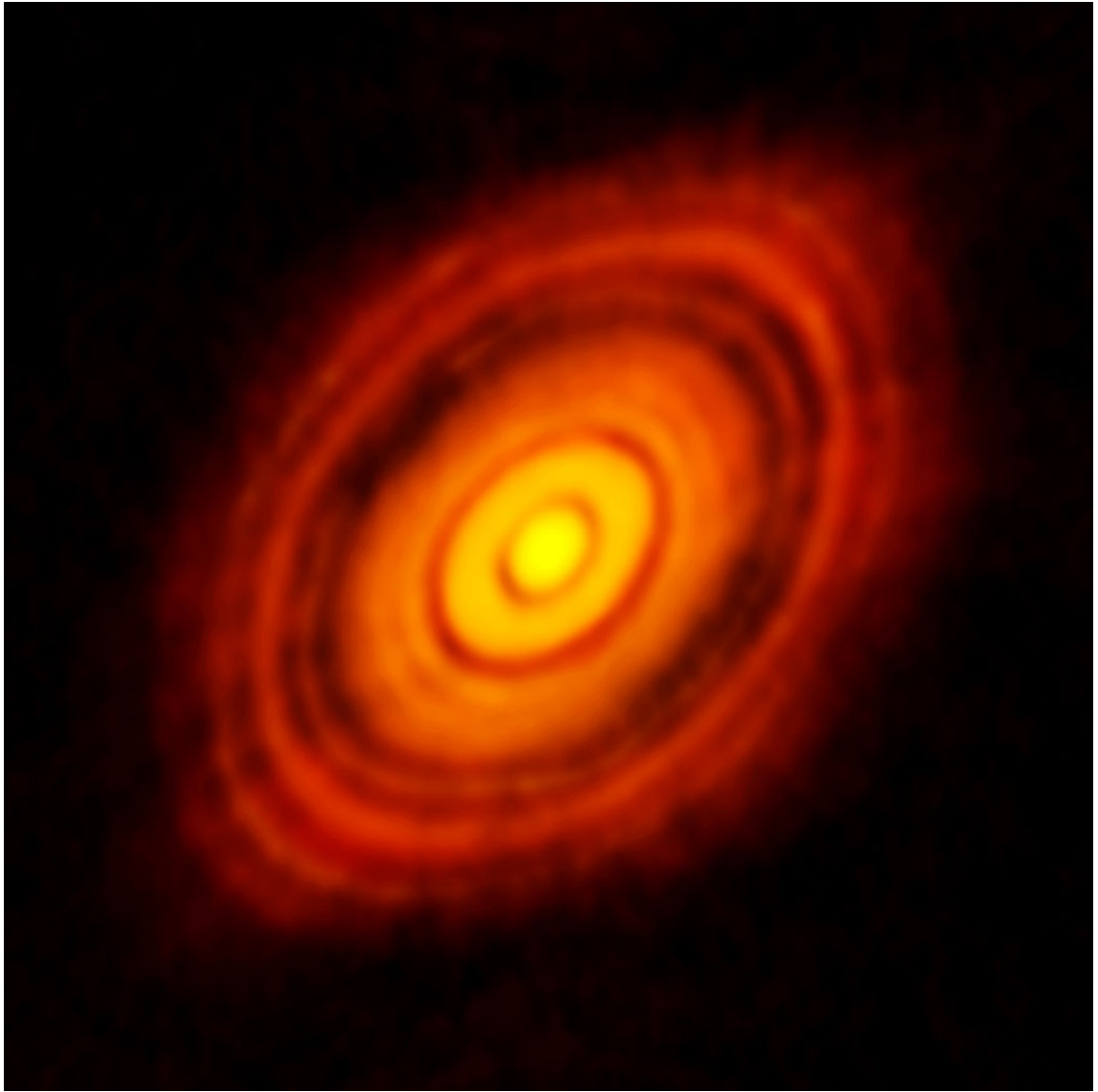


FIGURE 1.4: Image of the protoplanetary disc around HL Tau, a T Tauri star, taken by ALMA. The images of HL Tauri show rings within the disc. These could be formed by snow lines, or planets sweeping gaps within the disc by accreting the gas.

young stars that are less than 10 Myr old. A further 7 stellar objects were identified as classical T Tauri stars in this study. Three of the stellar objects appeared as purely reddened stars within the optical and infrared.

These observations formed the basis for the YSO Classes, which can be used as a rough timeline for protoplanetary disc evolution (Lada, 1987; Williams and Cieza, 2011). Class 0 objects contain deeply embedded infra-red sources. They are black-body objects, with spectral energy distribution (SED) peaks in the IR or mm part of the spectrum. Protoplanetary discs form very early on and grow rapidly during the Class 0 collapse phase. Class I objects have plumes and jets, but are still embedded, with sources having broad energy distributions that rise towards 2 micron wavelengths. The Class 0 and I phases of star formation only last a small fraction of the protoplanetary disc's life (~ 0.5 Myr; Williams and Cieza, 2011). Class II is where the fully fledged protoplanetary disc becomes optically visible (classic T Tauri stars). Class II sources have blackbody energy distributions, but flat or decreasing energy distributions towards the 2 micron wavelength. The median lifetime of a protoplanetary once it has left the embedded phase is $\sim 2-3$ Myr, although individually protoplanetary disc lifetimes vary greatly depending on the individual system. Class III have very weak visible discs and are sources that could be modelled with reddened black body energy distributions (weak-line T Tauri stars). They have little infrared excess and what excess there is likely comes from dust grain emission. Protoplanetary discs at this stage are also known as 'transition discs', where the disc is quickly dispersing. Transition discs are relatively rare ($\sim 10-20$ per cent of the disc population), which suggests that the transition phase is rapid.

Observations of protoplanetary discs have revealed that ≥ 1 mm dust grains within discs can survive $\sim 3-10$ Myr (Haisch et al., 2001). Observations of the gaseous component of the discs also suggest that discs survive on the time scale of a few Myr and then are rapidly dispersed ($\sim 3-5$ Myr Ansdell et al., 2017).

1.2.7 Disc disruption, mass loss, and destruction

Protoplanetary discs have been observed around most stars with ages of ~ 1 Myr, which are optically thick in infrared (IR), and have mostly disappeared around stars with ages of ~ 10 Myr (Haisch et al., 2001; Mamajek, 2009), meaning physical processes are actively dispersing protoplanetary discs.

Planet formation consumes material within the disc (Brandner et al., 2000). Within the solar planets there is a substantial deficit in the abundance of hydrogen and helium when compared to the original cosmic abundances from which the disc formed. The solar nebula contained many heavy elements which formed terrestrial planets, planetesimals and rocky cores. Even though the time scales between disc life and giant planet formation via core accretion are similar and therefore could be construed as tightly linked (both ~ 3 Myr), the lack of substantial amounts of hydrogen and helium being incorporated within planets along with the heavy elements means that the process of forming planets can only make a small contribution to the consumption of the gaseous component of discs. A disc of material which planets form out of should exist for many millions of years if planet formation is the only process removing material from the disc. The presence of planet-less and disc-less stars also shows that planet formation cannot be the main dispersal method.

The radial flow of material from the disc onto the host star is thought to contribute greatly to protoplanetary disc dispersal. Viscous accretion disc theory is based on the fact that the disc must transport angular momentum out radially to enable star formation (see Pringle, 1981). Viscous diffusion in the disc drives material inwards due a loss of energy. As the disc accretes mass onto its central star, the angular momentum of the disc is conserved by the disc expanding radially. The angular momentum of the material in the disc can be transported outward via magnetic fields, turbulence, and viscous material within the disc. As the disc expands due to this spreading, the accretion rate onto the star will also fall, meaning discs being dispersed by viscous accretion are never fully destroyed but become optically thin after $\geq 10^8$ yr (see Gorti et al., 2009), which does not reflect the quick dispersal times found in the previously mentioned observations.

Few stars are observed with partial discs, suggesting that the time-scale for transitioning between disc hosting and discless is small, and that processes acting to clear discs are rapid and efficient. Observations show that processes are acting on the scale of $\sim 10^5$ years to clear entire protoplanetary discs (Hartigan et al., 1990). This is known as the two-time scale problem, and the rapid dispersal of disc will place a time limit on planet formation.

There are a number of mechanisms that can drive gas from a protoplanetary disc throughout its lifetime. These mechanisms, depending when they disperse gas, can greatly affect and even inhibit planet formation. Depending on the timescale over which gas is driven from the protoplanetary disc, planet formation can be affected in two ways. If gas is being driven from the protoplanetary

discs before dust particles have managed to grow to sizes where they are able to decouple from the gas flow (~ 1 cm diameter), then the formation of planetesimals, Kuiper Belt objects (KBOs) and terrestrial planets will be prohibited. If the gas is dispersed before large ($\sim 5 - 15 M_{\oplus}$) terrestrial planets have formed, and if giant planets form via accretion onto large rocky cores, as described previously, this will inhibit the formation of giant planets (Adams et al., 2004).

The dispersal of gas and dust from discs impacts planet formation in other ways. As previously mentioned, the presence of a disc filled with gas and dust grains allows for planetary migration (see Section 1.2.5). Even a small presence of gas at late timescales (10–100 Myr) will affect the dynamical evolution of planets. Removing the gas removes the medium by which planets move, potentially reducing the eccentricities of planets and planetesimals and resulting in longer timescales for large planetesimals and terrestrial planets to form via collisions.

Our current understanding of planet forming processes and disc dispersal methods makes creating planets within these timescales difficult, and dispersing planet forming discs on such short time scales through planet formation and disc viscosity alone does not seem possible. Observations show that planet forming discs are dispersed within a few Myr, and the universality of planets seen today means that planets do form within these short time-scales. Therefore, stars must play an important role in the process of disc dispersal, and may also greatly impact planet formation.

1.3 Star clusters

Through extensive observations we have now built a relatively clear picture of the formation and evolutionary timeline of protoplanetary discs, and by extension the time scales involved in planet formation. These discs inherit their mass, composition and size from the surrounding star forming environment. The composition of the disc will in turn dictate, to some extent, the composition of the planets that subsequently form within it, provided no processes that inhibit planet formation are in action. Understanding stars and star forming environments is therefore fundamental to developing an understanding of planet formation.

Our understanding of the observed exoplanet diversity would be incomplete if considered solely within isolated disc environments. Stars and their protoplanetary discs form simultaneously, implying that planet formation is a natural outcome of star formation. Stars will, therefore, play a large part in defining the evolution of planets.

1.3.1 Star formation

Our understanding of star formation in recent years has changed as quickly and dramatically as our understanding of planet formation. Over the past 20 years, theories have moved from a quasi-static idea of formation to a process that occurs rapidly within turbulent clouds. The exact processes involved in forming stars are still not completely understood, and this is therefore just a brief description of current theories (McKee and Ostriker, 2007; Krumholz, 2014).

Previous theories

The favoured model, by Shu et al. (1987) which is based on the quasi-static picture, can be viewed in four stages: cloud assembly, cloud collapse, core accretion, and cloud dispersal.

In this model the molecular cloud assembles and cannot collapse under gravity because of the presence of a magnetic field. The magnetic field slowly 'leaks' out of the cloud as a result of ambipolar diffusion, due to the neutral hydrogen molecules not being coupled to the plasma, allowing them to undergo gravitational collapse. This causes a further increase in the density of the molecular cloud. The core of the cloud eventually overcomes a density threshold, allowing it to collapse under gravity to stellar densities. A protostar is created in

these dense regions, and is fed by in-flowing gas and dust from the surrounding medium. It is thought that the rotation of the protostar gives rise to the disc of material that forms around the protostar.

The protostar continues to accrete material from the surrounding medium and the disc of material around it. Eventually the rate at which material falls onto the protostar reduces due to the angular momentum of the material. This results in stellar winds being able to break free from the polar regions of the protostar, creating a bipolar outflow. Finally, the wind exceeds the accretion rate of in-falling material and the star appears as a main sequence star, and eventually loses all remaining traces of the disc, leaving behind a main sequence star.

Due to the constraints placed on the collapse of the cloud by the magnetic field, the timescales required to form stars via this process are very long (~ 100 Myr). The formation of binary or multiple star systems through core fragmentation is also prohibited, meaning that these systems must come from initially unbound objects, which is very hard to achieve.

Modern theories

Issues arose from the previous slow star formation theory, such as how a self-gravitating cloud of gas can support itself over many crossing times. Observations began to suggest that star formation occurred within one or two crossing times, rather than tens (Elmegreen, 2000a), with stars forming on timescales much shorter than those predicted by Shu et al. (1987). Recent theories focus on turbulence driven processes which can rapidly form stars, addressing the issue that the Shu et al. (1987) model had with timescales.

Over-densities within the galactic disc can develop due to the motion of spiral arms and shocks from supernovae; these dense regions form giant molecular clouds (GMC, Ballesteros-Paredes et al., 2007). Star formation and the cold interstellar medium (ISM) seem to be intrinsically linked. Star formation occurs within dense molecular clouds that are composed of hydrogen, and the turbulence within the GMCs is thought to influence substructure within the clouds. The properties of the clouds, such as the initial density profile and turbulence, will dictate star formation rates and stellar masses (Girichidis et al., 2011). These clouds can fragment into clumps, or prestellar cores. Some of the structures become self-gravitating cores of different masses, and may collapse to form stars if the internal gas pressure is not strong enough to withstand gravitational collapse (Jean's instability, Jeans, 1902).

Star formation typically begins with a prestellar core of $\sim 1 M_{\odot}$ at a temperature of ~ 10 K. Initially, the molecular hydrogen within the core loses energy by being in thermal equilibrium with the dust. Impacts between the H_2 and the dust grains transfers thermal energy, which can be radiated outwards from the core. As the core collapses, it is initially able to retain thermal balance by radiating away the kinetic energy released by the in falling cloud, maintaining the core's temperature at ~ 10 K. As the collapse is isothermal, the sound speed is constant. However, the density within the core keeps increasing, decreasing the Jean's mass, the minimum mass of a region that is required for collapse to occur.

At a critical density, the combination of gravitational energy release accelerating and the increasing column density means that heat is no longer able to radiate outward efficiently, causing the core to become optically thick to its own radiation. The temperature within the core increases and the collapse becomes adiabatic, resulting in the creation of the first protostar(s). As the cloud collapses, it is rotating, and forms a rotating disc of material. Stellar winds arise, either from radiation or magnetic fields, that sweeps the material into an outflow and reduces the efficiency of star formation within the core.

Some models of prestellar core evolution into stars show that cores can interact with one another, accreting material from one core onto another. Stellar multiplicity is also a ubiquitous outcome of star-formation (Duchêne and Kraus, 2013), which can arise from the prompt fragmentation of the prestellar core during gravitational collapse, although no single process appears to be able to account for all the observed multiplicity properties (Tohline, 2002). Modern theories today find the process of star-formation to be far more dynamical, rapid and environmentally dependant than previous theories.

1.3.2 Initial Mass Function

Star formation produces stars with a range of masses; from $0.08 M_{\odot}$ stars (brown dwarfs) to stars that are hundreds of times the mass of the Sun (O-type stars). The mass of a star is by far the most important factor in determining its evolution and lifetime. However, what dictates the mass of a forming star is currently poorly understood, and is a central issue to the study of star formation. One of the ways to probe the formation of stars is to look at the current population within the Galaxy and observe their mass distribution. Observations of the distribution of stellar masses throughout the Galaxy have been taken for decades to calculate this probability function, which is called the initial mass function (IMF, Adams

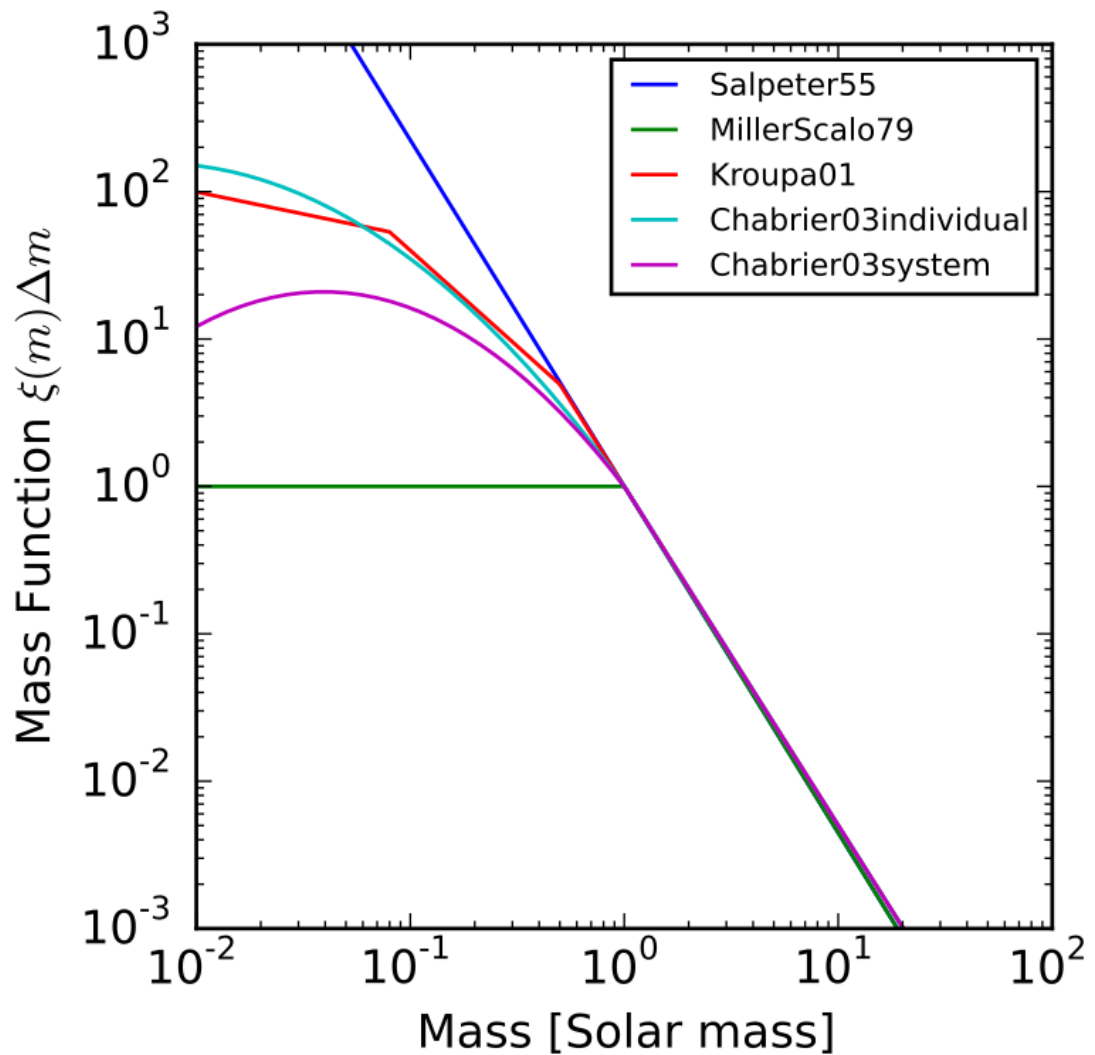


FIGURE 1.5: The initial mass functions from several studies (Salpeter, 1955; Miller and Scalo, 1979; Kroupa, 2001; Chabrier, 2003), courtesy of Johannes Buchner.

and Fatuzzo, 1996; Bastian et al., 2010). This provides a way of parameterising the relative number of stars as a function of their mass.

The observed IMF was first derived by Salpeter (1955). Since then there have been many different studies into variations of the IMF (see Fig. 1.5, Salpeter, 1955; Miller and Scalo, 1979; Kroupa, 2001; Chabrier, 2003; Maschberger, 2013) and studies into whether it is universal or not, and if universality means that there is a universal star formation process (Bastian et al., 2010; Kouwenhoven and Goodwin, 2010).

Theories on the origin of the IMF can be split approximately into two groups: models that are deterministic, and focus on the creation of cores, and models that

are stochastic and focus on the dynamics of the cloud that stars are forming from. Models that focus on prestellar cores postulate that there is a direct correlation between the mass of cores and the IMF, and therefore in these models the IMF is predetermined by the distribution of stellar core masses (Hennebelle and Chabrier, 2008; Hopkins, 2012). These models appeal to the resemblance of the IMF to the stellar core mass distribution. Models focused on stochastic accretion onto cores and dynamical interactions propose that final stellar masses are independent of core masses, and that any similarity between the IMF and the stellar core mass function is a coincidence (Bonnell et al., 2001; Clark et al., 2007). This dynamical view of star formation studies the effects of dynamical interactions and stochastic accretion, such as competitive accretion between cores (Larson, 1978).

1.3.3 Low mass star formation

Based on observations, an evolutionary path for low mass star formation has been built (Larson, 2003). Low mass stars start as cores and appear as main sequence stars after going through four separate phases, categories that have been based on the spectral energy distribution, as discussed in Section 1.2.6. Using these observational YSO categories as a guide, a timeline of stellar evolution can be built.

Class 0 objects are the earliest stages of disc and star formation that can be observed. Class 0 objects are still embedded within a cloud that it thought to be at least the same mass as the protostar; it is at this stage that the protostar accretes most of its mass. This phase is thought to last more than 10^5 yrs. The transition from Class 0 core to a Class I occurs when more than half of the surrounding envelope of material has been accreted onto the central protostar. Class I objects are still embedded, however the protostar is likely to be more massive than the surrounding envelope after the previous accretion phase. During this phase, the protoplanetary disc accretes material from the surrounding envelope until it is depleted, which lasts $\sim 10^5$ yrs. Class II objects are completely revealed, with fully fledged, thick discs orbiting a young star (classic T Tauri stars). The material within the disc, as previously mentioned, accretes onto the central star. This phase lasts for $\sim 1 \times 10^6$ yrs, during which planet formation occurs. Once there is no more matter accreting onto the star, and only a thin disc remains, and objects are classified as Class III (weak-line T Tauri stars).

1.3.4 High mass star formation

Massive star formation is not likely to be a scaled up version of low mass star formation due to the radiation that massive stars produce, which will be likely to affect the surrounding environment (Zinnecker and Yorke, 2007). Stars are considered massive when they are $\geq 8 M_{\odot}$, as this is the lower mass limit for SN progenitors (Smartt et al., 2010).

Studies of the Arches cluster, the densest known star cluster in the Milky Way, suggested that the largest star that can form via gravitational collapse is $\sim 150 M_{\odot}$ or that there is a sharp turn down in the IMF after this (Elmegreen, 2000b). It is potentially partially due to the Eddington luminosity, which defines the maximum amount of luminosity that can pass through a star's atmosphere without ejecting it into space. However this does not take into account that stars spin and therefore this limit does not hold (Crowther et al., 2010). Recent observations have revealed that R 136a1 has a mass of $\sim 265 M_{\odot}$, which disproves the maximum mass of a star that can form. Studies suggest that stars larger than $150 M_{\odot}$ can form through the collision and merging of massive stellar cores that form in binaries (Zinnecker and Yorke, 2007). However, the stellar densities needed for core merging to occur are extremely high (Bonnell and Bate, 2005).

Two main theories for the formation of massive stars from collapsing GMCs exist. The first, known as core collapse, is that the star forming molecular clouds fragment directly into stellar cores with masses of $20 - 50 M_{\odot}$. These massive cores can then accrete material from the surrounding environment to form a massive star with a disc, although this accretion will not substantially change the final mass of the star (Krumholz et al., 2005).

The second is that stars form via 'competitive accretion' (Bonnell et al., 2001). Cores form initially with masses that are only a small fraction of the final stellar mass. In-falling material from the surrounding environment can be accreted and, if the core is located within the centre of a star-forming region, can cause it to become sufficiently massive that the core becomes gravitationally dominant, leading to runaway growth.

Massive stars can greatly affect their surrounding environment during life (Boneberg et al., 2015), and death (Ouellette et al., 2007; Gounelle, 2015). In the immediate neighbourhood these effects are mostly destructive (as will be discussed in Section 1.3.8). However, further afield star formation may be triggered by the ionizing radiation from the massive star sweeping up material, creating

a dense shell of gas in which new stars can form, or from shock waves from expanding winds or SN-driven bubbles (Preibisch and Zinnecker, 2007). This is a debated form of star formation (Dale et al., 2015b).

The time to form a star may vary depending on the final mass of the star. In the competitive accretion models (Bonnell et al., 2001), massive stars gradually gain in mass over ~ 1 Myr (Wang et al., 2010), suggesting that high-mass stars form later than low-mass stars (Tan et al., 2014). This means that the entirety of their life is likely to be spent within a 1 of stars.

1.3.5 Star-forming regions and stellar groups

Observations show that $\sim 70 - 90$ per cent of stars reside in groups of stars (Gies, 1987; Bonnell et al., 2003). Observations of massive stars that are within the galactic field and appear to be isolated show that ~ 50 per cent originated from star forming-regions that contain many other stars, and therefore did not form in isolation (de Wit et al., 2005). More recent observations and simulations show that it is possible that all massive stars originated from stellar groups in star-forming regions (Parker and Goodwin, 2007; Gvaramadze and Bomans, 2008), and observations of star forming regions show most stars in the vicinity are clustered (Clarke et al., 2000).

As most stars form within groups (Lada and Lada, 2003), it is likely that the Sun and our planets formed in one, as well as the majority of other planets. Star and planet formation occurs simultaneously, and the formation of stars and planets are connected through discs. These discs can be affected by stars, therefore understanding the environment that stars are forming in is vital to understanding how it can potentially affect planet formation and evolution.

Practically all stars are thought to form as members of stellar groups that are embedded in GMCs. Two competing theories about the formation of stellar groups exist, although the reality may be an intermediate combination of the two (Wright et al., 2014). In 'clustered star formation', the majority of stars form within groups that contain thousands to hundreds of thousands of stars in regions that are parsec-sized (Kroupa, 2011). These stellar groups have smooth radial profiles and are centrally concentrated. As only 10 per cent of stars remain in gravitationally bound clusters after a few Myr, 90 per cent of these young clusters must become disrupted, potentially by gas not used in the formation of stars being expelled due to feedback (Goodwin and Bastian, 2006).

Recent images from the Herschel Space Observatory show the initial conditions of star formation, revealing that interstellar clouds are composed of filamentary structures (André et al., 2010) which fragment into many bodies. YSOs are correlated with the hierarchically structured ISM (Gutermuth et al., 2011) and are found over a wide range of stellar surface densities Bressert et al. (2010); Kruijssen et al. (2012), suggesting that there is no preferred scale for star formation to occur at.

In 'hierarchical star formation', stars form within significantly substructured (on pc scales) groups that vary with density across the regions. Bound stellar groups, or clusters, can form due to merging substructures in the densest, collapsing regions and low density regions become loosely bound or unbound groups (Bastian et al., 2007). The formation of many stars simultaneously within a fraction of a parsec produces groups of stars which vary greatly with regards to population; from a few tens to $\sim 10^6$ stars.

The term 'stellar cluster', or simply 'cluster', refers specifically to gravitationally bound groups of stars. The stars within these clusters can be loosely gravitationally bound to one another (open clusters) or tightly bound (globular clusters for example). However, the term 'cluster' is often used colloquially to simply describe a group of stars that formed from the same star-forming region. Used colloquially, the term cluster can refer to stellar groups which are gravitationally bound or unbound, and this has led to a great deal of confusion within the star-formation community. Throughout this thesis, the term cluster has been used to colloquially refer to a group of stars that formed from the same star-forming region, and does not make any assertions as to whether the stellar group is gravitationally bound or unbound.

1.3.6 Cluster Mass Function

Observations of star forming regions within the solar neighbourhood (Battinelli et al., 1994) and the Large Magellanic cloud (LMC, Elmegreen and Efremov, 1997) show that the initial mass distribution for young and old globular clusters, open clusters, associations and interstellar clouds are all power laws with a slope of ~ -2 . These observations, similar to the way that the IMF was produced, have formed a cluster mass function (CMF), a power law of the form:

$$\frac{\delta N}{\delta M} \propto M^{-\beta_c}, \quad (1.1)$$

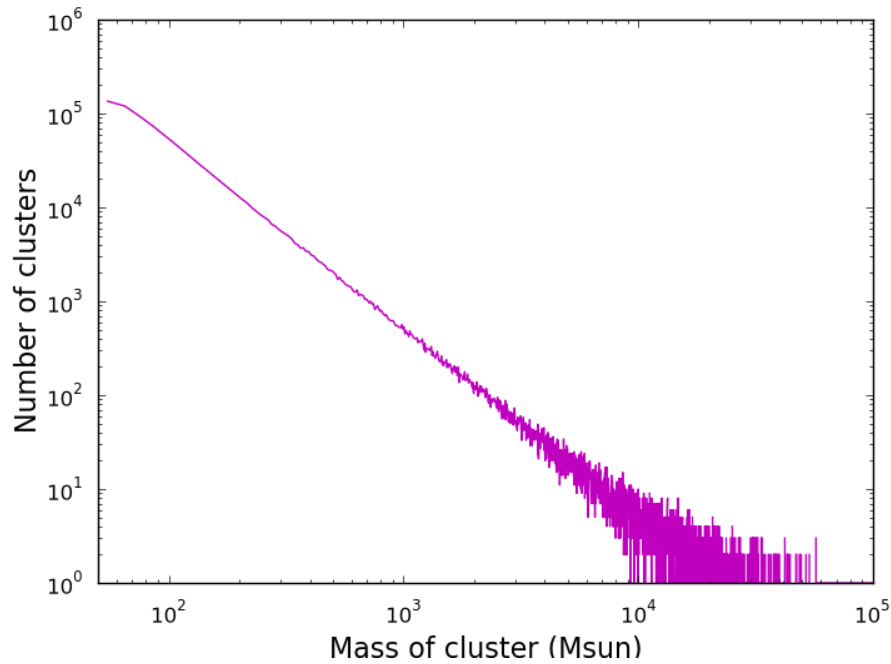


FIGURE 1.6: Star cluster mass function, with a slope of $\beta = 2$.

where M is the cluster mass and β_C describes the slope of the observed CMF; usually $\beta_C \sim 2$. More recent observations of the LMC and other galaxies have revealed a similar trend, and that there is an upper mass limit of $10^5 M_\odot$ to this relation (Gieles et al., 2006b), although this varies slightly depending on the observed galaxy ($\beta \approx 1.84 - 2.04$, Zhang and Fall, 1999; de Grijs et al., 2003; Hunter et al., 2003; Gieles et al., 2006a; de Grijs and Anders, 2006). A higher value of β , for example 2.04, will increase the number of low mass stellar clusters and decrease the number of high mass clusters. Decreasing the value of β , for example 1.84, would have the opposite effect, with a greater number of high mass clusters being present and a lower amount of low mass clusters. Fig. 1.6 shows the form of the CMF. Due to the slope of the CMF, there are many more low-mass ($\sim 100 M_\odot$) than there are high-mass ($\geq 10^3 M_\odot$) clusters.

Approximately 10 per cent of stars remain within bound clusters after a few Myr (Lada and Lada, 2003). Many other young stars are found in loose, comoving groups that contain O type and/or early B type stars (Blaauw, 1964). These regions are generally known as OB associations. OB associations have low densities, are not gravitationally bound and are therefore in the process of expanding and dispersing into the Galactic field, implying that they are relatively young.

Gravitationally bound clusters survive long after OB associations disperse, and can therefore tell us about the IMF of high density star forming regions. As mentioned in Section 1.3.4, massive stars can greatly influence their surrounding environment. The Orion Nebula Cluster (ONC), shown in Fig. 1.7, provides a good observational example of this. It is one of the most studied objects in the sky due to its proximity to Earth (~ 415 pc), allowing for detailed observations. The ONC is a cluster with an age of $\sim 1\text{--}2$ Myr, mass of $\sim 2000 M_{\odot}$, and ~ 3500 cluster members (Hillenbrand, 1997). Within the centre of the ONC is a very young (~ 1 Myr) open cluster, known as the Trapezium cluster, containing 4 massive stars (Hillenbrand and Hartmann, 1998). With on-going regions of star formation, to fully formed low and high mass stars, the ONC gives astronomers insight into all stages of the star formation process on many scales.

Several studies have proposed a fundamental relation between the cluster mass and the mass of the most massive star that can form (Weidner and Kroupa, 2006; Weidner et al., 2013), meaning that the CMF would ultimately control the IMF. In this scenario, forming a cluster containing one massive star that can explode as a supernova requires the presence of several thousand low-mass stars ($\sim 1000 M_{\odot}$, Adams, 2010; Parker et al., 2014a), and rules out the existence of low-mass clusters containing one or more massive stars.

However, low mass clusters containing massive stars containing stars with masses much greater than this theoretical limit have been detected. The γ Velorum cluster is an excellent example of this; a low mass cluster containing 242 members (Jeffries et al., 2014; Prisinzano et al., 2016), where the most massive member is γ^2 Velorum, a WC8/O8III binary with initial masses of $35 M_{\odot}$ and $31.5 M_{\odot}$ respectively (Eldridge, 2009) and the total cluster mass is only $\sim 100 M_{\odot}$. It is possible that these massive stars formed through mergers (Banerjee and Kroupa, 2018). However, as previously mentioned (see Section 1.3.4), the densities required to produce massive stars from mergers are extremely high, therefore this is unlikely. Maschberger and Clarke (2008) created a compilation of observations of low-mass clusters containing massive stars. Whilst the sampling was not complete or unbiased, they found no strong evidence that systematic suppression of the maximum stellar mass in low-mass clusters was occurring. Their results indicate that the mass of stars within low-mass clusters can be assumed to be randomly sampled from the IMF.

If the only limit on the mass of the star that can form is the total mass of the star-forming region itself then occasionally it would be expected that a low-mass star-forming region would contain one or more massive stars as observed in γ



FIGURE 1.7: A composite image of the Orion Nebula in visible and infrared using the Hubble Space Telescope, from NASA.

Velorum.

1.3.7 Cluster dynamics

The star formation process results in stars grouped together at densities that exceed the density within the Galactic disc by orders of magnitude (Lada and Lada, 2003; Bressert et al., 2010). The initial density of the group, and whether the stars are gravitationally bound to one another, will dictate whether the stars evolve into a bound cluster, or into a low-density association. Open clusters and associations share a similar fate, which is that they will eventually be dispersed by Galactic tides into the Galactic field, however the difference is the timescales. The time taken for open clusters to disperse can range from 100 Myr, to a few Gyr for the densest ones. As for associations, as they are unbound they are rapidly dispersed on timescales of 10 to 100 Myr.

As mentioned in Section 1.3.5, recent observations have revealed that stars form in substructured, hierarchical groups. However, observations of some young clusters (as young as 1 Myr), show that they are centrally concentrated, with smooth radial profiles, such as the ONC (Hillenbrand and Hartmann, 1998). Numerical studies have found that, due to two-body and violent relaxation, initially highly substructured star-forming regions can evolve to smooth and centrally concentrated clusters after only a few Myr (Scally and Clarke, 2002; Goodwin and Whitworth, 2004; Allison et al., 2010), making it possible that all star forming regions are initially substructured. A small amount eventually become smooth, and centrally concentrated clusters through dynamical evolution, whilst the rest become unbound associations (Parker and Meyer, 2012).

Stellar groups where gravity is important to the dynamical evolution of the cluster are known as collisional systems. Within these groups, many interactions with other stars are required to redistribute kinetic energy, and so collisional systems usually have high stellar densities, such as globular clusters or young, massive clusters. Over many crossing times (the time required for a significant fraction of an orbit to have occurred), the effects of so many interactions with other stars significantly affects the evolution of the stellar system. Relaxation-driven equipartition of energy causes heavier stars to sink towards the centre of the cluster and low-mass stars to migrate to the outskirts. This relaxation process provides a way for transporting kinetic energy out of the centre of the cluster, resulting in an increase in density.

The initial bulk motion (velocity) of the star forming-region will also greatly affect dynamical evolution. If the star-forming region is initially sub-virial (collapsing), then the region will violently relax. This violent relaxation can form gravitationally bound clusters. If the region is super-virial (expanding), the cluster will rapidly disperse outwards, forming (unbound) associations.

The evolution of a young cluster depends on its dynamics (Nicholson et al., 1992; Parker et al., 2014b; Sills et al., 2018), and possibly gas expulsion (Hills, 1980), although simulations have shown that if stars and gas are not coupled by the time feedback occurs, gas expulsion is not a dominant factor in cluster dispersal (Dale et al., 2015a). Whether a cluster is initially contracting (sub-virial), expanding (super-virial), or is stable (in virial equilibrium) will also affect its dynamical evolution.

The initial densities of star-forming regions are difficult to determine, and span a wide range (Bressert et al., 2010; King et al., 2012), but many are thought to be at least $\sim 100 M_{\odot} \text{pc}^{-3}$ at the epoch of star formation. Parker (2014) compare the present-day stellar densities and amount of spatial substructure in seven star-forming regions, including the ONC and Upper Scorpius, to infer the likely range of initial stellar densities in each of these star-forming regions. All are consistent with having an initial density in the range of $10 - 1000 M_{\odot} \text{pc}^3$.

The density of a cluster is an important consideration as dense clusters can be inhospitable to protoplanetary discs. Two clusters that presently have similar densities may have had very different initial densities because initially very dense clusters expand faster than lower density counterparts. By observing the properties of protoplanetary discs and planetary systems, we may be able to tell the kind of cluster environment that they formed in (Winter et al., 2019), and whether or not there are specific conditions for star-forming regions that make them conducive for planet formation.

Many factors impact planet formation, such as the length of time spent in proximity to other stars, the number of massive stars present, and the density of the cluster. Low mass clusters disperse more quickly than their high mass counterparts (Adams and Myers, 2001), meaning protoplanetary discs in low-mass clusters are less likely to be affected by external processes. Dynamical interactions within clusters, and whether a star cluster is bound (subvirial or virialized) or unbound (supervirial), could also significantly affect the formation process of planet and their evolution (Armitage, 2000; Bonnell et al., 2001; Scally and Clarke, 2001; Adams et al., 2006; Olczak et al., 2008; Parker and Quanz, 2012).

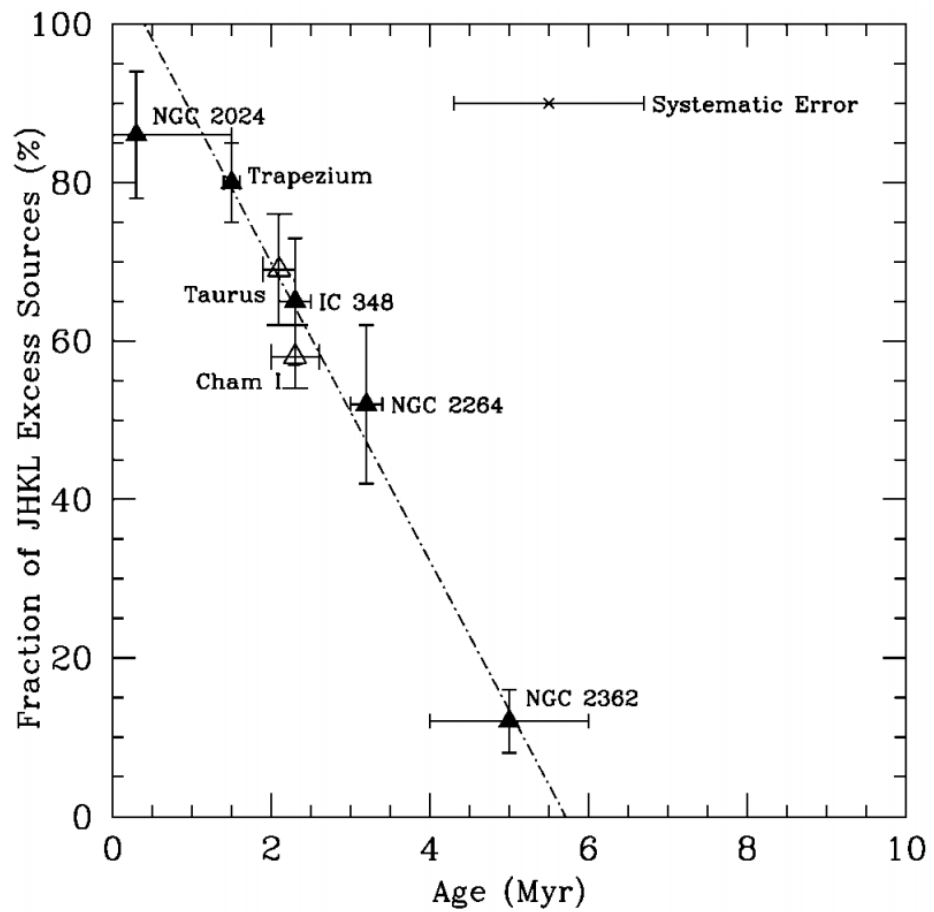


FIGURE 1.8: Plot from [Haisch et al. \(2001\)](#) showing the percentage of protoplanetary discs in observed clusters against the age of cluster.

1.3.8 Protoplanetary disc disruption and clearing in clusters

Studies have shown that discs within clusters survive at different rates. In the first study of its kind, [Haisch et al. \(2001\)](#) observed clusters which covered a large range of ages (0.3 – 30 Myr). These clusters, NGC 2024, Trapezium and IC348, were studied to collect data on the number of stars that were hosting discs (see [Fig. 1.8](#)). Near infrared continuum observations were taken of the central region of the disc ($r = 0.1$ AU). Comparing the youngest to the oldest cluster showed that discs disperse rapidly within a few Myr. The youngest cluster (NGC 2024), had a disc fraction greater than 80 per cent. By ~ 3 Myr, approximately 50 per cent of stars retain their discs. By ~ 6 Myr it appears that most discs have dispersed, giving a rough timescale for when stars will lose their discs within clusters.

As previously mentioned, gas dispersal methods are very inefficient ([Section 1.2.7](#)). Therefore, gas and dust should remain within the discs for many millions of years after planet formation. However, observations of discs within other clusters have also shown that disc lifetimes are short ([Zuckerman et al., 1995](#); [Pascucci et al., 2006](#); [Richert et al., 2018](#)). Very few stars appear to retain their discs by 10 Myr ([Haisch et al., 2001](#); [Mamajek, 2009](#); [Richert et al., 2015](#)), with observations showing that disc lifetimes are $\sim 3 - 5$ Myr. Therefore, there must be efficient external processes that can disperse discs.

Stellar winds

Protostellar winds and outflows will affect disc dispersal rates. After the collapse of the cloud into the protostar and protoplanetary disc, the disc actively begins to accrete material and produces a strong wind. This wind is created by the rotating magnetic field interacting with the inner disc, and this wind can have mass loss rates that are 0.3 – 0.5 times that of the accretion rate onto the protostar ([Shu et al., 1988](#)). Therefore, stellar winds cannot be responsible for dispersing significant amounts of disc material.

Stellar flybys

Passing stars' gravitational potential can affect and interact with the protoplanetary disc (see [Fig. 1.9](#), [Clarke and Pringle, 1993](#); [Armitage, 2000](#); [Bonnell et al., 2001](#); [Scally and Clarke, 2001](#); [Adams et al., 2006](#); [Olczak et al., 2008](#); [Parker and Quanz, 2012](#); [Rosotti et al., 2014](#); [Vincke et al., 2015](#); [Portegies Zwart, 2016](#); [Winter et al., 2018b](#)). Material from the protoplanetary disc can be stripped and accreted

onto the passing star. Close stellar interactions can also cause protoplanetary discs to be truncated or destroyed. Planetary orbits can be disrupted, liberated or accreted onto the passing star. The density of the star forming region will affect the rate of stellar interactions, with stars in low-density environments experiencing fewer dynamical interactions than dense and populous environments (Wright et al., 2014; Bressert et al., 2010).

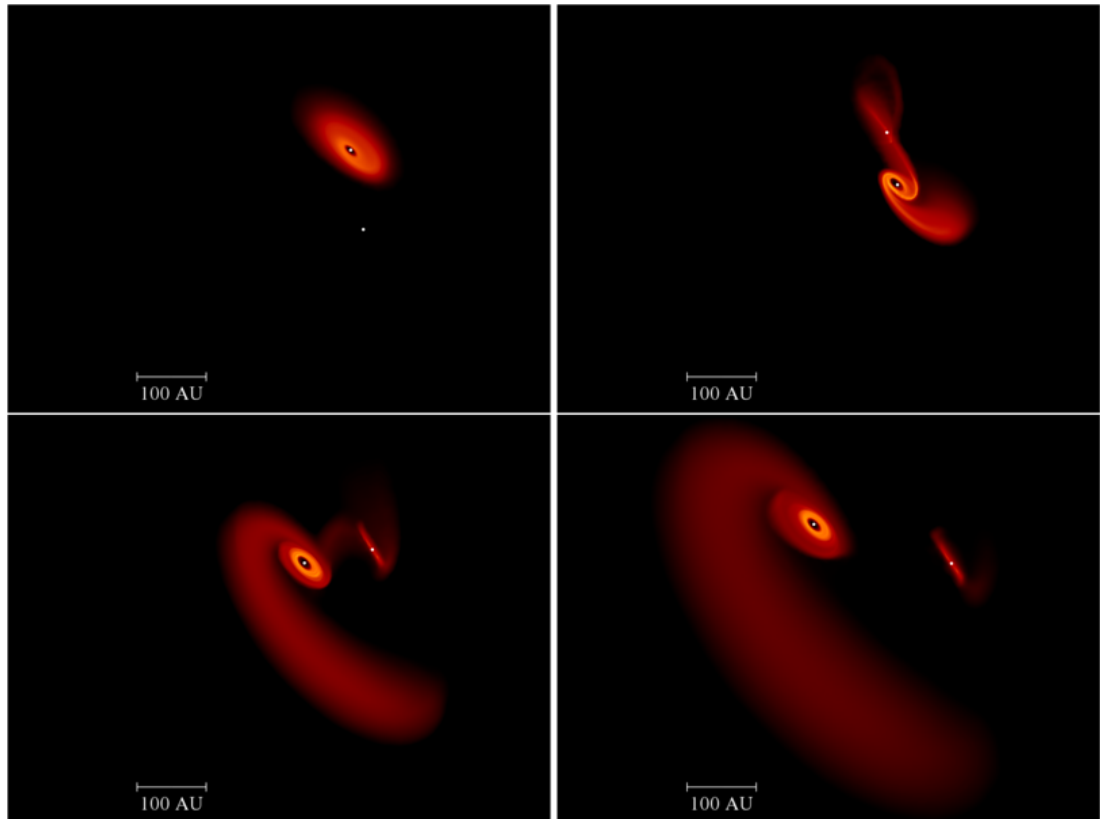


FIGURE 1.9: The evolution of a tidal encounter between a protoplanetary disc and a star at four different snapshots in time (Dai et al., 2015).

The orbits of objects within the Kuiper belt and Oort cloud show that it is possible there was a close encounter with another star during formation (Brasser et al., 2006; Punzo et al., 2014; Pfalzner et al., 2018). The wide and eccentric orbit of the potential Planet 9 also has implications for the formation of the Solar System. Planet 9 could have been captured by our Solar System from another star's protoplanetary disc (Mustill et al., 2016), although it is unlikely (Parker et al., 2017). It could also be the core of a giant planet that was ejected from its original

orbit by Jupiter during planet formation, or a captured rogue planet that formed in a similar way to stars (Sumi et al., 2011).

Photoevaporation

Photoevaporation by the central star and neighbouring massive stars is thought to be the dominant mechanism for dispersing protoplanetary discs. Photoevaporation occurs when ultraviolet radiation heats the material in the surface of the disc to a sufficiently high temperature ($\sim 500 - 10^4$ K) that it has enough thermal energy to overcome the gravitational binding energy of the disc. A pressure gradient drives the unbound gas into the surrounding ISM, causing a steady depletion and truncation of the disc. Internal or external sources can be responsible for photoevaporation of protoplanetary discs.

Internal Photoevaporation

Internal photoevaporation occurs for discs surrounding stars with masses greater than $\sim 1 M_{\odot}$, due to radiation produced by the host star. There are two types of ultraviolet radiation that are at work with the process of photoevaporation; extreme ultraviolet radiation (EUV), which ranges between 13.6 – 100 eV, and far ultraviolet radiation (FUV), which ranges between 6eV – 13.6 eV. EUV radiation ionizes hydrogen atoms within the disc, creating a layer of hot gas within the disc that has a temperature of $\sim 10^4$ K. FUV radiation acts externally to erode the protoplanetary disc from the outside in. FUV photons are absorbed principally by dust, and therefore FUV radiation can penetrate much deeper into the disc. At high column densities FUV photons dissociate molecules, heating the material that is impenetrable to EUV photons, and create a neutral flow of material away from the disc. X-ray radiation ($h\nu > 0.1$ keV) is also important in the case of internal photoevaporation as the disc is in close proximity to the star, and erodes the protoplanetary disc from the inside out.

Depending on the source of the ionization (or in the case of external photoevaporation the distance), photoevaporation can be dominated by EUV or FUV radiation. In the case where EUV radiation dominates the mass loss rate, EUV photons ionize the protoplanetary disc, causing the ionization front to be very close to the disc surface. The neutral gas flow evaporating from the protoplanetary disc moves subsonically through a thin photodissociation region (PDR), which is dominated by FUV photoevaporation. If EUV radiation is not dominating, the PDR increases in thickness and the ionization front moves away from the surface

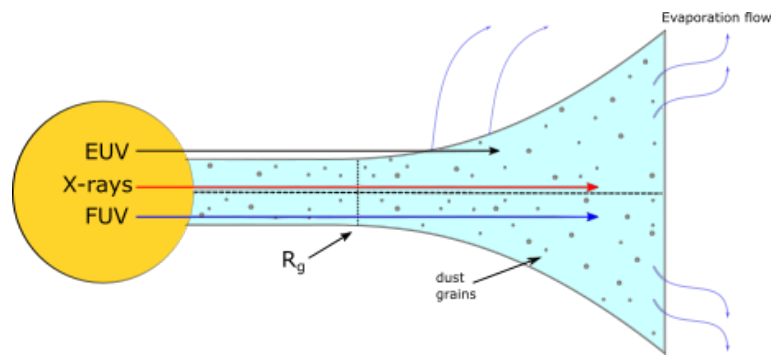
of the disc. The neutral flow of material travels supersonically through the thick PDR, eventually hitting the ionization front created by EUV radiation and creating a shock front. Beyond the shock, the material travels subsonically through a stationary ionization front (Johnstone et al., 1998).

The earliest ideas of photoevaporation considered disc heating due to EUV photons from OB stars (Hollenbach et al., 1994; Richling and Yorke, 1997; Font et al., 2004). However, this process by itself does not quickly or efficiently remove gas from the disc, and does not address the 'two-timescale' problem that T Tauri stars present, where discs survive for long time periods before suddenly dispersing.

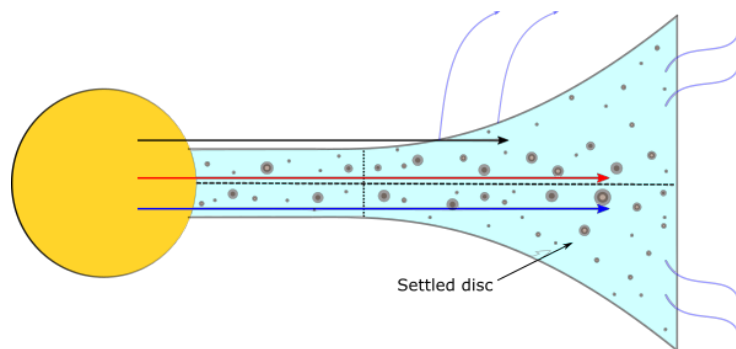
Clarke et al. (2001) developed a model called the 'UV-switch' to address the 'two-timescale' problem, where EUV photoevaporation and viscous evolution of the disc are combined (see Fig. 1.10). Viscous accretion of the disc onto the central star and internal photoevaporation of the disc at moderate radii act together to efficiently clear the entire disc. The 'UV switch' is turned on when the accretion rate of material flowing in from larger radii onto the inner disc falls to a low enough level ($\sim 10^{-10} M_{\odot} \text{ yr}^{-1}$) so that it roughly matches the rate that material is being lost from the disc due to photoevaporation. As the disc evolves, the accretion rate of material onto the inner disc falls. The material in the outer disc is no longer able to reach the inner disc as it is photoevaporated once it reaches $\sim 5 - 10$ AU.

As the inner disc is no longer being replenished, it rapidly empties onto the central star on viscous time scales ($\sim 10^5$ yr), resulting in the inner disc being cleared, as seen in Fig. 1.10(c). This leaves a hole within the centre of the disc, directly exposing the inner edge of the disc to UV photons. This UV radiation continues to evaporate material from the disc; this is known as a transition disc. Transition discs account for ~ 20 per cent of observed discs, and this transition phase takes approximately 10 per cent ($\sim 10^5$ yr) of the discs lifetime (Kenyon and Hartmann, 1995; Duvert et al., 2000). Based upon these observations, the transition period of a disc is relatively short.

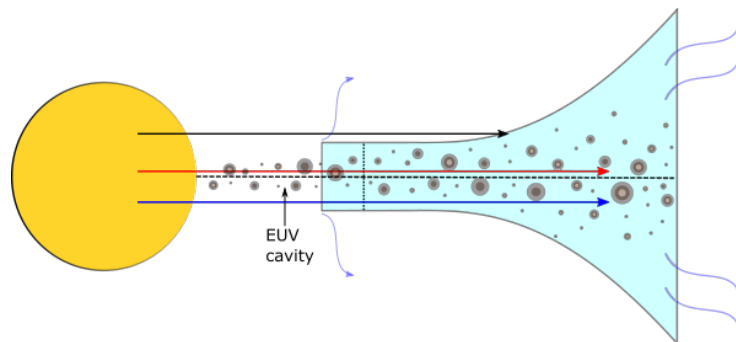
As it is the inner disc that is affected by EUV radiation, it is also the planet forming region that is affected. This could be potentially detrimental to planet formation, making the time it takes for EUV radiation to blow a hole in the inner disc very important. FUV radiation seems to predominantly remove mass that is not strongly bound from the outer disc. The FUV photons heat the material and cause significant erosion of the outer disc, which is where most of the mass of the disc lies.



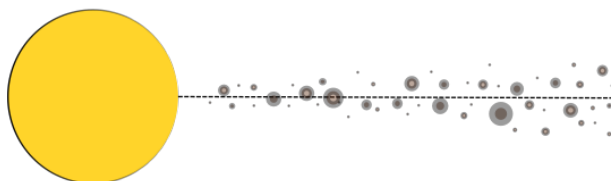
(a) Massive flared disc



(b) Settled disc



(c) Photoevaporating disc



(d) Debris disc

FIGURE 1.10: The evolutionary stages of a protoplanetary disc, depicting the process of planetesimal formation and disc clearing when including viscous accretion and internal photoevaporation of the discs by the host star. Graphics based on those made by Ian Czekala for astrobit.es.

X-rays can also play a major role in the evolution and dispersal of protoplanetary discs, especially when combined with the other forms of radiation. X-rays ionize the gas, reducing the positive charge on dust grains, therefore enhancing the heating caused by FUV radiation. Combined and under certain conditions, X-rays and FUV photons can also create a gap in the inner disc. Protoplanetary discs around solar-type stars will also be subjected to X-ray driven photoevaporative winds, the strength of which scales with the X-ray luminosity. These winds effectively suppress accretion by preventing material from reaching the star, creating a gap in the disc. By including internal X-ray photoevaporation in models, model accretion rates can be directly compared to typically observed T Tauri accretion rates, showing the relevance of X-ray photoevaporation in protoplanetary disc evolution. Models of protoplanetary discs that simulate the effects of X-ray driven internal photoevaporation show that the lifetime of discs are internally regulated by X-ray photoevaporation and strongly depend on the X-ray luminosity of the host star [Owen et al. \(2011\)](#).

External Photoevaporation

Star-forming regions can contain massive stars whose UV radiation is so strong that it can affect the protoplanetary discs of neighbouring stars ([Johnstone et al., 1998](#); [Armitage, 2000](#); [Adams et al., 2004](#); [Fatuzzo and Adams, 2008](#)). The external radiation heats the outer and upper layers of the disc, similar to internal photoevaporation, however the disc is evaporated from the outside in.

EUV radiation is produced by massive ($\geq 15 M_{\odot}$) stars. As explained earlier, in EUV-dominated flows the thermal pressure at the surface layer of the disc is determined by photoionization and the FUV produced pressure dominated region remains thin. Neutral gas that has been heated by FUV radiation moves through this thin layer towards the ionization front, and so the mass-loss rate is controlled by the EUV-induced ionization rate. EUV photons are absorbed by the ionization front, preventing them from reaching the disc. However, protoplanetary discs in close proximity to massive stars will experience a great deal of mass loss due to EUV radiation (see [Fig. 2.4](#)).

FUV photons are not absorbed and can penetrate and heat the gas, meaning FUV radiation usually dominates in external photoevaporation. FUV radiation is produced by all stars that are $\geq 1 M_{\odot}$ in mass, although O-type stars produce the majority, creating a combined background radiation field which is measured

in units of ‘Habing’ flux (G_0 , where $1G_0$ equals the estimated average UV background in the ISM, which is taken to be 1.6×10^{-3} ergs $\text{cm}^2 \text{s}^{-1}$). This radiation field can be substantial, and can greatly affect protoplanetary discs. FUV photons often initiate mass loss, creating a flow of neutral material from the disc that influences the size of the ionized envelope (Yorke and Richling, 2002).

FUV heating comes mainly from two mechanisms; grain photoelectric heating, and FUV pump heating and subsequent collisional de-exciting of H_2 molecules (Johnstone et al., 1998). In the first scenario, FUV photons are absorbed by dust grains. Occasionally, the absorption of a photon leads to an energetic electron being released, which then collides with gas atoms and ions, sharing its kinetic energy as heat. This mechanism is responsible for ~ 1 per cent of the absorbed FUV photon energy being converted into heat. The most common form of heating is caused when H_2 atoms absorb FUV photons, causing the electrons within H_2 atoms to become excited. At high densities at the disc surface, this vibrational energy is converted to heat via collisional de-excitation by other hydrogen atoms and molecules (Adams et al., 2004). In FUV-dominated flows, the thermal pressure at the surface of the disc is determined by FUV heating. The neutral gas expands as it is heated, resulting in this material being launched from the disc as a thermal wind. This supersonic wind pushes the ionization front away from the surface of the disc, creating a shock front. Shock fronts have been observed within star-forming regions, such as those in the Orion Nebula caused by external photoevaporation (see Fig. 1.11). After the shock, the material then travels subsonically through the stationary ionization front. The mass-loss rate in this scenario is determined by the pressure dominated region temperature, the FUV flux, and the opacity of the dust.

The effects of external photoevaporation appear to be observed in nearby star-forming regions (see Fig. 1.11), such as the ONC (McCaughrean and O’dell, 1996; Eisner et al., 2016, 2018) and σ Orionis (Ansdell et al., 2017). These observations show that protoplanetary discs within clusters hosting massive stars are subjected to photoevaporation.

The Solar System would have been impacted in substantially different ways depending on the mass, IMF, and initial density of the star-forming region. If massive stars were present during the formation of the Solar System, our protoplanetary disc could have been subjected to high levels of background radiation, and may have experienced external photoevaporation. FUV fluxes of $G_0 = 3000$ can evaporate the solar nebula past 30 AU within 15 Myr, with more extreme FUV fluxes ($G_0 = 30,000$) photoevaporating the solar nebula within 6 Myr (Adams,



FIGURE 1.11: Protoplanetary discs within the ONC that appear to be being affected by the radiation from the Trapezium OB association in the centre of the cluster. Whether these are protoplanetary discs or the remnants of disc is unknown. From NASA.

2010).

1.4 Formation of the Solar System

Observations of the present day Solar System can help place constraints on the type of star forming region that formed the Sun. Planetary orbits within the Solar System are mostly circular. The mean eccentricity of the orbits is 0.06, with a range from 0.00068 – 0.21. The orbits are almost completely aligned with the plane that is defined by the total angular momentum of the Solar System. This regularity provides powerful constraints on the formation of the Solar System (Adams, 2010).

'Edges' within the Solar System provide another set of constraints, and can tell us not only about planet formation, but also the type of stellar environment in which the Solar System formed. The outermost structure in the Solar System, the Oort cloud, is thought to extend to ~ 0.3 pc ($\sim 60,000$ AU), in which the objects are loosely bound to the Sun and are therefore easily perturbed by passing stars. Based on stellar fly by rates in embedded clusters, most of the Oort cloud would have been stripped if it formed within a dense, embedded cluster (Adams, 2010), and therefore the cloud likely grew slowly over time (Duncan et al., 1987).

The solar nebula must have extended to at least 30 AU, the orbit of Neptune, as planet formation occurred within this region. The Kuiper belt also experiences a significant drop in the number of KBOs at ~ 50 AU (Allen et al., 2000). It is likely that the Kuiper belt edge was created due to external photoevaporation (Adams et al., 2004; Adams, 2010). Isotopically selective UV photodissociation of CO isotopic isomers in the outer regions of the solar nebula is also the most likely cause for the mass-independent oxygen isotope fractionation observed in meteorites (Lyons and Young, 2005). Uranus and Neptune, both ice giants rather than gas giants, may indicate that the solar nebula experienced photoevaporation at the further edges of the disc (near $r = 30$ AU), as mentioned in Hollenbach and Adams (2004). The low gas content within the planets could imply that gas was expelled if they formed in situ with Jupiter and Saturn. Alternatively, they may have taken longer to form than the gas giants, and therefore less gas was present for them to accrete.

Orbits of objects like Sedna could not have been produced through planetary interactions. It is therefore likely that a stellar fly-by disrupted Sedna. There is also a small chance that it is a captured planet from another star (Kenyon and Bromley, 2004). The rate at which stellar encounters occur depends on the density of the environment that the Sun resided in when the encounter occurred.

1.4.1 Short-lived radioisotopes in chondrites

The original composition of the Sun's protoplanetary disc can be determined from chemical analysis of certain meteorites. Chondrites are stony meteorites and are composed of dust and small grains, and are some of the most primordial asteroids. They have never been a part of any bodies that were large enough to undergo melting or planetary differentiation, meaning their composition has remained unaltered since formation. Using Pb/Pb dating, the formation of chondrites has been dated to ~ 4.5 billion years ago (Bouvier et al., 2007; Amelin et al., 2011). Therefore, chondrites reflect the earliest composition and conditions of the Sun's protoplanetary disc. One of the most definitive pieces of evidence that the Sun formed within a cluster, and a potentially large cluster, is the presence of short-lived radio isotopes in chondrites, which can only have originated from neighbouring stars (which were likely massive) when the Solar System was forming.

It appears that chondrites are homogeneous throughout the Solar System (Jacobsen et al., 2008). Chondrites can contain calcium aluminium inclusions (CAIs), which are microscopic rocks that are enriched with specific elements (Krot et al., 2009). Chondrites are composed of a homogeneous mixture of pebbles and grains, which grew through small planetesimals sticking to one another. The fact that chondrites are undifferentiated (the metals are distributed throughout the chondrite and have not concentrated or formed a metallic core) shows that they could not have come from larger bodies, where the pressures and temperatures would have destroyed such mixtures and caused the creation of a core through differentiation. Chondrites are therefore some of the earliest solids that formed within the Sun's protoplanetary disc. Chondrites also have small dispersion ages, meaning their formation is extremely rapid (Thrane et al., 2006).

Short-lived radioactive species (SLRs) with half-lives less than 10 Myr, such as ^{26}Al and ^{60}Fe , have been detected in CAIs in carbonaceous chondritic meteorites in the Solar System (Lee et al., 1976; Marhas et al., 2008). These radioactive isotopes appear to be one of the dominant sources of heat during planetesimal formation (Urey, 1955; MacPherson et al., 1995) and could be important for long-term physical processes within forming planetary systems (Adams, 2010; Lichtenberg et al., 2016a).

In comparison to the interstellar medium (ISM), the Solar System appears to contain an over abundance of these SLRs (Cameron and Truran, 1977). Because of the short half-lives of SLRs and their homogeneous distribution throughout

the Solar System (Villeneuve et al., 2009), these isotopes must have been incorporated within the protoplanetary disc either shortly before or during the very early evolution of the Solar System.

SLRs can form through several mechanisms, though not all are viable methods for enriching the protosolar nebula. Cosmic ray spallation can form ^{26}Al in large enough quantities to match the levels measured in the Solar System, but cannot produce ^{60}Fe (Lee et al., 1998; Shu et al., 2001). SLRs are also produced in asymptotic giant branch (AGB) stars (Wasserburg et al., 1994; Busso et al., 1999, 2003; Trigo-Rodríguez et al., 2009); however AGB stars are not associated with star-forming regions and a chance encounter with them is highly unlikely (Kastner and Myers, 1994).

The most probable scenario is that these SLRs were produced in the cores of massive young stars, but the exact mechanism for their inclusion in the protosolar disc is still under debate. Star-forming regions often contain very massive stars, and these massive stars explode as supernovae (SNe) and can chemically enrich their immediate surroundings in short-lived radioisotopes.

One possibility is that the Sun (and its protoplanetary disc) formed from pre-enriched material (Gounelle et al., 2009; Gritschneder et al., 2012; Gounelle and Meynet, 2012; Gounelle, 2015). In this scenario, a first generation of stars produce SNe that pollute the surrounding medium and trigger a second generation of star formation, without destroying the GMC. This causes the second generation of stars to form from material pre-enriched in ^{60}Fe . Winds from a massive star in this second generation deliver ^{26}Al into the surrounding ISM, from which a third generation of stars, including the Sun, form. However, Parker and Dale (2016) show that this sequential star (and planet) formation scenario would lead to large age spreads (or even age dichotomies) due to dynamical mixing in young star-forming regions, which are not observed (e.g. Soderblom et al., 2014). Furthermore, this scenario requires a substantial fraction of stars to form via triggering, which is not common in simulations of star cluster formation (Dale et al., 2015b).

The other potential enrichment mechanism is direct enrichment of the protoplanetary disc from a nearby SN explosion (Chevalier, 2000; Ouellette et al., 2007). If enrichment occurs from a single supernova explosion, a star of $20 M_{\odot}$ would be sufficient to deliver similar abundances to those found in the Solar System (Wasserburg et al., 2006). Chevalier (2000) and Ouellette et al. (2007) propose that accretion of grains from the supernova ejecta could provide substantial amounts of ^{26}Al and ^{60}Fe , and that the high radiative luminosity could cause melting of

dust grains and the formation of chondrules. The disc, when closer than 1 pc from the SN explosion, would not incur large mass loss (< 1 per cent), and the disc does not absorb enough momentum from the shock to be liberated from the host protostar (Ouellette et al., 2007). A distance to the SN of between $\sim 0.1 - 0.3$ pc allows for sufficient enrichment without destroying too much of the disc (Scally and Clarke, 2001; Adams et al., 2004), although recent work by Lichtenberg et al. (2016c) suggests that the outer distance can be relaxed somewhat. However, SN ejecta is vastly enriched in ^{60}Fe relative to ^{26}Al (Woosley and Heger, 2007), meaning all models relying on SN injection result in a $^{26}\text{Al}/^{60}\text{Fe}$ ratio that is far lower than the initial solar ratio unless special conditions are adopted (Desch et al., 2011).

1.4.2 Birth environment of the Solar System

Over the past few years, observations have focused on trying to find the potential remnant of the Sun's birth cluster and models have begun to constrain the distances to clusters that could plausibly have formed. Accounting for previous orbits through the Galaxy and the impacts this can have on the dispersion of star-forming regions, it is thought that 10 – 40 per cent of the Sun's siblings should be located within 1kpc of the Sun (Portegies Zwart, 2009), and potentially the remnant of the cluster within 2kpc (Pichardo et al., 2012).

Based on the information gleaned from observations of the orbits of KBOs and the presence of daughter products of multiple radioactive isotopes in chondrites, it is clear that the Sun did not form in isolation, but in the vicinity of other stars, and at at least one massive star. It is common (see Fig. 1.5) that several thousand low-mass stars form with every massive star. Star clusters typically have radii of order 1 pc (Lada and Lada, 2003), which corresponds to initial densities of upward of $1000 \text{ stars pc}^{-3}$. The presence of thousands of stars means that photoevaporation of protoplanetary discs and disc truncation and disruption due to stellar flybys are potential problems discs can potentially face.

The Solar System may have been able to survive within a relatively dense ($\sim 10^3 \text{ stars pc}^{-3}$) cluster for as long as 250 Myr before being disrupted (Adams, 2010) so long as it spent a significant portion of time on the outskirts of the cluster and travelled to the central region of the cluster just before the SN explosion, although the probability of this occurring is small (Williams and Gaidos, 2007). However, external FUV radiation within a dense, massive cluster would be high

and as a result photoevaporation would greatly reduce the lifetime of the protoplanetary disc, potentially suppressing giant planet formation (Armitage, 2000).

Studies have looked at cluster properties that would allow for the formation of a planetary system like the Solar System whilst accounting for these external effects (Portegies Zwart, 2009; Parker et al., 2014a; Pfalzner et al., 2015; Portegies Zwart, 2019). Since massive stars usually form with several thousand other stars, these studies focus on clusters with $\sim 1000 - 3000$ stars, although Portegies Zwart (2009) considers clusters with as little as 300 stars. Parker et al. (2014a), who focus on 'typical' clusters containing massive stars, find that $\sim 0.5 - 1$ per cent of G-type stars are enriched and unperturbed, making high mass clusters inefficient at enriching protoplanetary discs via SN enrichment.

M67, an open cluster that has a very similar age and metallicity to the Sun, and is a similar distance from the Galactic centre, has been considered as the potential birth cluster of the Sun (Önehag et al., 2011). Recent 3D models of the Milky Way have traced the orbits of M67 and the Sun through time show that it is highly unlikely that the Sun originated from M67 (Pichardo et al., 2012), meaning that either the birth cluster of the Sun still has yet to be discovered, or that it has been fully dispersed into the Galactic field.

As mentioned in Section 1.3.6, observational examples of low mass clusters containing massive stars have been found, such as the γ^2 Velorum cluster, a low mass cluster containing 242 members (Jeffries et al., 2014; Prisinzano et al., 2016), where the most massive member is γ^2 Velorum, a WC8/O8III binary with initial masses of $35 M_{\odot}$ and $31.5 M_{\odot}$ (Eldridge, 2009). If the only constraint during star formation is that a star cannot form with a mass greater than that of its birth cluster (Elmegreen, 2006), this means that stastically speaking it is possible to form a low mass cluster ($\sim 100 M_{\odot}$) containing high mass stars.

Embedded clusters typically have radii of order 1 pc (Lada and Lada, 2003), meaning that clusters with low masses will likely have a lower stellar density than their higher-mass counterparts. These lower stellar densities may imply that the stars that are enriched by SNe suffer fewer dynamical interactions, and hence could be more viable environments for the formation and evolution of a quiescent Solar System.

1.5 Aims

In this Chapter I have reviewed the processes behind planet and star formation and how the surrounding environment affects and shapes them. As the majority of stars seem to host planets, and the majority of stars form in clusters, understanding the effects of cluster environments on planet formation may be fundamental to understanding the diversity of observed exoplanets. The old theories of planet formation have changed dramatically with the detection of exoplanets, and many new challenges face astrophysicists, from the timescales involved to how star forming environments shape planet formation.

The birth environment of the Solar System is currently unknown. There is significant tension between the apparent need for a large birth cluster containing massive stars to provide nuclear enrichment to protoplanetary discs and to explain the orbits of objects such as Sedna, and the need for a smaller, less dynamically active cluster to avoid potentially destructive dynamical and radiative effects. A wide range of star-forming regions containing massive stars that can create analogues to the Solar System has been explored, with masses as low as $\sim 500 M_{\odot}$ being investigated (Portegies Zwart, 2009); however, this ignores the majority of star forming regions. Lower mass star forming regions outnumber $\geq 500 M_{\odot}$ clusters by almost 10 to 1 (see Fig. 1.6). Though the total numbers of stars born from these low-mass star forming regions is not 10:1 when compared to the numbers that originate from higher mass clusters (see Section 2.1), these low-mass regions may be less prone to close encounters that disrupt discs, and less extreme UV radiation, as the presence of even one massive star in a low-mass region is unusual.

Previous studies have focused on smooth, centrally concentrated star-forming regions, similar to the ONC. However, observations of young star-forming regions show that many initially begin highly substructured, and over a few Myr become smooth and centrally concentrated due to two-body relaxation. If, and how, this initial substructure affects the amount of UV radiation and subsequent photoevaporation that protoplanetary discs are subjected to is unknown.

The aim of this thesis is to explore the parameters that have yet to be considered when analysing how star-forming environments shape planets. I will explore whether low-mass ($\sim 100 M_{\odot}$) star-forming regions that contain massive stars could be the potential birth environment for the Solar System, and how efficient low-mass star forming regions containing one or two massive stars are at enriching protoplanetary discs (Chapter 3). I shall also consider the dependence

of protoplanetary disc dispersal rates due to external photoevaporation in different mass star-forming regions when the initial conditions of clusters are varied (Chapter 4). Finally, I shall examine how UV radiation fields vary based on the initial spatial distribution of stars, and whether stars with masses $<15 M_{\odot}$ contribute significantly to UV radiation (Chapter 5).

Chapter 2

Methods

In this Chapter I describe the cluster simulations used throughout this thesis, focusing on the cluster set-up and selection and the N -body simulations used to examine the effects that cluster dynamics have on enrichment and destruction of protoplanetary discs.

I use Monte Carlo codes and N -body simulations to model and evolve clusters containing massive stars and analyse the results. I describe the method to select low-mass clusters containing massive stars from the cluster mass function (Section 2.1), before describing the subsequent N -body and stellar evolution of these clusters (Section 2.2 and 2.3). Finally, I discuss how disc mass loss and the UV radiation field are calculated (Section 2.4.1 and 2.5).

2.1 Creating clusters

In order to determine the fraction of low-mass clusters that contain massive stars, cluster masses are randomly sampled from the following analytic fit to the observed star cluster mass function (CMF):

$$N(M) \propto M^{-\beta_C}, \quad (2.1)$$

where M is the cluster mass and β_C describes the slope of the observed CMF. A value of $\beta_C = 2$ is adopted in accordance with Lada and Lada (2003) although, as described in Section 1.3.6, this value does vary depending on the observed star-forming region. I sample this function for cluster masses between $50 - 10^5 M_\odot$, which results in the distribution shown by the (top) magenta line in Fig. 2.1.

I then populate these clusters with stars drawn randomly from the IMF, which is described in Section 1.3.2. The mass function developed by Maschberger (2013) is used in this thesis, and has a probability density function of the form:

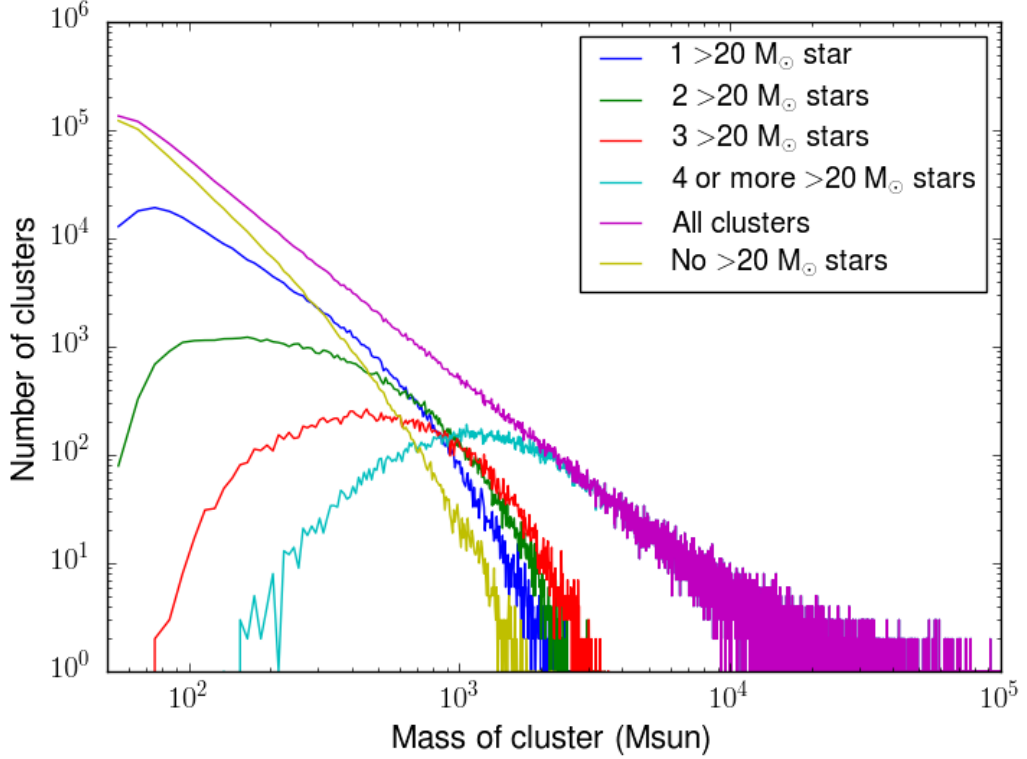


FIGURE 2.1: Star cluster mass functions for clusters containing different numbers of massive stars. Stars with masses $>20 M_{\odot}$ were specifically selected because of their exceptionally short lives, exploding as SN within a few Myr, which allows for enrichment to take place while planet formation is still occurring.

$$p(m) \propto \left(\frac{m}{\mu}\right)^{-\alpha} \left(1 + \left(\frac{m}{\mu}\right)^{1-\alpha}\right)^{-\beta} \quad (2.2)$$

Here, $\mu = 0.2 M_{\odot}$ is the average stellar mass, $\alpha = 2.3$ is the [Salpeter \(1955\)](#) power-law exponent for higher mass stars, and $\beta = 1.4$ is used to describe the slope of the IMF for low-mass objects (which also deviates from the log-normal form; [Bastian, Covey, and Meyer, 2010](#)). Finally, this IMF is sampled from within the mass range $m_{\text{low}} = 0.1 M_{\odot}$ to $m_{\text{up}} = 50 M_{\odot}$. Stars more massive than $50 M_{\odot}$ are not sampled here so that the simulated star forming regions produce clusters which represent star-forming regions found in the local Solar neighbourhood.

A "soft-sampling" technique is adopted to fill the clusters, i.e. if the total stellar mass sampled from the IMF equals or exceeds the stipulated cluster mass, then

the cluster is considered to have been populated, and the process is repeated with the next cluster (Elmegreen, 2006). This method of randomly sampling the IMF implies that the only formal limit on the most massive star that can form is the upper limit to the IMF (Parker and Goodwin, 2007). The debate on whether to use random or selected sampling is an important issue with regard to the clusters selected for this thesis. Sorted sampling would rule out the case where a low mass cluster could produce a massive star, due to the physical dependence on the mass of the cloud (Weidner and Kroupa, 2006). However, if the only limit on the mass of the star that can form is the total mass of the star-forming region itself, then occasionally it would be expected that a low-mass star-forming region could contain one or more massive stars.

As mentioned in Section 1.3.6, low-mass star-forming regions rarely contain massive stars, but such regions are observed (e.g. γ^2 Vel, a low-mass region containing at least two massive stars, Jeffries et al., 2014). Because Cerviño et al. (2013) show that it is statistically impossible to distinguish between each scenario, and given their significant contribution to the integrated stellar mass function (see Fig. 2.1), I therefore investigate low-mass star-forming regions ($100 M_{\odot}$) that contain massive stars. I will assume that it is possible to form a massive star that explodes as a SN in a cluster containing a few hundred low-mass stars, and will explore how protoplanetary discs within these clusters are affected by the radiation of the massive star or stars.

As it is low-mass clusters containing massive stars that are of most interest, the CMFs for clusters that contain one or more stars with mass $>20 M_{\odot}$ are plotted. Fig. 2.1 shows that there is an equal probability of a cluster with a stellar mass of $1000 M_{\odot}$ occurring as a low-mass ($50\text{--}200 M_{\odot}$) cluster containing one or two massive stars; low mass clusters containing one massive star are 100 times more abundant than the higher mass clusters. Whilst the total population of stars originating from each type of star-forming region will depend on the mass range that is considered, the number of stars produced in low-mass star forming regions ($\sim 100 M_{\odot}$) is non-negligible (see Section 3.4). Therefore, these low-mass environments should be considered when searching for the birth environment of the Solar System and its analogues.

I select the median regions in terms of the total number of stars from within the mass ranges of $100 \pm 1M_{\odot}$ and $1000 \pm 10M_{\odot}$, with the stipulation that they have to contain massive stars. For the $100 M_{\odot}$ mass regions, the median region containing one and two massive stars was specifically selected. For the $1000 M_{\odot}$ the average cluster that contained three or more massive stars was selected.

2.2 Simulation set-up

Both observations (e.g. [Cartwright and Whitworth, 2004](#); [Sánchez and Alfaro, 2009](#); [Gouliermis et al., 2014](#)) and simulations ([Schmeja and Klessen, 2006](#); [Girichidis et al., 2012](#); [Dale et al., 2013](#)) of star-forming regions indicate that stars form with a hierarchical, or self-similar spatial distribution (i.e. they are substructured). It is almost impossible to create substructure through dynamical interactions; rather it is usually completely erased over a few crossing times ([Scally and Clarke, 2002](#); [Parker et al., 2014b](#)).

The simulations presented in this thesis are created with initial substructure by following the box-fractal method in [Goodwin and Whitworth \(2004\)](#). As mentioned in Chapter 1, clusters form in highly turbulent clouds, which are highly substructured, giving rise to highly substructured star clusters. These clusters then lose their substructure as they evolve, and become smooth and approximately spherical. To create substructure, a fractal distribution of stars is created. First a cube of side N_{div} ($N_{div} = 2$ is used throughout) is defined, inside which the fractal will be created. A first generation parent is placed at the centre of the cube. From the centre of the cube, N^3 sub-cubes are created, with a first generation child in the centre of each. The fractal is then created by determining which first generation children become parents themselves and spawn children in the same manner. Which children become parents is determined by the fractal dimension, D , with the probability that a child becomes a parent being $N_{div}^{(D-3)}$. If the fractal dimension is low then less children will become parents, meaning the final cluster will contain more structure, and if the fractal dimension is high then more children will become parents, meaning the structure will be more smooth.

A small amount of noise is added to the positions of the generated children to stop the cluster having a grid like appearance. Some of these children then become parents and the process is repeated until there are substantially more children than have been specified. Finally, some of the children are then randomly removed from the outer edges to produce a spherical cluster from the cube, the random selection process making sure that the fractal shape is maintained, until the specified number of children are remaining. These children are then randomly assigned masses from the IMF and become the stars within the cluster ([Allison et al., 2010](#); [Parker et al., 2014b](#)).

I adopt three different fractal dimensions: $D = 1.6$ (highly substructured), $D = 2.0$ (moderately substructured), and $D = 3.0$ (smooth). Note that the fractal dimensions obtained from [Goodwin and Whitworth \(2004\)](#) give approximate

fractal values with some statistical variation around these values. The clusters are defined by the half-mass radius, a value that is set at the beginning of each simulation run. The half-mass radius is the radius within which half the mass of the cluster resides.

There are several ways to distribute the mass of a cluster. Recent papers (e.g. Allison et al., 2009) adopt a fractal mass distribution to reproduce the clumpy and filamentary conditions that are observed in young star forming regions. Another approach is to adopt a mass distribution similar to that of a globular cluster, known as a Plummer sphere (Plummer, 1911). The Plummer sphere is a good approximation for the ONC as it is observed today, and describes clusters with a smooth radial mass profile that is centrally concentrated. The mass-density profile of the Plummer sphere can be written as

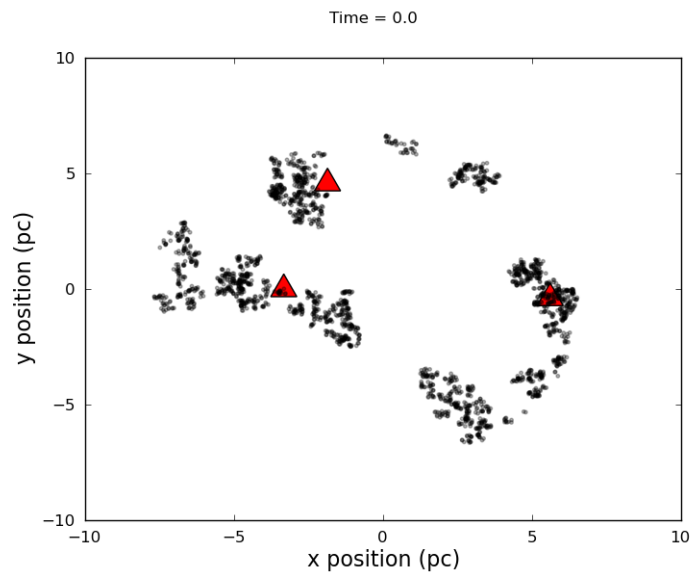
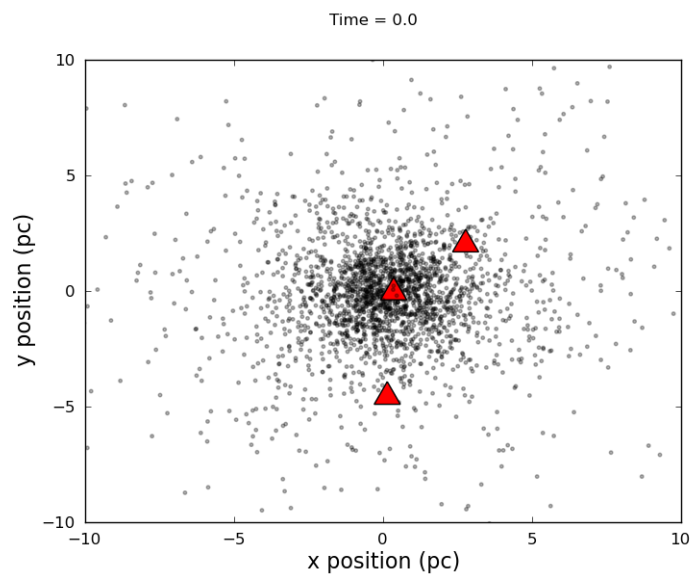
$$m(r) = \frac{3M_{cl}}{4\pi r_{pl}^3} \frac{1}{\left[1 + \left(\frac{r}{r_{pl}}\right)^2\right]^{5/2}} \quad (2.3)$$

where $\rho_m(r)$ is the radius-dependent density, M_{cl} is the mass of the cluster, and r_{pl} is the 'Plummer radius' (Kroupa, 2008). Both fractal and Plummer sphere mass distributions are used in Chapter 4.

The velocities of stars in the fractals are also correlated on local scales, in accordance with observations (Larson, 1981; André et al., 2010). The children in the fractals inherit their parent's velocity, plus a small amount of noise which successively decreases further down the fractal tree. This means that two nearby stars have very similar velocities, whereas two stars which are distant can have very different velocities. Again, this is an effort to mimic the observations of star-forming regions, which indicate that stars in filaments have very low velocity dispersion (André et al., 2010).

Finally, the velocities of the stars are scaled in the fractal to the desired virial ratio α_{vir} , where $\alpha_{vir} = T/|\Omega|$; T and Ω are the total kinetic energy and total potential energy of the stars, respectively. Three different virial ratios are adopted for the simulations: $\alpha_{vir} = 0.3$ (subvirial, or collapsing), $\alpha_{vir} = 0.5$ (virial equilibrium) and $\alpha_{vir} = 0.7$ (supervirial).

Each median cluster is evolved through every permutation in Table 2.1 for 10 Myr using the Starlab environment (Portegies Zwart et al., 1999, 2001). For each realisation of the initial conditions, 20 versions of the same simulation are run, identical apart from the random number seed used to set the positions and velocities, in order to gauge the inherent stochasticity in the evolution.

(a) Highly substructured ($f_d = 1.6$)

(b) Plummer sphere

FIGURE 2.2: (a) and (b) show the same $1000 M_{\odot}$ cluster at time 0 Myr, but with different spatial mass distributions. Fig. (a) shows a highly substructured and clumpy initial mass distribution ($f_d = 1.6$), and Fig. (b) shows the cluster with a Plummer sphere mass distribution. The black points are individual stars and the red triangles show massive ($\geq 20 M_{\odot}$) stars.

TABLE 2.1: The initial conditions for all simulations where α_{vir} is the virial ratio, f_D is the fractal dimension, and ps stands for Plummer sphere. All configurations of these initial conditions were run.

N_{stars}	$N_{\text{stars}} (>20 M_{\odot})$	α_{vir}	f_D	$\rho (M_{\odot} \text{ pc}^{-3})$
145	2	0.3; 0.5; 0.7	1.6; 2.0; 3.0	10; 100
113	1	0.3; 0.5; 0.7	1.6; 2.0; 3.0	10; 100
2377	5	0.3; 0.5; 0.7	1.6; 2.0; 3.0; ps	10; 100

2.3 N -body simulations

N -body simulations provide the most efficient way of numerically simulating dynamical interactions and evolution within clusters. Every star within the simulation is provided with a mass, as described above, and is considered as a point-like particle. Newtonian gravity is used to determine the force that all these particles exert on one another at each time-step within the simulation. This allows for the trajectory of stars to be calculated for the next time step, and this process is repeated for the duration of the simulation. The smaller the time steps are, the more accurate the calculation but the longer the run time for the simulation.

As mentioned in Section 1.3.7, many small interactions between stars (or particles) within dense stellar groups can greatly affect the evolution of the system. Interactions between stars can also result in binary systems, which can affect stellar evolution and potentially protoplanetary discs, especially for massive stars (Portegies Zwart and Verbunt, 1996; Sana et al., 2012). Calculating these small interactions within simulations provides a challenge. Using brute-force direct-summation methods can result in high running costs and difficulties with the enormous range of time scales (from days to $10^4 - 10^6$ yrs). There is also the issue that the time step sizes required to accurately integrate the trajectory of a star can vary considerably. To overcome the enormous dynamic range in time involved in collisional N -body problems, variable time-step schemes are used (Aarseth, 2003). Particles are arranged in a hierarchy of time-step levels which are organised in powers of two, with reference to a base time step level, and can then move between levels at synchronised points according to the amount of accuracy needed.

Due to the high precision needed when calculating the trajectory of a star, a Hermite integration scheme is used. This uses a 4th-order polynomial to fit a function between two points, as long as the value and the first derivative of the

function at the points is known. This prediction scheme is used to fit \mathbf{a} (the acceleration vector) with a fourth order polynomial using four previously recorded times

$$\mathbf{a}_t = \mathbf{a}^{(1)}(\Delta t) + \frac{\mathbf{a}^{(2)}}{2!}(\Delta t)^2 + \frac{\mathbf{a}^{(3)}}{3!}(\Delta t)^3 + \frac{\mathbf{a}^{(4)}}{4!}(\Delta t)^4, \quad (2.4)$$

where $\mathbf{a}^{(n)}$ is the n^{th} derivative of the acceleration with respect to time, and Δt is the difference between the current and most recent (t_0) time.

From Newton's law of gravity, the equation of motion for the i^{th} particle in a cluster containing N particles is:

$$\mathbf{a}_i = - \sum_{j=1, j \neq i}^N \frac{Gm_j(\mathbf{r}_i - \mathbf{r}_j)}{|\mathbf{r}_i - \mathbf{r}_j|^3} \quad (2.5)$$

where \mathbf{a}_i is the acceleration vector of the i^{th} particle, which is calculated with respect to the j^{th} particle. \mathbf{r}_i and \mathbf{r}_j are the radial vectors of the i^{th} and j^{th} particles, and G is the gravitational constant ($G = 6.67 \times 10^{-11} \text{m}^3 \text{kg}^{-1} \text{s}^{-2}$). The first derivative of this is given by

$$\dot{\mathbf{a}}_i = - \sum_{j=1, j \neq i}^N \frac{Gm_j(\mathbf{v}_i - \mathbf{v}_j)}{|\mathbf{r}_i - \mathbf{r}_j|^3} + 3 \sum_{j=1, j \neq i}^N \frac{(\mathbf{r}_i - \mathbf{r}_j) \cdot (\mathbf{v}_i - \mathbf{v}_j) \mathbf{a}_{ij}}{|\mathbf{r}_i - \mathbf{r}_j|^2}. \quad (2.6)$$

At the beginning of each timestep, the values of \mathbf{a}_0 and $\mathbf{a}_0^{(1)}$ are calculated. These values are then used to predict the position of the particles (r) at the end of this time step

$$\mathbf{r} = \mathbf{r}_0 + \mathbf{v}_0 \Delta t + \frac{1}{2} \mathbf{a}_0 \Delta t^2 + \frac{1}{6} \dot{\mathbf{a}}_0 \Delta t^3, \quad (2.7)$$

where \mathbf{r}_0 is the radial and \mathbf{v}_0 is the velocity vector of the particle at the beginning of the timestep. The velocity (\mathbf{v}) of the particle at the end of the step is calculated using \mathbf{a} , $\mathbf{a}_0^{(1)}$ and \mathbf{v}_0 , using

$$\mathbf{v} = \mathbf{v}_0 + \mathbf{a}_0 \Delta t + \frac{1}{2} \dot{\mathbf{a}}_0 \Delta t^2. \quad (2.8)$$

Next, the acceleration and its first derivative (\mathbf{a} and $\dot{\mathbf{a}}$) are calculated at the end of the timestep. The Taylor series for the acceleration \mathbf{a} can be expanded up to order $\ddot{\mathbf{a}}$,

$$\mathbf{a} = \mathbf{a}_0 + \dot{\mathbf{a}}_0 \Delta t + \frac{1}{2} \ddot{\mathbf{a}}_0 \Delta t^2 + \frac{1}{6} \dddot{\mathbf{a}}_0 \Delta t^3. \quad (2.9)$$

An expansion of the first derivative can also be made, up to the $\ddot{\mathbf{a}}$ term:

$$\dot{\mathbf{a}} = \dot{\mathbf{a}}_0 + \ddot{\mathbf{a}}_0 \Delta t + \frac{1}{2} \dddot{\mathbf{a}}_0 \Delta t^2. \quad (2.10)$$

The higher order terms of acceleration ($\ddot{\mathbf{a}}_0$ and $\dddot{\mathbf{a}}_0$) can be simultaneously solved and then eliminated, giving

$$\mathbf{r} = \mathbf{r}_0 + \frac{1}{2}(\mathbf{v} + \mathbf{v}_0)\Delta t + \frac{1}{12}(\mathbf{a}_0 + \mathbf{a}) + C(\Delta t^5), \quad (2.11)$$

$$\mathbf{v} = \mathbf{v}_0 + \frac{1}{2}(\mathbf{a} + \mathbf{a}_0)\Delta t + \frac{1}{12}(\dot{\mathbf{a}}_0 - \dot{\mathbf{a}})\Delta t^2 + C(\Delta t^5). \quad (2.12)$$

These equations are fourth order accurate and also time symmetric, and therefore give excellent energy conservation. At the beginning of each time step, all stars are synced. The acceleration of each particle is calculated using Eqns. 2.4, and is used to predict the position of the particle at the end of the time step. Based on this first calculation, particles are assigned a time-step rung based on the level of accuracy needed (see Fig. 2.3). The particles with the smallest time-step segments will have their velocities, accelerations, and positions calculated to the highest precision. Particles that are on lower rungs (larger time-step segments) will have their positions predicted using a low-order Taylor series. During the time-step, particles can move between rungs at specific points depending on the level of accuracy needed. At the end of the time-step, all particles are re-synchronised and the process is repeated until the end of the simulation.

In order to reduce the amount of rounding errors and the repeated multiplication and division of constants to values, and the computational expense, the parameters within N -body simulations are assigned standardised specialist units (Heggie and Mathieu, 1986). Once the simulation is complete, all values are converted back to physical units.

2.3.1 Software packages

The Starlab package is a collection of programs that are specifically developed for simulating and analysing realistic star clusters. The main time integration program within Starlab is kira (Makino and Aarseth, 1992), which uses a Hermitic integration scheme.

Stellar evolution is implemented within the simulations using the SeBa look-up tables (Portegies Zwart and Verbunt, 1996). The stellar mass and radius are what dictates a star's evolution, and detailed calculations of the stellar structure

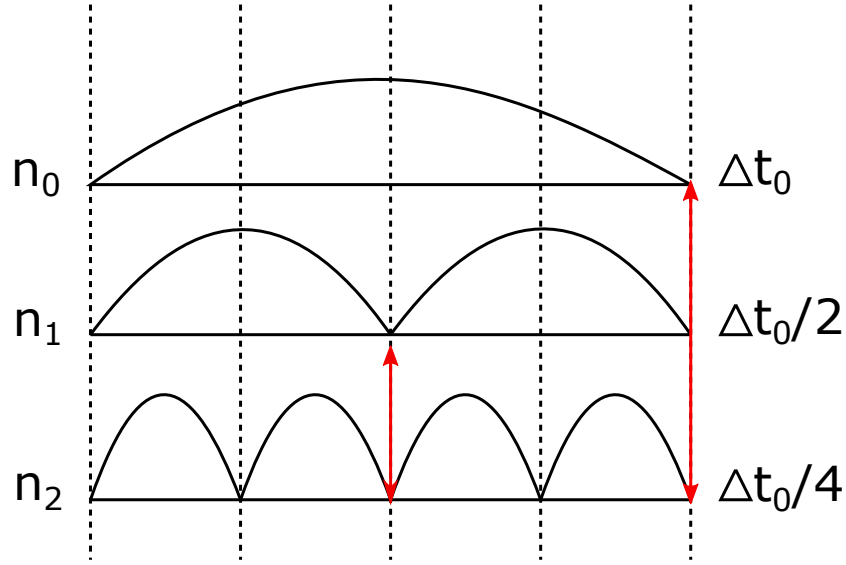


FIGURE 2.3: Illustration of a block time stepping scheme. Particles are organised on timesteps in a hierarchy, with relation to base timestep Δt_0 . Particles can move between rungs (denoted as $n_0, n_1 \dots$) at synchronisation points, which are indicated by the red arrows [Dehnen and Read \(2011\)](#).

are made (which are described in detail by [Eggleton et al., 1989](#)). These values are then presented in the SeBa look up tables, and give results like those seen in [Table 2.2](#).

In these simulations, only single stellar evolution is considered using SeBa. The potential impacts of stars forming in binaries shall be discussed in [Chapter 7](#).

2.4 Protoplanetary discs

For the work which will be discussed in [Chapter 3](#), no disc physics has been included in the simulations. Whether a disc has become enriched or not is based on its position in relation to the SN when it explodes, with the distance to the SN being between $\sim 0.1 - 0.3$ pc ([Adams et al., 2004](#)) although, as stated before, these limits can probably be relaxed ([Lichtenberg et al., 2016c](#)).

For [Chapter 4](#), disc masses are assigned to each star. Theoretical constraints from the Minimum Mass Solar Nebula (MMSN, [Weidenschilling, 1977](#); [Hayashi, 1981](#)) and observations ([Andrews et al., 2013](#); [Ansdell et al., 2016](#)) suggest that an upper limit of $M_{\text{disc}} = 0.01 M_{\star}$ for disc masses. The initial disc masses in these simulation are 10 per cent of the host star mass ($M_{\text{disc}} = 0.1 M_{\star}$) to over compensate for potential mass accretion that may occur during a disc's lifetime.

TABLE 2.2: The evolutionary tracks from SeBa for stars within the low-mass cluster with two massive stars, a cluster which is used in Chapter 3.

Stellar ID	Evolutionary step	Time (Myr)
20	main sequence to Hertzsprung gap	6.62000
20	Hertzsprung gap to horizontal branch	6.62999
20	horizontal branch to super giant	7.23004
20	super giant to neutron star	7.76999
124	main sequence to hyper giant	3.98000
124	hyper giant to black hole	4.41001

These discs are then subjected to mass loss due to external radiation from massive stars. A range of initial radii are sampled due to the large range of observed disc radii: 10, 50, 100, 200 and 1000 AU (Segura-Cox et al., 2016; Yen et al., 2017; Ansdell et al., 2018). A single value for each disc radius is adopted, focusing primarily on 100 AU discs. A range of disc radii (10–1000 AU) are also examined for one set of simulation initial conditions, to understand the impact of varying the size of protoplanetary discs. In reality, the radius of the disc will change due to internal processes such as viscous evolution, and due to internal and external photoevaporation, but these simulations are unable to account for this (and the changing disc density profile) in these N -body simulations.

2.4.1 Photoevaporation

As mentioned in Section 1.3.8, the mass loss rate of discs at a certain distance from a neighbouring massive star is determined by the strength of the star’s FUV ($h\nu < 13.6$ eV) and EUV ($h\nu > 13.6$ eV) fluxes at that distance. Mass loss due to FUV photons is caused by heating the circumstellar disc, which creates an unbound neutral layer that can drift towards the ionization front, where it meets the EUV field. FUV is independent of the distance from the massive star because the only requirement is that the FUV flux is strong enough to heat the disc above its escape velocity. With EUV, the mass loss rate depends on the EUV flux and so is directly dependent on the distance from the massive star(s) (see Fig.2.4). The same prescriptions for FUV and EUV photoevaporation as Scally and Clarke (2001) are used in this thesis.

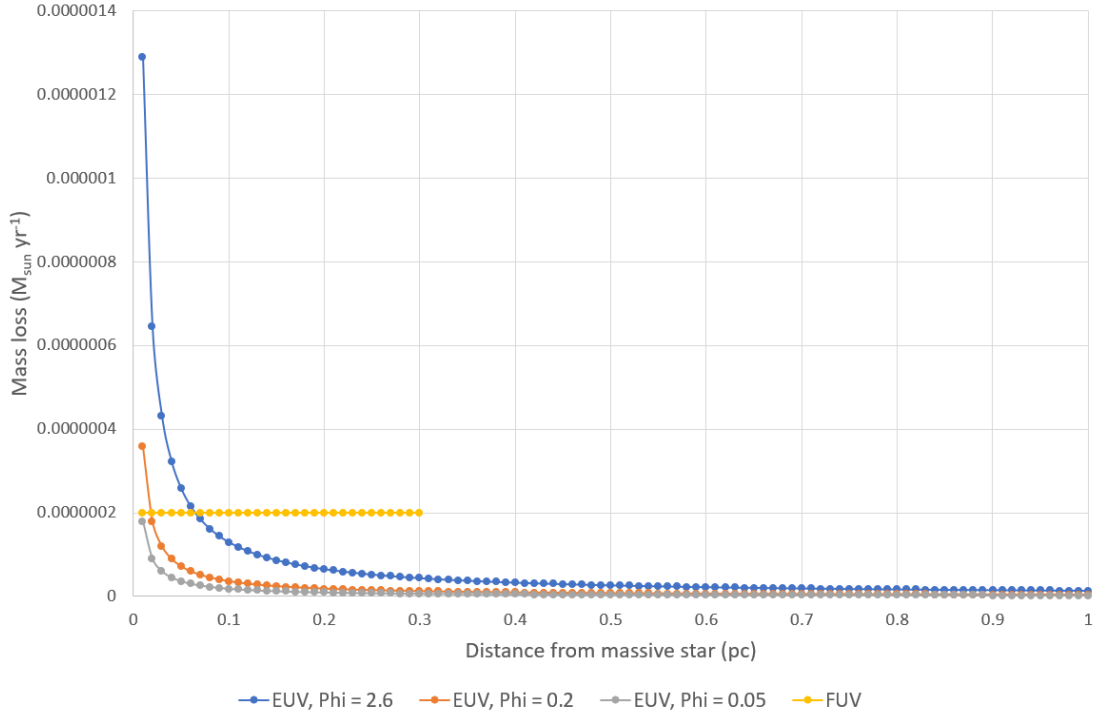


FIGURE 2.4: Using the photoevaporation prescriptions described, the amount of disc mass loss per year that a 100 AU protoplanetary disc will experience due to external EUV and FUV radiation is shown. The amount of mass loss depends on the discs proximity to the massive stars, and values of Phi taken from [Scally and Clarke \(2001\)](#).

Mass loss due to photoevaporation is dependent on the radius, density and velocity of material within the protoplanetary disc, as well as the incoming UV radiation. The density distribution is calculated by assuming that the neutral material flows supersonically, and the radius is measured to the disc surface. It is assumed in these models that the flow of material has spherical geometry, which is true at large radii. Mass loss due to external radiation can be written as

$$\dot{M}_d = m_H n_0 v_0 4\pi r_0^2, \quad (2.13)$$

where \dot{M}_d is the mass loss rate of the disc in yrs, m_H is the mass of a proton-electron pair, n_0 is the electron density at the base of the disc, v_0 is the flow velocity of the material, and r_0 is the radius of the region being photoevaporated.

In the outer EUV dominated regions, where atomic hydrogen dominates the EUV opacity, photoevaporation occurs when the flux from a massive star is equal to the recombinations in the disc

$$\frac{1}{3}\alpha n_0^2 r_d \sim \frac{\Phi_i}{4\pi d^2}, \quad (2.14)$$

where Φ_i is the ionizing (EUV) photon luminosity of the massive star (with units of 10^{49}s^{-1}), α is the recombination coefficient to all except ground state, r_d is the disc radius, and d is the distance from the massive star to the disc, making the flux

$$F \propto n_0 r_d^2 \propto d^{-2}. \quad (2.15)$$

Hence, $n_0 \propto r_0^{-1/2} d^{-1}$, and

$$\dot{M}_d \propto n_0 r_d^2 \propto r_0^{3/2} d^{-1}, \quad (2.16)$$

making mass loss due to external EUV radiation dependent on distance from the massive star, which can be seen in Fig. 2.4.

Φ can also be written as

$$\Phi = \frac{4}{3}\pi r^3 \alpha_2 n_0^2(r). \quad (2.17)$$

Rearranging the above equation for n_0 gives

$$n_0 \propto \sqrt{\frac{\Phi_i}{d^2 r_d}}, \quad (2.18)$$

which can then be substituted into Equation 2.16, giving

$$\dot{M}_d \approx \sqrt{\frac{\Phi_i}{d^2}} r_d^{3/2}, \quad (2.19)$$

In the case of FUV dominated regions (and the inner EUV-dominated regions), the material is flowing at a constant supersonic speed (v_0), and dust opacity dominates the recombination-induced atomic hydrogen opacity and sets the column density of the region between the ionization front and the protoplanetary disc to some constant ($n_0 r_d$) (Johnstone et al., 1998), giving

$$\dot{M}_d \propto r_d. \quad (2.20)$$

This means that dust controlled regions can be modelled as being insensitive to distance, although in reality there will be a weak dependence. Following the example of Scally and Clarke (2001), and based on the size of the FUV-dominated ionization bubble within the star forming region $\theta^1\text{C Ori}$ (0.3pc), any star within

0.3pc of a massive star in these simulations will experience photoevaporation due to external FUV radiation.

Using the same physical parameters that were assumed by [Störzer and Hollenbach \(1999\)](#), and [Hollenbach et al. \(2000\)](#), this gives the mass lost by a disc in an EUV dominated region as

$$\dot{M}_{\text{EUV}} \approx 8 \times 10^{-12} r_d^{3/2} \sqrt{\frac{\Phi_i}{d^2}} M_{\odot} \text{yr}^{-1}, \quad (2.21)$$

and an FUV dominated region as

$$\dot{M}_{\text{FUV}} \approx 2 \times 10^{-9} r_d M_{\odot} \text{yr}^{-1}, \quad (2.22)$$

where r_d is the radius of the disc in astronomical units, Φ_i is the ionizing EUV photon luminosity from each massive star in units of 10^{49} s^{-1} ($\Phi = \frac{4}{3} \pi r^3 \alpha_2 n_0^2(r)$), and d is the distance from the massive star in parsecs. The UV photon rate (Φ_i) for the massive stars ($> 15M_{\odot}$) is dependent on stellar mass and values from [Vacca et al. \(1996\)](#) and [Sternberg et al. \(2003\)](#) are adopted.

These photoevaporation rates were derived assuming a disc density profile $\Sigma \propto r_d^{-2}$ ([Hollenbach et al., 2000](#); [Hartmann, 2009](#)); however, my analysis does not take into account the evolution of the surface density profile if the disc radius were to change significantly. This will be discussed more in Chapter 7 regarding proposed future work.

When selecting a value for Φ_i , where Φ is the UV photon rate for the massive stars ($> 15M_{\odot}$), several different studies were compared, as can be seen in Fig.2.5 ([Vacca et al., 1996](#); [Scally and Clarke, 2001](#); [Sternberg et al., 2003](#); [Martins et al., 2005](#)). The Φ values from [Crowther \(2005\)](#) and [Crowther et al. \(2006\)](#) were used. By using these lower Φ values, it ensures that these results are conservative.

Disc masses are set at 10 per cent the mass of their host star ($M_{\text{disc}} = 0.1M_{\text{star}}$), and Equations 2.21 and 2.22 are used to subtract mass from the discs when applicable. The mass loss rates of protoplanetary discs are independent of disc masses, and only dependent on disc radius in these models.

2.5 UV radiation fields

Using the range of initial mass distribution of stars described in Section 2.2, the amount of UV radiation that every star receives from all other cluster members is

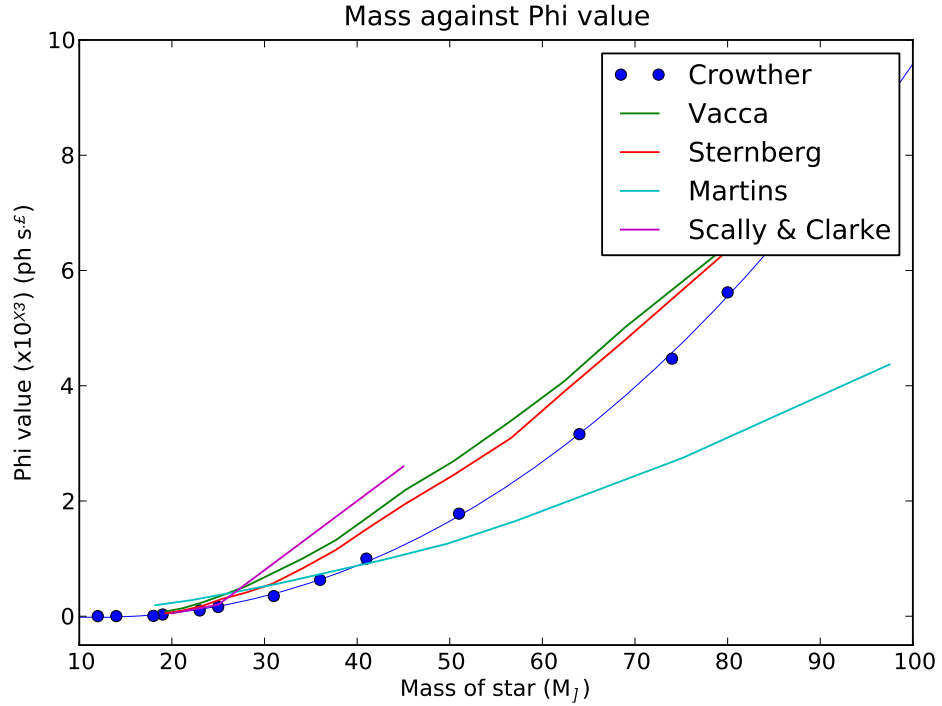


FIGURE 2.5: Φ_i values of massive stars from several different studies (Vacca et al., 1996; Scally and Clarke, 2001; Sternberg et al., 2003; Martins et al., 2005; Crowther, 2005; Crowther et al., 2006). The values used within this thesis come from Crowther (2005) and Crowther et al. (2006).

calculated. Using FUV and EUV luminosity values from Armitage (2000), the UV luminosity for every mass star was found (see Fig. 2.6) by calculating the flux:

$$F_{UV} = \frac{L_{UV}}{4\pi d^2}, \quad (2.23)$$

where F_{UV} is the FUV or EUV flux that the 'disc' receives, L_{UV} is the FUV or EUV luminosity of each star, and d is the distance from each star to the 'disc'. The amount of flux that discs receive from every star within the simulation was calculated and recorded for every timestep. The FUV fluxes are expressed in units of G_0 , where $G_0 = 1$ corresponds to $F_{FUV} = 1.6 \times 10^{-3} \text{ erg s}^{-1} \text{ cm}^{-2}$. The FUV radiation within a cluster is thousands of times that of the ISM, therefore FUV fluxes in clusters are expressed in terms of G_0 , which is approximately the value for the ISM (Habing, 1968). No protoplanetary discs are included within these simulations, however how this work should be expanded is discussed in

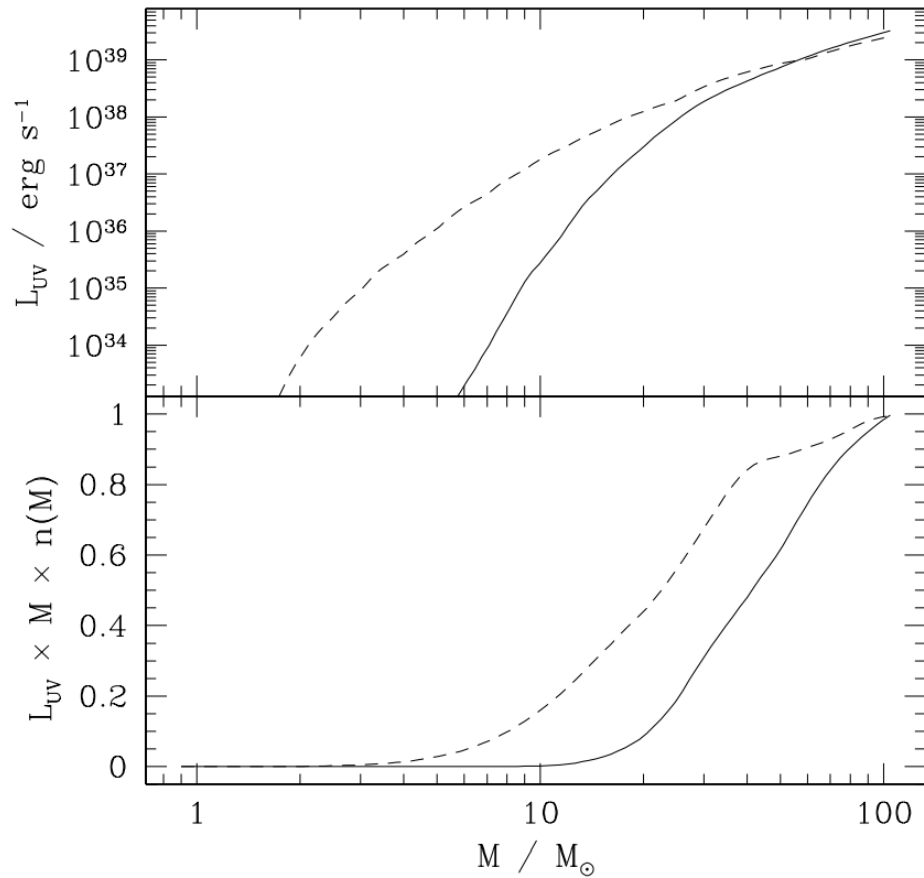


FIGURE 2.6: Figure from [Armitage \(2000\)](#) showing how the luminosity of stars varies with mass. The upper panel shows the luminosity in EUV (solid line) and FUV (dashed line) for stars of mass M_* (where M is in units of M_\odot). The lower panels shows, for a [Salpeter \(1955\)](#) IMF, the relative contributions to the total EUV and FUV flux from stars of different masses. The units in the lower panel are arbitrary.

Chapter 7.

The methods outlined in this Chapter have been taken and applied in Chapters 3, 4, and 5 to various questions about the direct enrichment and photoevaporation of protoplanetary discs that still remain.

Chapter 3

Supernova enrichment of planetary systems in low-mass clusters

In this Chapter, the rate at which protoplanetary discs are enriched by the death of massive stars within low-mass star forming regions is examined. The presence and abundance of short lived radioisotopes (SLRs) in chondritic meteorites implies that the Sun formed in the vicinity of one or more massive stars that explode as supernovae (SNe). Massive stars are more likely to form in massive star clusters ($>1000 M_{\odot}$) than lower mass clusters. However, photoevaporation and dynamical interactions with passing stars can inhibit planet formation in clusters with radii of ~ 1 pc. I investigate whether low-mass ($50 - 200 M_{\odot}$) star clusters containing one or two massive stars are a more likely avenue for early Solar System enrichment.

A similar fraction of stars experience SN enrichment in low mass clusters as in high mass clusters, despite their lower densities. Because of the high number of low mass star-forming regions containing one or two massive stars, the absolute number of enriched stars is non-negligible in comparison to the absolute number of enriched stars produce in high mass star-forming regions. The results show that direct enrichment of protoplanetary discs from SNe occurs as frequently in low mass clusters containing one or two massive stars ($>20 M_{\odot}$) as in more populous star clusters ($1000 M_{\odot}$).

The work in this Chapter has been published in the Monthly Notices of the Royal Astronomical Society (Nicholson and Parker, 2017).

3.1 Introduction

As discussed in Chapter 1, understanding the conditions of the birth environment where the Solar System formed is one of the major questions in planet and star formation, as well as astrobiology (e.g. Adams, 2010; Pfalzner et al., 2015; Portegies Zwart, 2009). As stars do not form in isolation, but rather with many other stars in regions that often contain very massive stars (Lada and Lada, 2003; Bressert et al., 2010), the birth environment of stars should be considered when discussing planet formation. In addition to their destructive properties, massive stars explode as SNe and can chemically enrich their immediate surroundings in SLRs.

In comparison to the ISM, the Solar System appears to contain an over abundance of these SLRs (Cameron and Truran, 1977). These radioactive isotopes appear to be one of the dominant sources of heat during planetesimal formation (Urey, 1955; MacPherson et al., 1995) and could be important for long-term physical processes within forming planetary systems (Adams, 2010; Lichtenberg et al., 2016a). Because of the short half-lives of SLRs and their homogeneous distribution throughout the Solar System (Villeneuve et al., 2009), these isotopes must have been incorporated within the protoplanetary disc either shortly before or during the very early evolution of the Solar System.

SLRs can form through several mechanisms, though not all are viable methods for enriching the protosolar nebula (Lee et al., 1998; Shu et al., 2001; Wasserburg et al., 1994; Busso et al., 1999, 2003; Trigo-Rodríguez et al., 2009; Gounelle et al., 2009; Gritschneider et al., 2012; Gounelle and Meynet, 2012; Gounelle, 2015). I focused on the potential enrichment mechanism that is direct enrichment of the protoplanetary disc from a nearby SN explosion, which was discussed in detail in Chapter 1.

Direct enrichment requires that the Sun formed near to high mass stars ($>20 M_{\odot}$) and due to the form of the IMF, it is common that several thousand low-mass stars form along with every massive star. Stars in these dense clusters are likely to undergo significant dynamical interactions. N -body simulations which follow direct enrichment in massive clusters have shown that the number of G-dwarf stars that are enriched, but unperturbed by dynamical interactions is $\sim 0.5 - 1$ per cent (Parker et al., 2014a), making high mass clusters inefficient at enriching protoplanetary discs.

Low mass clusters containing massive stars may be more efficient. Embedded clusters typically have radii of the order of 1 pc (Lada and Lada, 2003, though see

the more recent discussion in [Pfalzner et al., 2016](#)), meaning that clusters with low masses are likely to have a lower stellar density than their higher-mass counterparts. These lower stellar densities may imply that the stars that are enriched by SNe suffer fewer dynamical interactions, and hence could be more viable environments for the formation and evolution of a quiescent Solar System.

In this Chapter I present work on whether low-mass star clusters containing massive stars can facilitate the enrichment of planetary systems without these systems suffering perturbing dynamical interactions with other stars.

3.2 Methods

In Chapter 2 I described the method used to select low-mass clusters containing massive stars from the cluster mass function, before describing the subsequent N -body and stellar evolution of these clusters. I shall briefly summarise the method again.

3.2.1 Creating low-mass clusters

In order to determine the fraction of low-mass clusters that contain massive stars, I randomly sampled cluster masses from the analytic fit (see Equation 2.1) to the observed star cluster mass function. These clusters were then populated with stars drawn randomly from the IMF parameterised in [Maschberger \(2013\)](#). A "soft-sampling" technique was adopted, allowing for low mass clusters to contain massive stars; these are the clusters of interest.

In Fig. 3.1 I show the CMFs for clusters that contain one star with mass $>20 M_{\odot}$ (blue line) and two stars with masses both $>20 M_{\odot}$ (green line). From Fig. 3.1 it is immediately apparent that there is an equal probability of a cluster with a stellar mass of $1000 M_{\odot}$ occurring as a low-mass ($50\text{--}200 M_{\odot}$) cluster containing two massive stars; low mass clusters containing one massive star are 100 times more abundant than the higher mass clusters.

Given that random sampling of the CMF and IMF can produce low-mass clusters containing massive stars in equal or greater proportion to more massive clusters, I explored the dynamical evolution and enrichment probabilities in these low-mass clusters. To achieve this, the 'median' of these low-mass clusters ($50 < M_{\text{cl}}/M_{\odot} < 200$), that contain the median number of stars and one or two massive ($>20 M_{\odot}$) stars that will explode as SNe within 10 Myr was selected. The

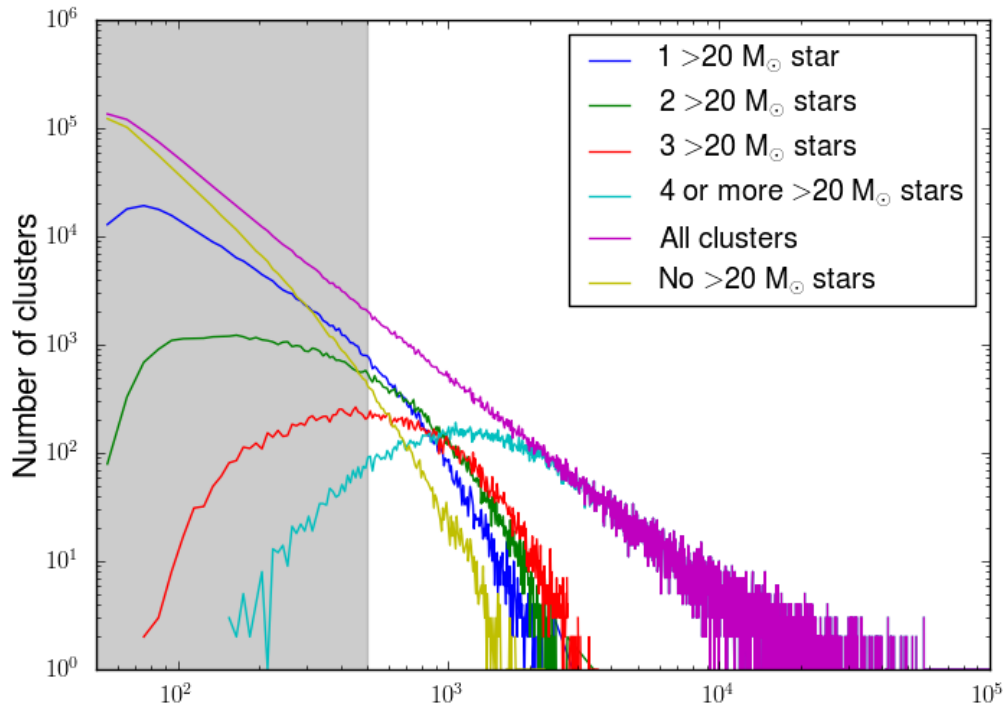


FIGURE 3.1: Star cluster mass functions for clusters containing different numbers of massive ($> 20 M_{\odot}$) stars. The grey shaded region indicates on Fig 1.6 the mass range that has yet to be investigated for potentially Solar System forming environments.

median cluster containing two ($>20 M_{\odot}$) stars contains 145 stars in total and the median cluster containing one ($>20 M_{\odot}$) star contains 113 stars.

3.2.2 *N*-body simulations

The median star clusters (in terms of the number of stars) that contain one/two massive stars are evolved in *N*-body simulations with different initial conditions. Substructured star forming regions were set up using fractal distributions, following the method of described in Chapter 2. Three different fractal dimensions were adopted: $D = 1.6$ (highly substructured), $D = 2.0$ (moderately substructured) $D = 3.0$ (smooth). Note that the fractal dimensions obtained from Goodwin and Whitworth (2004) give approximate fractal values with some statistical

TABLE 3.1: The initial conditions for all simulations where α_{vir} is the virial ratio, D is the fractal dimension and r_F is the initial radius of the cluster. All configurations of these initial conditions were run. The clusters with 113 and 145 particles contained one and two massive ($>20 M_{\odot}$) stars respectively.

N_{stars}	$N_{\text{stars}} (>20 M_{\odot})$	α_{vir}	D	r_F
145	2	0.3; 0.5; 0.7	1.6; 2.0; 3.0	0.2; 1.0; 2.0 pc
113	1	0.3; 0.5; 0.7	1.6; 2.0; 3.0	0.2; 1.0; 2.0 pc

variation around these values. Three different radii are selected for the fractals: $r_F = 0.2 \text{ pc}$, $r_F = 1.0 \text{ pc}$ and $r_F = 2.0 \text{ pc}$.

Finally, the velocities of the stars in the fractal are scaled to the desired virial ratio α_{vir} , where $\alpha_{\text{vir}} = T/|\Omega|$; T and Ω are the total kinetic energy and total potential energy of the stars, respectively. Three different virial ratios are adopted in the simulations: $\alpha_{\text{vir}} = 0.3$ (subvirial, or collapsing), $\alpha_{\text{vir}} = 0.5$ (virial equilibrium) and $\alpha_{\text{vir}} = 0.7$ (supervirial, or expanding).

Each median cluster was evolved for 27 sets of simulations ($r_F = 0.2, 1.0, 2.0 \text{ pc}$; $\alpha_{\text{vir}} = 0.3, 0.5, 0.7$; $D = 1.6, 2.0, 3.0$) for 10 Myr using the *kira* integrator within the *Starlab* environment (Portegies Zwart et al., 1999, 2001). In order to determine the locations of the SNe, stellar evolution was implemented using the *SeBa* look-up tables (Portegies Zwart and Verbunt, 1996), which are also part of *Starlab*. For each realisation of the initial conditions 20 versions were run of the same simulation, identical apart from the random number seed used to set the positions and velocities, in order to gauge the inherent stochasticity in the evolution.

3.3 Results

In this section, the results from low mass clusters containing one massive star are presented. I focus on one set of initial conditions, which best reflect the observed properties of young star-forming regions, for each cluster – a subvirial ($\alpha_{\text{vir}} = 0.3$), highly substructured cluster ($D = 1.6$) with initial radius $r_F = 1.0 \text{ pc}$ – before summarising the results from the other initial conditions.

Two median clusters were analysed, one containing a single massive star and the other containing two. I concentrate on the cluster containing two massive stars due to the potential for a greater enrichment fraction; however the analysis of both clusters is the same, and the median cluster containing one massive star shall be discussed in detail in Section 3.3.4.

3.3.1 Cluster evolution and supernova enrichment

The median clusters chosen from the Monte Carlo sampling of the CMF and IMF resulted in a cluster containing 145 stars, of which two were massive stars ($42 M_{\odot}$ and $23 M_{\odot}$). Stars with these masses explode as SNe after ~ 4 and ~ 8 Myr respectively (Hurley et al., 2000) and I therefore focus on clusters that will reach a maximum density at or around these ages (to maximise the number of low-mass stars that could be enriched by the SN explosions).

Star-forming regions with medium density initial conditions (~ 100 stars pc^{-3}) and subvirial motion ($\alpha_{\text{vir}}=0.3$) will collapse to form a spherical cluster on timescales of ~ 5 Myr (Parker, 2014), and so simulations with radii $r_F = 1.0$ pc, subvirial velocities and a high degree of initial substructure ($D = 1.6$) are focused on in order to facilitate this cool-collapse (Allison et al., 2010).

An example of the morphology of a typical cluster immediately before the first SN (at 4.4 Myr) is shown in Fig. 3.2. The SN progenitors are shown by the large red triangles and have clearly migrated to the centre of the cluster.

The cumulative distributions of the distances from each low-mass star to the first SN is shown in Fig. 3.3. Each of the twenty realisations of these initial conditions is shown by a coloured line, and the "enrichment zone" is shown by the vertical dashed lines. The enrichment zone is the distance range from the SN (0.1 – 0.3 pc) thought to be most conducive to Solar System enrichment levels. Within 0.1 pc the effects of FUV and EUV radiation are likely to destroy the protoplanetary disc, whereas beyond 0.3 pc the amount of enrichment is too low. Even at 0.3 pc, the effects from external photoevaporation are great. However, this 0.1 - 0.3 pc range may be an underestimate and recent work has shown that sufficient enrichment can take place much further away from the SN (Lichtenberg et al., 2016c).

The average number of stars that lie within the enrichment zone during the first SN is 9 out of 145 stars. I now consider the enrichment probability from the second, later SN which explodes at 7.8 Myr. The spatial distribution of the cluster at this time is shown in Fig. 3.4. It is already apparent from this figure that the cluster has expanded somewhat in the ~ 3.4 Myr between SN explosions. Again, the SN progenitor is indicated by a red triangle in Fig. 3.4.

The cumulative distribution of distances from the second SN is shown in Fig. 3.5. This second SN event at 7.8 Myr polluted an average of 4 stars and from inspection of Figs. 3.3 and 3.5 it can be clearly seen that the fraction of polluted

stars from the first SN is more than double the fraction polluted by the second event. The number of stars polluted by both SNe is found to be negligible.

3.3.2 Dynamical histories of polluted stars

The fraction of stars that are enriched by SNe pollution is insufficient to determine whether these systems could nurture a young Solar System. Dynamical encounters in natal star-forming environments occur frequently, and can disrupt protoplanetary discs and/or dramatically alter the architecture of fledgling planetary systems.

For this reason, the dynamical history of each star that is enriched by the supernovae is tracked and Fig. 3.6 plots the nearest neighbour distance from each enriched star at all times in the simulation. Each coloured line represents every enriched star in one of the default $N = 145$, $\alpha_{\text{vir}} = 0.3$, $D = 1.6$, $r_F = 1.0$ pc simulations. The vertical dashed lines indicate the time of the two SNe.

Two stars (the cyan and black lines in Fig. 3.6) undergo interactions that could potentially disrupt the planetary system, where the perturbing star encroaches within 1000 AU. However, in contrast to the simulations of very dense clusters in Parker et al. (2014a) where 80 per cent of enriched stars are affected by previous/subsequent interactions, only a small fraction of enriched stars (15 per cent) in these lower density initial conditions suffer perturbing interactions.

3.3.3 Other initial conditions

In my default model ($\alpha_{\text{vir}} = 0.3$, $r_F = 1.0$ pc, $D = 1.6$) the median total number of stars that are enriched per event is ~ 13 (~ 9 per cent) although this percentage is considering stars across the entire mass range and stars which may have experienced stellar interactions and disc perturbations. When focusing on Solar analogous, the fraction of enriched G-dwarf stars that were unperturbed for the duration of the 10 Myr simulation (~ 0.5 per cent) is comparable to the maximum number of *G-dwarfs* (stars with similar mass to the Sun, $0.8 - 1.2 M_{\odot}$) that were enriched in the more populous clusters studied in Parker et al. (2014a) (~ 1 per cent).

In an attempt to increase the fraction of enriched stars, a host of initial conditions are explored for the star clusters. However, no initial conditions result in a significantly higher ($>$ twice) fraction of enriched stars. The principal reason for this is the effects of two-body relaxation. In order to enrich more than half of the

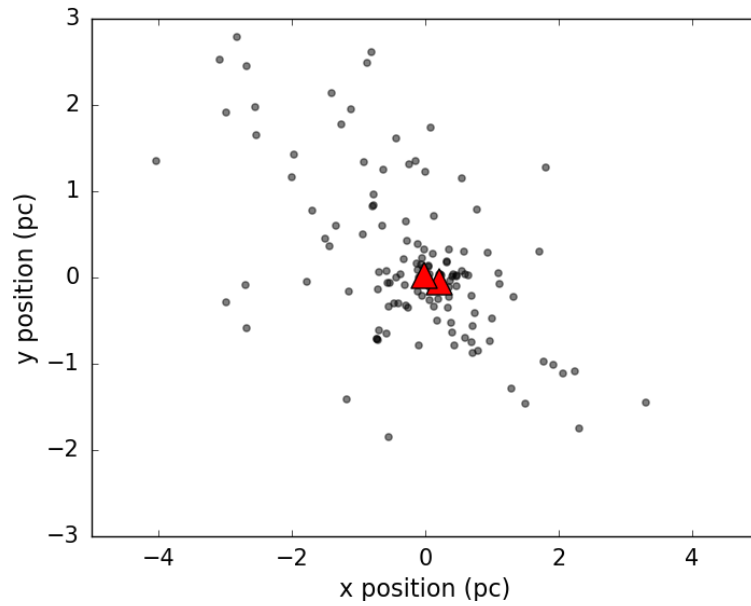


FIGURE 3.2: Snapshot of the cluster before the first SN event. The massive stars are shown by red triangles, other stars are grey points.

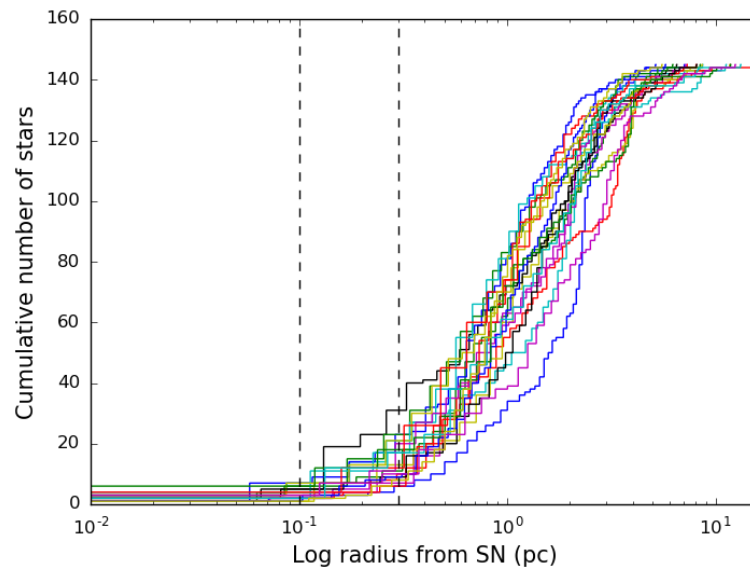


FIGURE 3.3: Cumulative distribution of stars from the first SN event. Coloured lines indicate 20 runs of the simulation. Dashed grey lines indicate 0.1 – 0.3 pc range where stars receive sufficient enrichment from the SN.

stars in a low-mass cluster, the required stellar density *at the time of the SN(e) explosion(s)* corresponds to a radius of only $\sim 0.4\text{pc}$, which is impossible to achieve after 5 Myr of evolution.

Two-body relaxation causes even moderately dense systems (100 stars pc^{-3}), such as the default model, to expand significantly in the first 10 Myr, as shown in Fig. 3.7. Here, the coloured lines represent the median local stellar density with time in each of the 20 realisations of these initial conditions. The solid black line is the mean central density across all 20 simulations (where the central density is defined as the density within the half-mass radius). Clearly, the clusters have expanded significantly before the SN explosions (shown by the vertical dashed lines).

Irrespective of the initial conditions, the clusters never attain significant enrichment because the initial density is either too high (and two-body relaxation causes significant expansion), or the initial density is so low that despite the initial subvirial motion of the stars, significant clustering of the stars never occurs. The fraction of enriched G-dwarf stars that remain unperturbed throughout the duration of the simulation, ranges between $\sim 0.07\text{--}0.55$ per cent across all applied initial conditions.

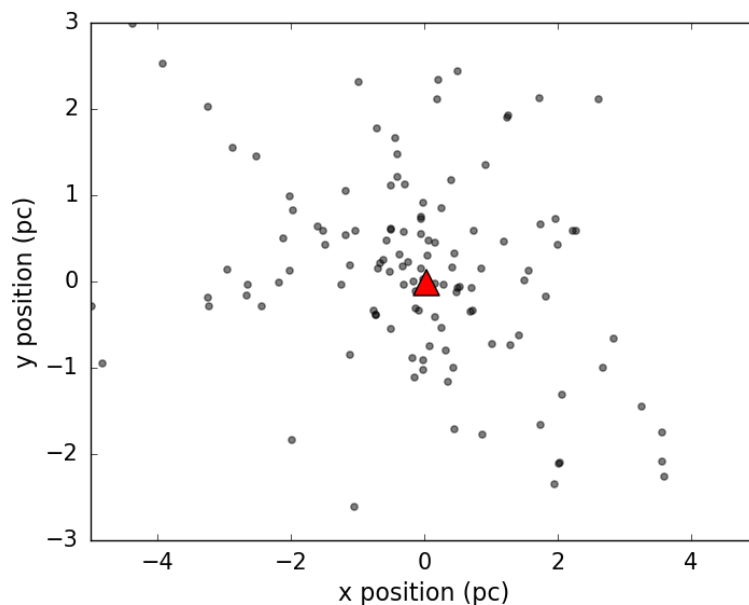


FIGURE 3.4: Snapshot of the cluster before the second SN event. The massive star is shown by a red triangle, other stars are grey points.

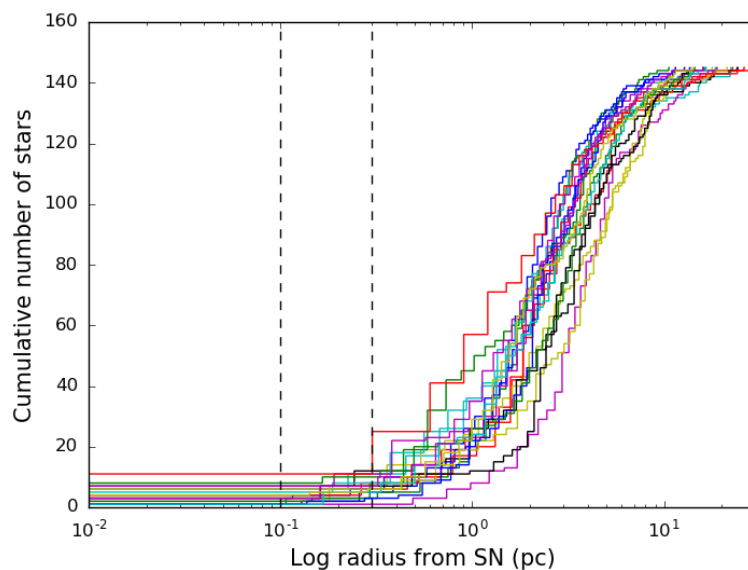


FIGURE 3.5: Cumulative distribution of stars from the second SN event. Coloured lines indicate 20 runs of the simulation. Dashed grey lines indicate 0.1 - 0.3 pc range where stars receive sufficient enrichment from the SN.

3.3.4 Low mass clusters containing one massive star

The second median cluster chosen from the Monte Carlo sampling contained 113 stars, of which one was massive ($24 M_{\odot}$), resulting in a SN explosion at ~ 7 Myr. The same set of initial conditions are focused on ($\alpha_{\text{vir}} = 0.3$, $r_F = 1.0$ pc, $D = 1.6$) before summarising the others.

An average of six stars were enriched by the SN (~ 5 per cent), a similar number to the median cluster containing two massive stars. The dynamical interaction and cluster density histories were also similar, resulting in ~ 0.1 – 0.4 per cent of G-dwarfs being enriched and unperturbed. With almost identical enrichment fractions and dynamical histories, the difference between clusters containing one or two massive stars is small.

Fig. 3.1 indicates that there are \sim ten times as many clusters containing one massive star than clusters containing two. Intermediate mass star clusters (~ 1000 stars), such as the simulated clusters in [Parker et al. \(2014a\)](#), are rarer, with nearly 100 low mass clusters containing one massive star for every $\sim 1000 M_{\odot}$ cluster. When integrating the numbers of enriched stars produced by low mass star clusters containing one or two massive star(s) to the massive clusters that [Parker et al.](#)

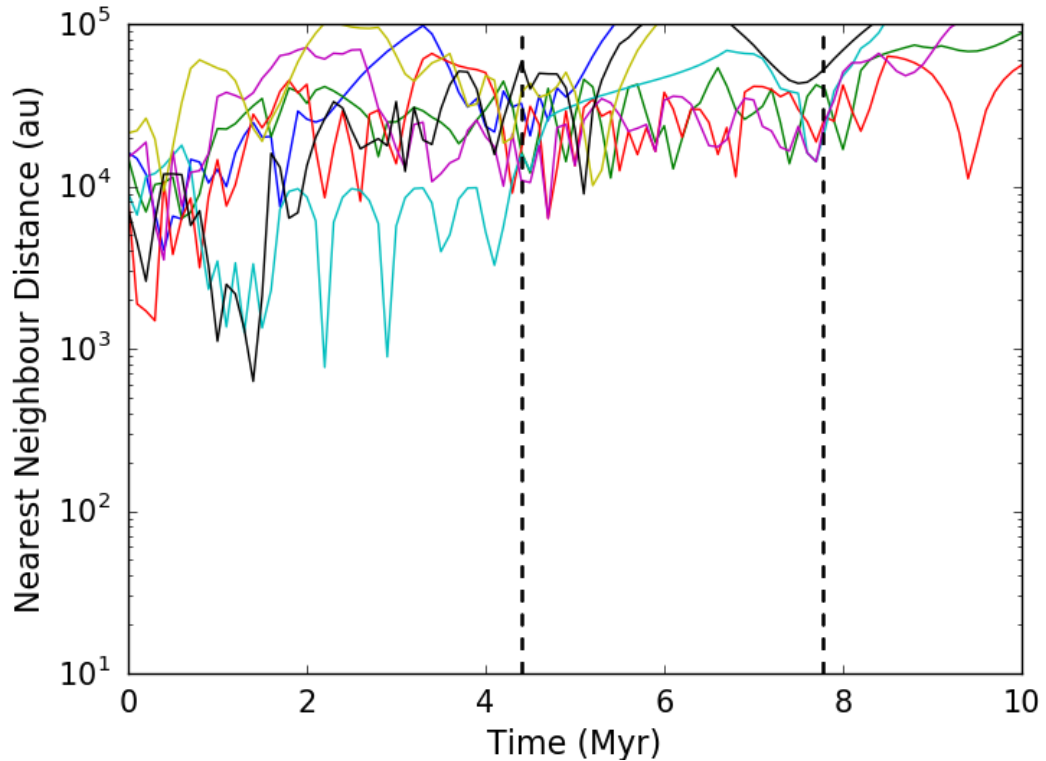


FIGURE 3.6: The closest interaction history for every enriched star with time for one of the 20 simulation runs. The black dashed lines show the times of the SN events.

(2014a) simulated, the number of enriched stars is of the same order.

3.4 Discussion

The results of the parameter study suggest that low-mass clusters ($M_{\text{clus}} < 200 M_{\odot}$) containing one or two massive stars occur much more frequently than intermediate mass clusters ($M_{\text{clus}} \sim 1000 M_{\odot}$), which have previously been thought to be more conducive to isotopic enrichment (Adams, 2010; Parker et al., 2014a). When the clusters are evolved as N -body simulations, the fraction of enriched Sun-like stars ($0.8 - 1.2 M_{\odot}$) is found to be lower (~ 0.1 – 0.6 per cent) in contrast to the simulations in Parker et al. (2014a) that contain ~ 2100 stars and enrich around 1 per cent of Sun-like stars. However, because the ratio of low mass clusters containing one or two massive stars to intermediate mass clusters is $\sim 1:100$, the raw

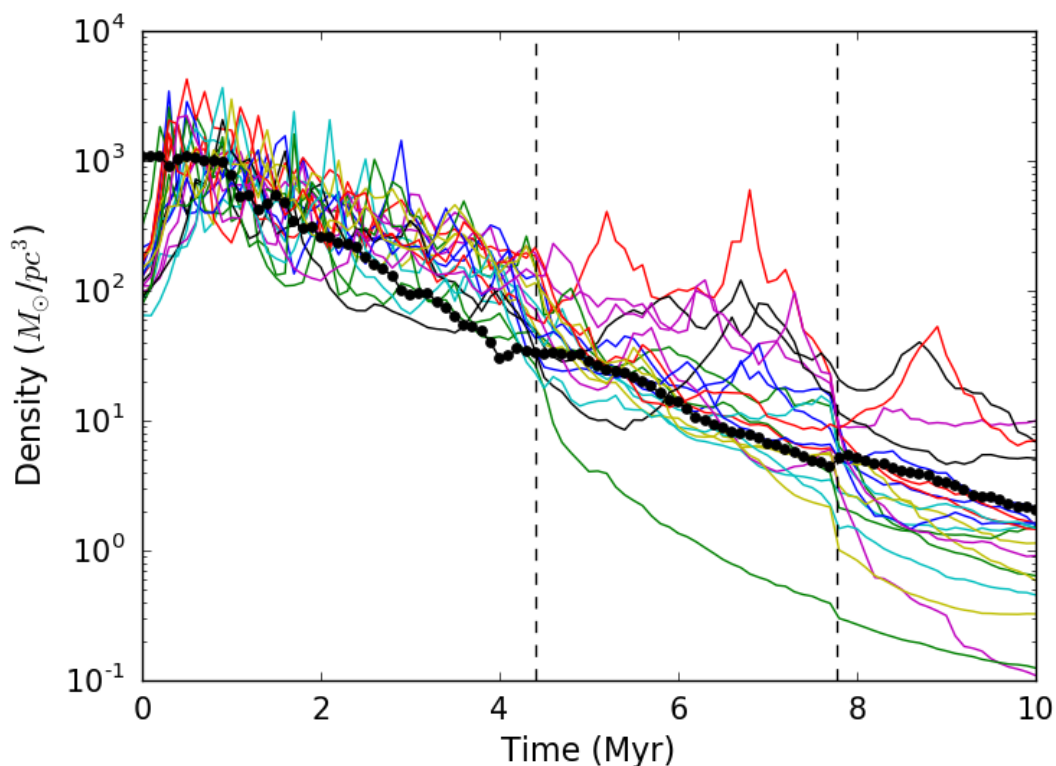


FIGURE 3.7: Evolution of the median local volume density in each simulation as a function of time. Coloured lines indicate each of the 20 simulations and the black line indicates the average central density. Vertical dashed grey lines indicate times of the supernovae.

numbers of enriched stars are comparable.

I calculate the fraction of enriched and unperturbed G-dwarfs produced by low mass clusters so that the results can be compared to the fraction produced in high mass clusters [Parker et al. \(2014a\)](#). By running the simulation 20 times with different starting positions and velocities, the rate at which G-dwarf stars are enriched in this specific cluster has been thoroughly tested. However, the number of G-dwarf stars present in these simulated low mass clusters is subject to low number statistics, and therefore the fraction of enriched G-dwarf stars will most likely depend on the random sampling of the IMF. To test this, several low mass clusters with different IMFs should be simulated so that the fraction of enriched G-dwarf stars for a broad range of low mass star-forming regions can be calculated and compared to the one found here.

The choice of default initial conditions for the N -body simulations ($r_F = 1.0$ pc,

$D = 1.6$, $\alpha_{\text{vir}} = 0.3$) results in an initial density of $100 \text{ stars pc}^{-3}$. With these densities, a cluster is expected to form on timescales similar to the first SN in the median two massive star cluster (4 – 5 Myr, Parker, 2014; Parker et al., 2014b) and hence expect enrichment for a high fraction of stars. However, two-body relaxation completely dominates the evolution of these low-mass star-forming regions and the median stellar density decreases so that the fraction of enriched stars is similar to that for the higher-mass clusters. Therefore, the fraction of stars enriched in low-mass clusters is not greater than in high mass clusters.

However, due to the high number of low mass clusters containing one or two massive stars, they are as viable environments for the initial conditions for Solar System formation as high-mass clusters. I find that ~ 10 per cent of low-mass star-forming regions contain at least one massive star ($>15 M_{\odot}$) when using the "soft-sampling" technique described in Chapter 2, and 1 per cent of low-mass regions contain two massive stars. Furthermore, when taking into account the decreasing probability of forming a high-mass star-forming region (Eqn. 2.1), the number of low-mass ($M_{\text{cl}} = 100 \pm 1 M_{\odot}$) regions containing at least one massive star is ~ 3100 , which is actually greater than the total number of high-mass ($M_{\text{cl}} = 1000 \pm 10 M_{\odot}$) star-forming regions (1200). Of these 1200 high-mass regions, ~ 1000 contain at least one massive ($>15 M_{\odot}$) star.

If these numbers are translated into the total number of stars that may be affected by photoevaporation, the average number of stars in the $M_{\text{cl}} = 100 \pm 1 M_{\odot}$ star-forming regions containing at least one massive star is ~ 110 , so in the 3100 low-mass regions that contain at least one massive star there are $\sim 341\,000$ stars in total. The average number of stars in the high mass star-forming regions ($M_{\text{cl}} = 1000 \pm 10 M_{\odot}$) is ~ 1710 , and so the 1000 regions that contain at least one massive star host a total of $\sim 1\,700\,000$ stars that could be affected by photoevaporation. In short, the fraction of stars originating in low-mass star-forming regions containing at least one massive star is ~ 20 per cent of the total number of stars originating from high-mass regions containing at least one massive star. If it is stipulated that the high-mass regions must contain three or more massive stars, only ~ 580 regions out of 1200 fulfill this criteria and host a total of $986\,000$ stars. The fraction of stars originating in low-mass star-forming regions containing at least one massive star is ~ 35 per cent of the total number of stars originating from high-mass regions containing at least three massive stars.

The total number of stars that each star-forming environment produces will greatly depend on the mass ranges considered. Commonly the term $1000 M_{\odot}$ cluster refers to a large mass range ($\sim 500\text{-}2000 M_{\odot}$) rather than the small range

considered here. The numbers here are highly changeable depending on the considered mass range (bin size). The population of stars originating in low-mass clusters is likely to be smaller still than the population produced in high-mass star-forming regions when considering a broader range at higher masses. However, this rough calculation highlights the non-negligible contribution of low-mass star forming regions containing massive stars to the total population of stars, and that there is a large enough number to make these star-forming regions worthy of investigation.

This also makes no assumption about the disruption and dissolution of these star-forming regions, and how many stars from each type of region eventually enter the Galactic field. The Galactic potential will influence the destruction of low-mass star-forming regions much more than high-mass regions (Binney and Tremaine, 2008), which take longer to dissolve into the Galactic field (and some remain as long-lived open clusters). Dynamical interactions between passing stars that could disrupt or destroy the natal Solar System also occur less frequently in lower-mass clusters, and the effects of photoevaporation and truncation from other massive stars are also reduced, potentially making low mass clusters a more viable birth environment for the Solar System. My results are in broad agreement with the conclusions in Portegies Zwart (2009), who suggest that the Sun's birth cluster had a likely mass of between 500 – 3000 M_{\odot} . This suggests that this constraint can be relaxed even further, and that the Sun could have originated in a cluster with mass between 100 – 3000 M_{\odot} . Therefore, the majority of planet-hosting field stars may come from lower-mass regions.

I have shown that the Sun is equally as likely to obtain the required isotopic enrichment levels in a low mass cluster (50 – 200 M_{\odot}) than in (less common) high mass clusters. Present and future facilities, such as the Gaia mission, may eventually be able to constrain the birth environment of the Sun by tracing it and other stars with similar chemical properties back to their formation site (Portegies Zwart, 2009; Martínez-Barbosa et al., 2016). For the moment, observational examples of low-mass clusters (50 -200 M_{\odot}) need to be observed, such as γ Velorum, which could be equally plausible birth environments for the Solar System compared to higher-mass star clusters.

3.5 Conclusions

I analyse Monte Carlo and N-body simulations of star cluster formation and evolution to determine whether enrichment of protoplanetary discs with short-lived radioisotopes can occur from core-collapse supernovae in low-mass star clusters. My conclusions are the following:

(i) Populating star clusters drawn from the observed cluster mass function with stars drawn randomly from the stellar initial mass function leads to a significant fraction of low-mass ($<200 M_{\odot}$) clusters that contain one or two massive stars. These low-mass clusters with massive stars occur far more often than $1000 M_{\odot}$ clusters, which have previously been thought to be the most likely environments for enrichment from supernovae to occur.

(ii) A typical low-mass cluster is evolved using N -body models with stellar evolution for a wide range of initial conditions (initial radius, virial ratio, and degree of substructure) and it is found that the typical fraction of unperturbed enriched G-dwarf stars is of order ~ 0.1 – 0.6 per cent, similar to the fraction of unperturbed enriched G-dwarfs in high-mass clusters.

(iii) The principal reason for the low fraction of enriched stars in both low and high-mass clusters is two-body relaxation. Even if the SN enrichment occurs at early times (~ 4 Myr), the cluster has already expanded, with the stellar density decreased by a factor of ten. Stellar densities that do not result in significant expansion from two-body relaxation are inherently so diffuse that little or no enrichment can occur.

(iv) As a percentage, the fraction of enriched stars in low-mass clusters is similar to the fraction of enriched stars in more populous clusters. However, the higher number of low-mass clusters from the cluster mass function means that the raw number of enriched stars that enter the Galactic field from lower-mass clusters is similar to that from intermediate mass clusters.

Based on these conclusions, the constraints placed on the direct enrichment scenario are reduced and I find that it is as efficient to enrich protoplanetary discs in low mass clusters ($M_{\text{clus}} \sim 50 - 200 M_{\odot}$) as in populous clusters ($M_{\text{clus}} \sim 1000 M_{\odot}$). It is likely that the efficiency of enriching protoplanetary discs and creating Solar System analogues will decrease in more massive clusters where disc truncation or destruction from EUV and FUV radiation from massive stars will dominate.

Chapter 4

Rapid destruction of protoplanetary discs due to external photoevaporation

In this Chapter I analyse N -body simulations of star-forming regions to investigate the effects of external FUV and EUV photoevaporation from massive stars on protoplanetary discs. By varying the initial conditions of simulated star-forming regions, such as the spatial distribution, net bulk motion (virial ratio), and density, I investigate which parameters most affect the rate at which discs are dispersed due to external photoevaporation. Disc dispersal is found to be faster in highly substructured star-forming regions than in smooth and centrally concentrated regions. Sub-virial star-forming regions undergoing collapse also show higher rates of disc dispersal than regions that are in virial equilibrium or are expanding.

In moderately dense ($\sim 100 M_{\odot} \text{pc}^{-3}$) regions, half of all protoplanetary discs with radii ≥ 100 AU are photoevaporated within 1 Myr, three times faster than is currently suggested by observational studies (Haisch et al., 2001; Richert et al., 2018). Discs in lower-density star-forming regions ($\sim 10 M_{\odot} \text{pc}^{-3}$) survive for longer, but half are still dispersed on short timescales (~ 2 Myr). This demonstrates that the initial conditions of the star forming regions will greatly impact the evolution and lifetime of protoplanetary discs. These results also imply that either gas giant planet formation is extremely rapid and occurs before the gas component of discs is evaporated, or gas giants only form in low-density star-forming regions where no massive stars are present to photoevaporate gas from protoplanetary discs.

The work in this Chapter has been accepted for publication in the Monthly Notices of the Royal Astronomical Society (Nicholson et al., 2019).

4.1 Introduction

As discussed in Chapter 1, the evolution and dispersal of protoplanetary discs controls the planet formation process, and observations suggest that disc lifetimes are between $\approx 3 - 5$ Myr (e.g. [Zuckerman et al., 1995](#); [Haisch et al., 2001](#); [Pascucci et al., 2006](#); [Richert et al., 2018](#)). Internal processes remove mass from the protoplanetary disc and, after several Myr, disc accretion slows significantly to the point where these processes begin removing more mass than can be replaced, leading to very rapid disc dispersal ([Clarke et al., 2001](#); [Owen et al., 2011](#)).

Proplyd host stars do not form in isolation, but rather in clusters and associations with stellar densities that exceed that of the Galactic field by a few orders of magnitude ([Lada and Lada, 2003](#); [Bressert et al., 2010](#)). Tens to thousands of stars can form in these regions that are a fraction of a parsec in size ([Clarke et al., 2000](#)). External processes, such as close stellar interactions, can also cause proplyds to be truncated or destroyed, as well as disrupting the orbits of fledgling planets ([Armitage, 2000](#); [Bonnell et al., 2001](#); [Scally and Clarke, 2001](#); [Adams et al., 2006](#); [Olczak et al., 2008](#); [Parker and Quanz, 2012](#); [Rosotti et al., 2014](#); [Vincke et al., 2015](#); [Portegies Zwart, 2016](#); [Winter et al., 2018b](#)). The density of the star forming region will affect the rate of stellar interactions, with stars in low-density environments experiencing fewer dynamical interactions than those in higher density environments ([Wright et al., 2014](#); [Bressert et al., 2010](#)). Furthermore, star-forming regions can contain massive stars ($>15 M_{\odot}$), whose intense radiation fields are significantly higher than those in the interstellar medium ([Armitage, 2000](#); [Adams et al., 2004](#); [Fatuzzo and Adams, 2008](#)). This high-energy radiation heats the gaseous material of the upper layers of the disc until the thermal energy of the heated layer exceeds the gravitational potential of the disc, causing it to escape as a photoevaporative wind ([Hollenbach et al., 1994](#); [Johnstone et al., 1998](#)). This mass loss will affect the evolution of protoplanetary discs, and reduce the reservoir of material available to form gas giant planets ([Haworth et al., 2018b](#)). How much the initial density and substructure of a star-forming region affects the rate of protoplanetary disc dispersal due to external photoevaporation has yet to be studied.

Previous studies into the effects of external photoevaporation on protoplanetary discs in star-forming regions have tended to calculate the background UV radiation without directly calculating the disc mass-loss ([Armitage, 2000](#); [Adams et al., 2004](#)). [Scally and Clarke \(2001\)](#) did calculate mass-loss rates in simulations specifically tailored to match the ONC, but assumed rather low stellar densities

($\sim 40 M_{\odot} \text{pc}^{-3}$), whereas [Parker \(2014\)](#) suggests that the initial density of the ONC may have been much higher ($> 100 M_{\odot} \text{pc}^{-3}$).

These previous studies of external photoevaporation used spherically smooth spatial distributions with primordial mass segregation to model the environment of the ONC as observed today. However, observations of star forming regions show that stars form in highly substructured filamentary environments, where the stars are moving with subvirial velocities. I focus on initial conditions that more closely reflect observations of young star forming regions ([Cartwright and Whitworth, 2004](#)), and determine how much external photoevaporation affects the evolution of protoplanetary discs. Therefore, the massive stars are not centrally concentrated, but randomly distributed in the simulated star-forming regions. I run suites of simulations that cover a range of initial conditions, with varying initial density, spatial distribution and net bulk motion (virial ratio). I then calculate and compare the mass-loss rates due to external photoevaporation for each set of initial conditions.

4.2 Method

Similar to the method in Chapter 2, I shall briefly describe the method to select low-mass star-forming regions containing massive stars, before describing the subsequent N -body and stellar evolution of these regions.

Given their significant contribution to the integrated stellar mass function, as discussed in Chapter 1, low-mass star-forming regions ($100 M_{\odot}$) that contain either one or two massive stars are investigated – these represent an unusual sampling of the IMF but allow the effects of photoevaporation in less populous star-forming regions to be investigated. Hence there are three different star-forming region set-ups; a $100 M_{\odot}$ region with one massive star ($38 M_{\odot}$), a $100 M_{\odot}$ region with two massive stars (42 and $23 M_{\odot}$) and one $1000 M_{\odot}$ region with 5 massive stars ($43, 33, 26, 17$ and $17 M_{\odot}$).

These regions were selected as the median outcomes of Monte Carlo sampling of 1×10^6 star-forming regions ([Nicholson and Parker, 2017](#)), and then filled with stellar masses drawn from the IMF (see Eqns. 2.2, [Maschberger, 2013](#)). I then selected the median regions in terms of the total number of stars from within the mass ranges of $100 \pm 1 M_{\odot}$ and $1000 \pm 10 M_{\odot}$, with the stipulation that they had to contain massive stars. For the $100 M_{\odot}$ regions, the median region containing one

and two massive stars were specifically selected. For the $1000 M_{\odot}$ the average cluster that contained three or more massive stars was selected.

The simulations are created with initial substructure by following the box-fractal method in [Goodwin and Whitworth \(2004\)](#). A range of fractal dimensions for varying amounts of substructure are used: $D = 1.6$ (highly sub-structured), $D = 2.0$ (moderately sub-structured), and $D = 3.0$ (smooth). Star-forming regions with stellar densities of $100 M_{\odot} \text{pc}^{-3}$ or $10 M_{\odot} \text{pc}^{-3}$ were created for the $1000 M_{\odot}$ regions; for the $100 M_{\odot}$ regions an initial density of $100 M_{\odot} \text{pc}^{-3}$ was set. Such densities bracket the range observed in present-day star-forming regions ([Bressert et al., 2010](#)) as well as allowing for potentially higher *primordial* densities ([Parker, 2014](#)). Finally, a set of simulations with a Plummer sphere distribution ([Plummer, 1911](#)) were created to facilitate comparisons with previous studies. I use the IMF from the $1000 M_{\odot}$ simulations to create two clusters with Plummer sphere distributions that have initial densities of 10 and $100 M_{\odot} \text{pc}^{-3}$.

Each of the star-forming regions are evolved for 10 Myr using the *kira* integrator within the *Starlab* environment, as described in Chapter 2. No binary or multiple stellar systems are included in these simulations. To gauge the amount of stochasticity in the disc photoevaporation, 20 realisations of the same initial conditions are run, identical apart from the random number seed used to assign the positions and velocities.

I use the same prescriptions for FUV and EUV photoevaporation as described by Eqns. 2.22 and 2.21 in Chapter 2 ([Scally and Clarke, 2001](#)). These photoevaporation rates were derived assuming a disc density profile $\Sigma \propto r_d^{-2}$ ([Hollenbach et al., 2000](#); [Hartmann, 2009](#)).

Observations of star forming regions show that disc radii can extend to several 100s of AU (e.g. [Ansdell et al., 2018](#)). However, the typical initial radius of protoplanetary discs is still debated in the literature and observations show a huge range ([Segura-Cox et al., 2016](#); [Yen et al., 2017](#)); therefore a wide range of initial radii are sampled: 10, 50, 100, 200 and 1000 AU. A single value for each disc radius is adopted, focusing primarily on 100 AU discs, and then the analysis is repeated for the five values. In reality, the radius of the disc will change due to internal processes such as viscous evolution, and due to internal and external photoevaporation, but I am unable to account for this (and the changing disc density profile) in the *N*-body simulations. My analysis also does not take into account the evolution of the surface density profile if the disc radius were to change significantly.

The initial disc masses are also debated, with theoretical constraints from the

MMSN (Weidenschilling, 1977; Hayashi, 1981) and observations (Andrews et al., 2013; Ansdell et al., 2016) suggesting an upper limit of $M_{\text{disc}}=0.01 M_{\star}$. The initial disc masses in these simulation are set to 10 per cent of the host star mass ($M_{\text{disc}} = 0.1 M_{\star}$). Disc masses of 10 per cent are selected so that the upper range of masses is being sampling. While accretion onto the protoplanetary discs is not accounted for, the discs are large enough in mass that the accretion onto the disc can be neglected as it will be minimal in comparison. For completeness, a set of simulations where the disc masses were 1 per cent of the stellar host mass were run, which is more consistent with the MMSN estimates.

I subtract mass from the discs according to Eqns. 2.22 and 2.21. The current protoplanetry disc mass is calculated by subtracting the mass lost during the current time step. As the protoplanetary disc has a fixed radius and viscous spreading is not implemented, the disc mass can reach zero and thus be completely photoevaporated in a finite amount of time. In the case of viscous spreading, as explained in Section 1.2.7, viscous accretion causes the protoplanetary disc to indefinitely thin and spread, eventually causing the disc to become optically thin, leading to difficulties in knowing if a disc is present or not. Whilst not as realistic as including viscous spreading, the fixed radius in these simulations allows for an exact time at which the protoplanetary disc has fully dispersed to be calculated.

The rate of photoevaporation due to EUV radiation is dependent on distance from the ionising source, d , whereas the photoevaporation rate due to FUV is largely independent of distance from the source (see Section 2.4.1 Störzer and Hollenbach, 1999). Following Störzer and Hollenbach (1999) and Scally and Clarke (2001), I apply Eqn. 2.22 if the disc-hosting stars are within 0.3 pc of the ionising source, noting that this distance is calibrated to models where $\theta^1\text{C Ori}$ is the most massive star ($40 M_{\odot}$), which is commensurate with the most massive star in these simulations. However, it should be noted that this is likely an underestimate of the amount of photoevaporation due to FUV fields in star-forming regions (Facchini et al., 2016; Haworth et al., 2018b). The maximum distance from a massive star at which stars still experience FUV radiation is fixed to 0.3pc in these simulations. However, in reality this distance will change depending on the mass and luminosity of the star. As

$$F_{FUV} \propto \frac{L}{d^2}, \quad (4.1)$$

and the flux threshold (F_{FUV}) at which photoevaporation is switched on is

constant, then the maximum distance from a massive star at which photoevaporation is triggered will vary proportionally to \sqrt{L} . Therefore, massive stars with lower masses, and correspondingly lower luminosities, should have smaller FUV bubble sizes.

4.3 Results

I focus on $1000 M_{\odot}$ star-forming regions, which typically contain a few massive stars ($M_{\star} > 15M_{\odot}$) that act as photoionising sources (c.f. Scally and Clarke, 2001). The specific $1000 M_{\odot}$ cluster studied here contains 5 massive stars; 43.2, 32.7, 25.7 and two at $17 M_{\odot}$ with Φ_i values of 1.1, 0.47, 0.19 and ~ 0.013 respectively. I focus on the results for two different initial stellar densities, $\sim 10 M_{\odot} \text{pc}^{-3}$ and $\sim 100 M_{\odot} \text{pc}^{-3}$ to cover a range of observed densities in star forming regions, and, apart from the final section, the assumed initial mass for every disc is $0.1 M_{\star}$.

The results from varying different initial properties within the star forming regions are presented, focusing on the spatial distribution (fractal dimension, D) and net bulk motion (virial ratio, α_{vir}). Protoplanetary discs that have a radius of 100 AU are focused on, however the effects of external photoevaporation on discs with different radii and mass are discussed later in Sections 4.3.3 and 4.3.4.

I compare the simulation results to the observed disc fractions in both Haisch et al. (2001) and Richert et al. (2018), which cover a broad range of young star forming regions, using stellar ages from the models in Siess et al. (2000). The caveats associated with these models are discussed in Section 4.4.

I later present two low mass clusters ($100 M_{\odot}$) with an initial density of $\sim 100 M_{\odot} \text{pc}^{-3}$ that are subvirial ($\alpha_{\text{vir}} = 0.3$) and highly substructured ($D = 1.6$). These clusters contain either one ($38 M_{\odot}$) or two ($42 M_{\odot}$ and $23 M_{\odot}$) massive stars. The corresponding Φ_i values are $\Phi_i = 0.76$ and $\Phi_i = 1.01, 0.11$ respectively.

4.3.1 Substructure in star-forming regions

First, the results from four simulations of star forming regions are presented, where in each simulation the star forming region has a different initial spatial distribution; $D = 1.6$ (highly substructured), $D = 2.0$ (moderately substructured), $D = 3.0$ (smooth) and a Plummer sphere spatial distribution. In all simulations the star-forming region is subvirial ($\alpha_{\text{vir}} = 0.3$).

Fig. 4.1 shows the average fraction of stars that have retained their (100 AU) discs from 20 runs of each simulation, where the initial substructure of the star-forming region is varied. The results for regions with two different initial stellar densities are presented; 10 and 100 $M_{\odot} \text{pc}^{-3}$ respectively.

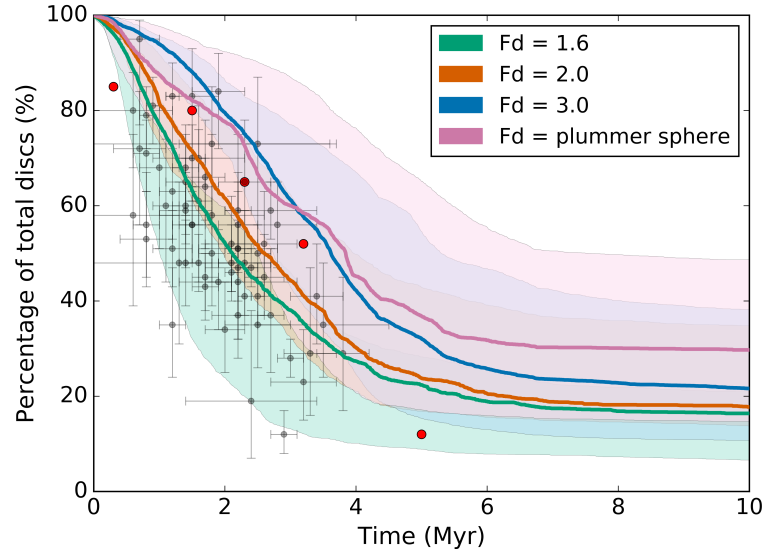
Fig. 4.1(a) shows the results from a star forming region with an initial density of 10 $M_{\odot} \text{pc}^{-3}$. Within highly sub-structured regions ($D = 1.6$), the time taken for half of the stars to lose their discs due to external photoevaporation is 2.12 Myr. In moderately sub-structured regions ($D = 2.0$), this time increases to 2.60 Myr. However, the average percentage of remaining discs with time in both remain relatively similar throughout the 10 Myr. For regions with an initially smooth and spherical distribution ($D = 3.0$), the time taken for half of the discs to disperse is 3.62 Myr. Discs within Plummer spheres have the longest lifetimes (3.85 Myr), with an average of ~ 29.7 per cent of discs surviving for longer than 10 Myr.

Plummer (1911) models (and other models that describe smooth star clusters such as a King (1966) profile or an Elson et al. (1987) profile) are intended to model dynamically relaxed systems, whereas young star-forming regions have yet to relax. Therefore, even a smooth box fractal ($D = 3.0$) contains kinematic substructure, which causes the dynamical evolution of such a region to be more violent than a smooth Plummer sphere. It is therefore unsurprising that fewer discs survive in kinematically substructured fractal regions than in Plummer spheres with a similar density.

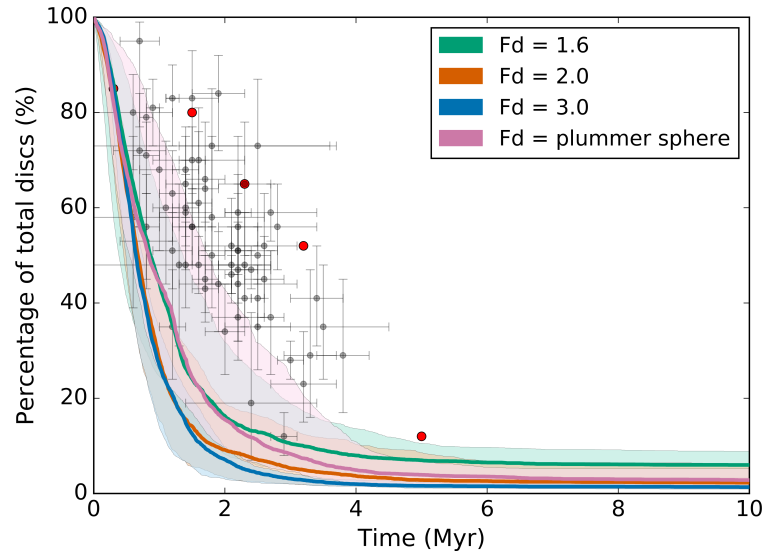
Fig. 4.1(b) shows the results for star forming regions with an initial density of 100 $M_{\odot} \text{pc}^{-3}$. For discs in the highly sub-structured regions ($D = 1.6$), the time taken for half of the stars within the cluster to lose their protoplanetary discs is 0.87 Myr. The majority of discs within the highly substructured region ($D = 1.6$) are dispersed after 10 Myr, with ~ 6 per cent surviving for the length of the simulation. The majority of discs within smooth, spherical regions are also dispersed within a short time frame, with only ~ 3 per cent remaining after 10 Myr.

Table 4.1 summarises the average time taken for half of the stars in a star-forming region to lose their discs for each spatial distribution and table 4.2 summarises the percentage of discs remaining at the end of the 10 Myr simulation.

In the low density simulations, regions with more spatial substructure photoevaporate discs faster than smoother regions of a comparable density (Fig. 4.1(a)). The reason for this is that the more substructured regions are initially further from dynamical equilibrium than the smooth regions, and low-mass stars undergo more close interactions with the high mass stars as the regions relax. The



(a) Density = $10 M_{\odot} \text{ pc}^{-3}$



(b) Density = $100 M_{\odot} \text{ pc}^{-3}$

FIGURE 4.1: The average percentage of stars retaining their 100 AU disc over time within a sub-virial ($\alpha_{\text{vir}} = 0.3$) cluster. The amount of substructure in the star-forming region is varied from highly substructured ($D = 1.6$) to smooth and centrally concentrated (Plummer Sphere). Two different initial densities (10 and $100 M_{\odot} \text{ pc}^{-3}$) are considered. Each coloured line represents a different initial spatial distribution. The red data points are observational values from Haisch et al. (2001). The grey data points are from Richert et al. (2018) using stellar ages from the models in Siess et al. (2000). The coloured shaded regions show the complete range of values from the 20 runs for each set of initial conditions.

TABLE 4.1: The mean time taken for half of the stars within the star-forming region to lose the gas from their 100 AU protoplanetary discs in a $1000 M_{\odot}$ sub-virial ($\alpha_{\text{vir}} = 0.3$) region with two different initial densities; 10 and $100 M_{\odot} \text{pc}^{-3}$. Four different spatial distributions are analysed; $D = 1.6$ (highly sub-structured), $D = 2.0$ (moderately sub-structured), $D = 3.0$ (smooth), and a Plummer sphere distribution. The quoted errors are derived from the full range.

Fractal dimension (D)	Half life of protoplanetary discs	
	$\rho = 10 M_{\odot} \text{pc}^{-3}$	$\rho = 100 M_{\odot} \text{pc}^{-3}$
1.6	$2.12^{+0.51}_{-1.11}$ Myr	$0.87^{+0.50}_{-0.49}$ Myr
2.0	$2.60^{+1.36}_{-0.62}$ Myr	$0.67^{+0.21}_{-0.22}$ Myr
3.0	$3.62^{+1.68}_{-0.89}$ Myr	$0.65^{+0.10}_{-0.16}$ Myr
Plummer Sphere	$3.85^{+3.70}_{-1.34}$ Myr	$0.84^{+0.90}_{-0.29}$ Myr

TABLE 4.2: The average percentage of 100 AU discs remaining after 10 Myr within a sub-virial ($\alpha_{\text{vir}} = 0.3$) star forming region from 20 realisations of each simulation. The amount of substructure is varied from highly substructured ($D = 1.6$) to a smooth and centrally concentrated Plummer sphere. The highest and lowest values from the 20 different runs are also shown. Two different initial densities (10 and $100 M_{\odot} \text{pc}^{-3}$) are considered. The quoted errors are derived from the full range.

Fractal dimension (D)	Percentage of discs remaining after 10 Myr	
	$\rho = 10 M_{\odot} \text{pc}^{-3}$	$\rho = 100 M_{\odot} \text{pc}^{-3}$
1.6	$16.40^{+4.58}_{-9.8}$	$5.99^{+2.88}_{-2.67}$
2.0	$17.75^{+17.03}_{-4.04}$	$2.27^{+4.04}_{-0.92}$
3.0	$21.60^{+16.63}_{-10.88}$	$1.35^{+0.63}_{-0.42}$
Plummer Sphere	$29.70^{+18.95}_{-14.98}$	$2.81^{+2.36}_{-1.63}$

clustering of stars spatially will also contribute to this, as initially a higher percentage of stars are within closer proximity to a massive star in highly substructured cluster than in smooth, evenly distributed clusters.

Interestingly, in the high-density simulations (Fig. 4.1(b)), whilst the fraction of discs remaining after 10 Myr is lower than in the low density simulations, the initially more substructured star-forming regions contain more discs than the

smooth regions after 10 Myr (and their disc-destruction half-life is longer, see Table 4.1). This may be attributed to the higher ejection rate of massive stars in dense, substructured star-forming regions (Parker et al., 2014b), which means that some of the ionising sources are no longer near the majority of the proplyds as early as 1 Myr after the start of dynamical evolution.

4.3.2 Virial ratio

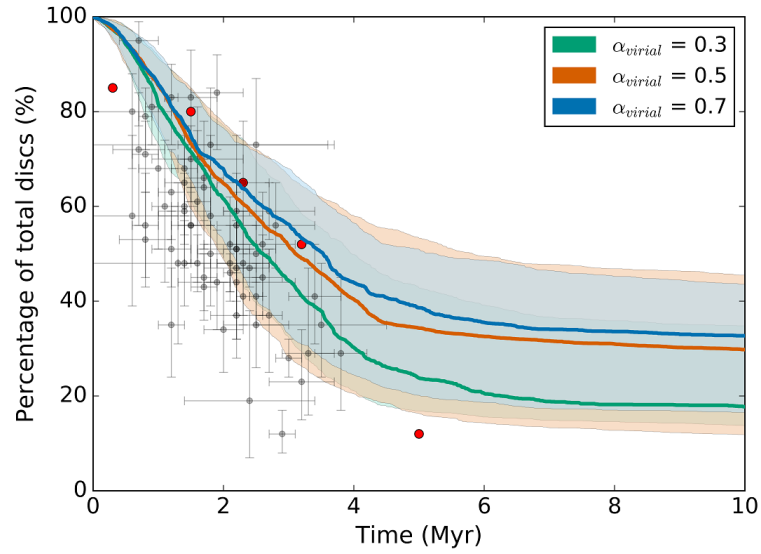
I explore how changing the net bulk motion of the star-forming region affects the rate of disc dispersal due to external photoevaporation. Simulations of the star-forming region with three different virial ratios are run; 0.3 (subvirial, or collapsing), 0.5 (virial equilibrium), and 0.7 (supervirial, or expanding). The fractal dimension is kept constant, adopting $D = 2.0$ and as before I analyse simulations with two different initial densities; $10 M_{\odot} \text{ pc}^{-3}$ and $100 M_{\odot} \text{ pc}^{-3}$.

Table 4.3 summarises the average time taken for half of the stars in each region to lose their (100 AU) discs for a given bulk virial ratio. Table 4.4 shows the percentage of discs remaining at the end of the 10 Myr simulation. Fig. 4.2 shows the average fraction of stars that have retained their discs from the 20 runs of each simulation for a star forming region where the initial bulk motion (virial ratio) is varied.

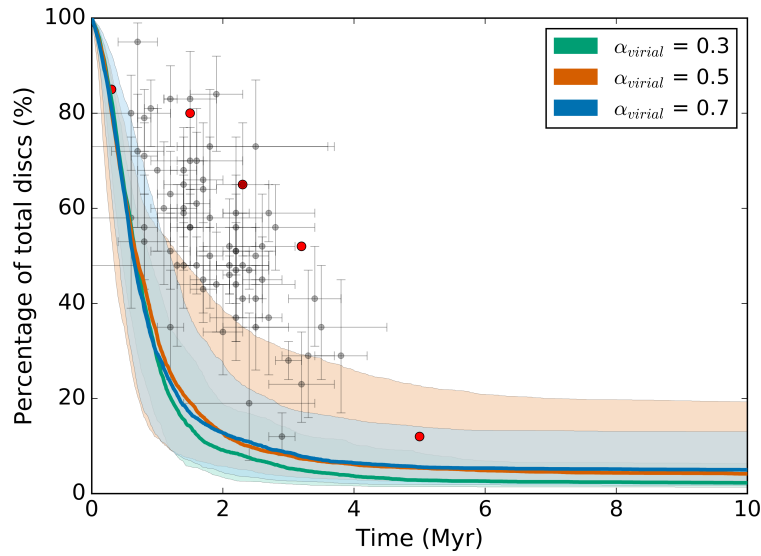
Fig. 4.2(a) shows the average mass loss rate in a star forming region with an initial density of $10 M_{\odot} \text{ pc}^{-3}$. The time taken for half of the stars within a collapsing (sub-virial) star-forming region to lose their discs is 2.60 Myr. In regions that are expanding (supervirial), this time increases to 3.53 Myr. The percentage of discs within the subvirial region after 10 Myr is 17.8 per cent, in comparison to discs within an expanding region where the percentage rises to 32.7 per cent.

The initial net bulk motion of low density star-forming regions affects the amount of discs that are photoevaporated due to external radiation, with subvirial regions evaporating more discs at a faster rate than either virialised or supervirial regions.

Fig. 4.2(b) shows the results for a star-forming region with an initial density of $100 M_{\odot} \text{ pc}^{-3}$. The time taken for half the stars within a collapsing region to lose their discs is 0.67 Myr. This time is similar for regions in virial equilibrium and expanding regions (0.68 and 0.63 Myr respectively). The lower disc half-life for the supervirial regions could again be due to massive stars being ejected in the (sub)virial regions. The percentage of discs remaining after 10 Myr in sub-virial



(a) Density = $10 M_{\odot} \text{ pc}^{-3}$



(b) Density = $100 M_{\odot} \text{ pc}^{-3}$

FIGURE 4.2: The average percentage of stars retaining their 100 AU disc with time in a $1000 M_{\odot}$, moderately substructured ($D = 2.0$) star forming region with an initial density of 10 and $100 M_{\odot} \text{ pc}^{-3}$. Each coloured line represents a different virial ratio. The red data points are observational values from Haisch et al. (2001). The grey data points are from Richert et al. (2018) using ages from the stellar model in Siess et al. (2000). The shaded regions show all values between the maximum and minimum values from all 20 runs of the simulations.

TABLE 4.3: The time taken for half of the stars within the cluster to lose the gas within their 100 AU protoplanetary discs in a $1000 M_{\odot}$, moderately sub-structured ($D = 2.0$) star forming region for two different initial densities; 10 and $100 M_{\odot} \text{ pc}^{-3}$. Three different virial ratios are analysed: $\alpha_{\text{vir}} = 0.3$ (sub-virial, or collapsing), $\alpha_{\text{vir}} = 0.5$ (virial equilibrium), and $\alpha_{\text{vir}} = 0.7$ (super-virial, or expanding). The quoted errors are derived from the full range.

Half life of protoplanetary discs		
Virial Ratio (α_{vir})	$\rho = 10 M_{\odot} \text{ pc}^{-3}$	$\rho = 100 M_{\odot} \text{ pc}^{-3}$
0.3	$2.60^{+1.36}_{-0.62}$ Myr	$0.67^{+0.21}_{-0.22}$ Myr
0.5	$3.10^{+2.73}_{-1.15}$ Myr	$0.68^{+0.66}_{-0.35}$ Myr
0.7	$3.53^{+1.72}_{-1.40}$ Myr	$0.63^{+0.57}_{-0.23}$ Myr

TABLE 4.4: The average percentage of 100 AU discs remaining after 10 Myr from 20 runs of simulations within a moderately substructured ($D = 2.0$) cluster. The bulk motion (virial ratio) of the star-forming region is varied, from collapsing (sub-virial, $\alpha_{\text{vir}} = 0.3$) to expanding (super virial, $\alpha_{\text{vir}} = 0.7$). The quoted errors are derived from the full range.

Percentage of discs remaining after 10 Myr		
Virial Ratio (α_{vir})	$\rho = 10 M_{\odot} \text{ pc}^{-3}$	$\rho = 100 M_{\odot} \text{ pc}^{-3}$
0.3	$17.75^{+17.03}_{-4.04}$ %	$2.27^{+4.04}_{-0.92}$ %
0.5	$29.77^{+15.73}_{-17.95}$ %	$4.16^{+15.14}_{-2.06}$ %
0.7	$32.67^{+10.9}_{-16.14}$ %	$5.00^{+8.04}_{-3.23}$ %

star forming regions is 2.27 per cent whereas in regions where the net motion is expansive, this is increased to 5.00 per cent.

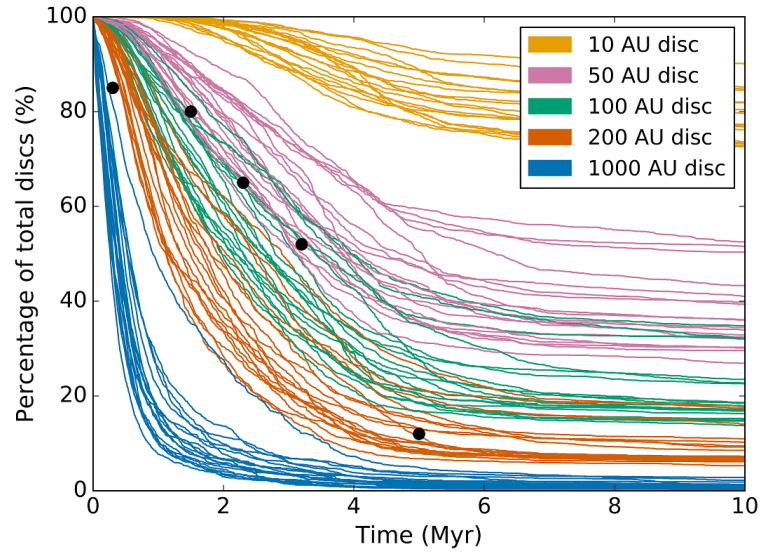
4.3.3 Disc radii

Here the rates of disc dispersal are presented for different initial disc radii in a star-forming region with two different initial densities (10 and $100 M_{\odot} \text{ pc}^{-3}$). The region has a fractal dimension of $D = 2.0$ (moderately substructured) and a virial ratio of $\alpha_{\text{vir}} = 0.3$ (sub-virial).

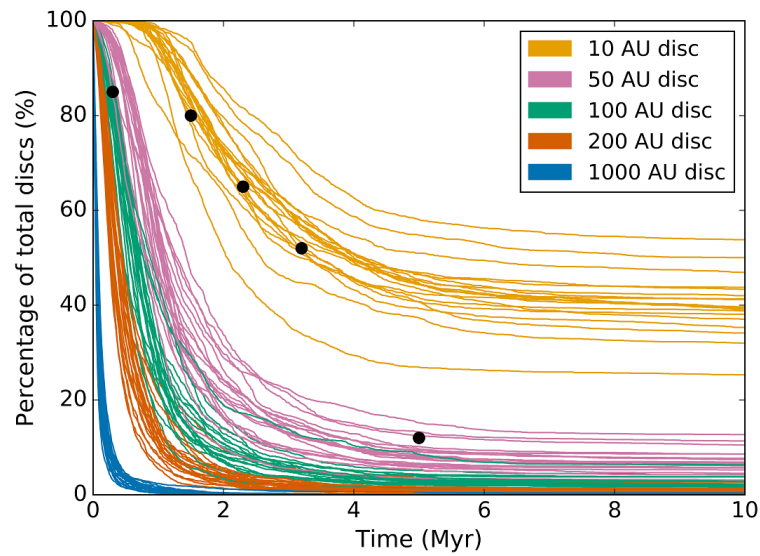
Fig. 4.3 shows the percentage of protoplanetary discs with initial radii ranging between 10 – 1000 AU that have some remaining mass over 10 Myr in a $1000 M_{\odot}$ star-forming region with different initial stellar densities; $10 M_{\odot} \text{ pc}^{-3}$ in Fig 4.3(a) and $100 M_{\odot} \text{ pc}^{-3}$ in Fig. 4.3(b).

In the lower-density star-forming regions (Fig. 4.3(a)), the time taken for half of the 100 AU discs to be completely photoevaporated is 2.60 Myr. Discs with radii of 10 AU have much greater lifetimes, with an average of ~ 77 per cent of discs surviving the full length of the simulation. The majority of discs with very large radii (1000 AU) are still depleted within very short timescales. Disc depletion rates begin to switch off after ~ 4 Myr due to a combination of a large decrease in density of the star forming region, which peaks at ~ 2 Myr, and the death of the most massive star at 4.33 Myr.

Fig. 4.3(b) shows that the majority (90 per cent or more) of discs with radii > 10 AU are completely photoevaporated before the end of the 10 Myr simulation in moderately dense star-forming regions. The time taken for half of the stars in the region to lose their 100 AU discs is 0.67 Myr. The vast majority of the largest discs (1000 AU) are photoevaporated completely within 2 Myr, with half of the stars in the region losing their discs within < 0.1 Myr.



(a) Density = $10 M_{\odot} \text{ pc}^{-3}$



(b) Density = $100 M_{\odot} \text{ pc}^{-3}$

FIGURE 4.3: The percentage of total remaining discs over time for a $1000 M_{\odot}$ star-forming region with an initial density of ~ 10 and $100 M_{\odot} \text{ pc}^{-3}$ (panels (a) and (b) respectively). The cluster is moderately sub-structured ($D = 2.0$) and is sub-virial ($\alpha_{vir} = 0.3$). Each colour represents a different initial disc radius. The disc masses are 10 per cent of the host star mass. Each coloured line is one run of the simulation. The black data points are observational values from [Haisch et al. \(2001\)](#).

4.3.4 Disc masses

For the previous simulations, it has been assumed that the disc masses are 10 per cent of the host star's mass, which is likely to be an overestimate. Observations and various studies suggest that the disc mass is as low as 1 per cent of the host star's mass (Weidenschilling, 1977; Hayashi, 1981; Andrews et al., 2013), therefore simulations are run with a disc mass of 1 per cent. Changing the initial mass of the disc reduces the mass budget of protoplanetary discs but does not affect the mass loss rates.

Fig. 4.4 shows the results for a star-forming region with the two different initial densities (10 and 100 $M_{\odot} \text{pc}^{-3}$ respectively), where the initial disc masses are set to $M_{\text{disc}} = 0.01 M_{\star}$.

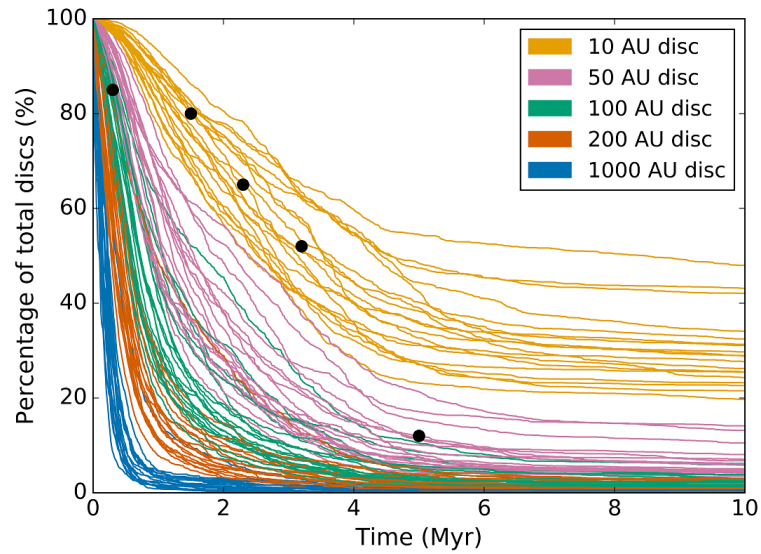
Fig. 4.4(a) shows that on average the time taken for half of the stars within the low density star forming region to lose their 100 AU disc is 0.71 Myr, less than half of the time taken for discs with 10 per cent of the mass of their stellar host. For discs with a radii of 10 AU, the half life is 3.31 Myr.

The timescale for half of the 100 AU discs to dissipate in the moderately dense (100 $M_{\odot} \text{pc}^{-3}$) star forming region (see Fig. 4.4(b)) is ~ 0.14 Myr. For discs with a radius of 10 AU, the half life is ~ 0.84 Myr. Less than 5 per cent of 10 AU discs survive for more than 3 Myr.

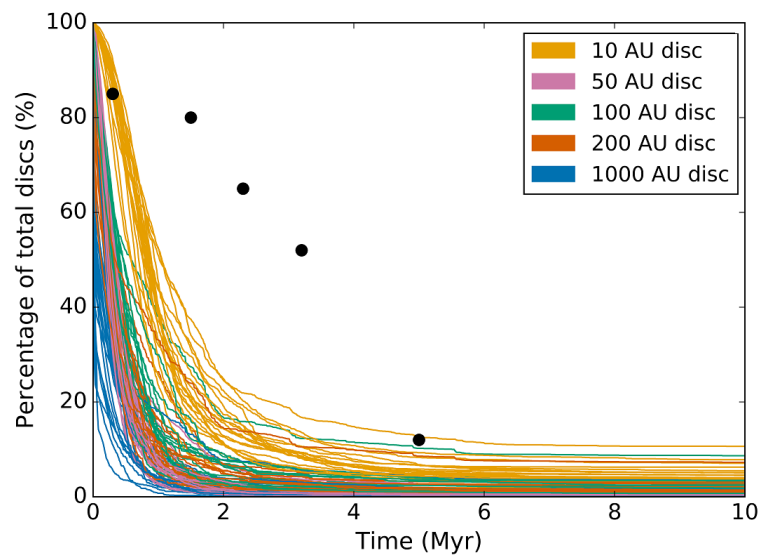
4.3.5 Mass of star-forming regions

Simulations were also run for two different low mass star-forming regions (100 M_{\odot}) with an initial density of $\sim 100 M_{\odot} \text{pc}^{-3}$, which were sub-virial ($\alpha_{\text{vir}} = 0.3$) and substructured ($D = 1.6$). These low-mass regions contain one (38 M_{\odot}) or two (42 M_{\odot} and 23 M_{\odot}) massive stars, which again represents an unusual sampling of the IMF (Parker and Goodwin, 2007), but is observed in nature (e.g. γ^2 Vel, Jeffries et al., 2014). From randomly sampling the IMF it is found that 10 per cent of all low-mass (100 M_{\odot}) star-forming regions can host a massive star, and 1 per cent of regions will host two massive stars. I note that the lack of massive star(s) in *any* star-forming region would preclude disc destruction from photoevaporation, though as discussed in Section 3.4 it is unclear which type of star-forming region (in terms of total mass, M_{cl}) contributes the most (planet hosting) stars to the Galactic field.

In both of these low mass regions, half of the discs with radii of 100 AU dissipated before ~ 1 Myr (Fig. 4.5). The time taken for half of the discs to be destroyed



(a) Density = $10 M_{\odot} \text{ pc}^{-3}$



(b) Density = $100 M_{\odot} \text{ pc}^{-3}$

FIGURE 4.4: The percentage of total remaining discs over time for a star forming region of $1000 M_{\odot}$ with an initial density of ~ 10 and $100 M_{\odot} \text{ pc}^{-3}$ respectively, a fractal dimension of $D = 2.0$ and a virial ratio of $\alpha_{\text{vir}} = 0.3$. The initial disc masses are 1 per cent of the host star mass. Each colour represents a different disc radius. Each coloured line is one run of a simulation. The black data points are from observational values from [Haisch et al. \(2001\)](#).

TABLE 4.5: The time taken for half of stars in a star forming region to lose the gas within their 100 AU protoplanetary discs in a 1000 M_{\odot} , moderately sub-structured ($D = 2.0$) region for two different initial densities; 10 and 100 $M_{\odot} \text{pc}^{-3}$ and two different masses of disc, 10 per cent and 1 per cent. Three different virial ratios are analysed: $\alpha_{\text{vir}} = 0.3$ (sub-virial, or collapsing), $\alpha_{\text{vir}} = 0.5$ (virial equilibrium), and $\alpha_{\text{vir}} = 0.7$ (super virial, or expanding). The quoted errors are derived from the full range.

Half life of cluster protoplanetary discs						
		Disc mass = $0.1 M_{\star}$		Disc mass = $0.01 M_{\star}$		
Disc Radius (AU)	$\rho = 10 M_{\odot} \text{pc}^{-3}$	$\rho = 100 M_{\odot} \text{pc}^{-3}$	$\rho = 10 M_{\odot} \text{pc}^{-3}$	$\rho = 10 M_{\odot} \text{pc}^{-3}$	$\rho = 100 M_{\odot} \text{pc}^{-3}$	$\rho = 100 M_{\odot} \text{pc}^{-3}$
10	> 50% remaining	$3.92^{+5.91}_{-1.87}$ Myr	$3.31^{+5.16}_{-0.9}$ Myr	$0.84^{+0.22}_{-0.27}$ Myr		
50	$3.94^{+5.96}_{-0.82}$ Myr	$1.04^{+0.40}_{-0.24}$ Myr	$1.22^{+1.18}_{-0.35}$ Myr	$0.28^{+0.07}_{-0.09}$ Myr		
100	$2.60^{+1.36}_{-0.62}$ Myr	$0.67^{+0.21}_{-0.22}$ Myr	$0.71^{+0.96}_{-0.21}$ Myr	$0.14^{+0.05}_{-0.05}$ Myr		
200	$1.55^{+1.34}_{-0.44}$ Myr	$0.36^{+0.09}_{-0.11}$ Myr	$0.39^{+0.58}_{-0.12}$ Myr	$0.06^{+0.03}_{-0.02}$ Myr		
1000	$0.37^{+0.55}_{-0.11}$ Myr	$0.06^{+0.02}_{-0.02}$ Myr	$0.15^{+0.20}_{-0.05}$ Myr	$0.02^{+0.02}_{-0.01}$ Myr		

TABLE 4.6: The average percentage of 100 AU discs remaining after 10 Myr within a moderately substructured ($D = 2.0$) star forming region for two different initial densities, (10 and $100 M_{\odot} \text{ pc}^{-3}$), with two different initial disc masses, 10 per cent and 1 per cent. The bulk motion (virial ratio) of the star forming region is varied, from collapsing (sub-virial, $\alpha_{\text{vir}} = 0.3$) to expanding (super-virial, $\alpha_{\text{vir}} = 0.7$). The quoted errors are derived from the full range.

Disc Radius (AU)	Percentage of discs remaining after 10 Myr					
	Disc mass = $0.1 M_{\star}$		Disc mass = $0.01 M_{\star}$		Disc mass = $0.01 M_{\star}$	
	$\rho = 10 M_{\odot} \text{ pc}^{-3}$	$\rho = 100 M_{\odot} \text{ pc}^{-3}$	$\rho = 10 M_{\odot} \text{ pc}^{-3}$	$\rho = 100 M_{\odot} \text{ pc}^{-3}$	$\rho = 100 M_{\odot} \text{ pc}^{-3}$	$\rho = 100 M_{\odot} \text{ pc}^{-3}$
10	$77.29^{+12.79}_{-4.71}$	$39.49^{+14.34}_{-14.17}$	$28.81^{+19.13}_{-9.09}$	$3.99^{+6.65}_{-2.18}$		
50	$34.44^{+18.08}_{-7.57}$	$6.73^{+5.97}_{-3.62}$	$4.79^{+9.34}_{-1.43}$	$0.40^{+1.53}_{-0.23}$		
100	$17.75^{+17.03}_{-4.04}$	$2.27^{+4.04}_{-0.92}$	$2.27^{+3.91}_{-1.13}$	$0.08^{+0.59}_{-0.08}$		
200	$7.12^{+10.79}_{-1.82}$	$0.74^{+1.95}_{-0.36}$	$1.09^{+1.81}_{-14.17}$	$0.00^{+0.38}_{-0.00}$		
1000	$1.09^{+1.73}_{-0.9}$	$0.0^{+0.38}_{-0.00}$	$0.29^{+0.51}_{-0.29}$	$0.00^{+0.04}_{-0.00}$		

in a region with one massive star is 0.95 Myr. This time is reduced to 0.37 Myr for the cluster with 2 massive stars.

At the end of the 10 Myr simulation, 15.5 per cent of discs within the region with one massive star survive. Within the region containing 2 massive stars, less than 5 per cent of discs remain, double the number of discs remaining in higher mass regions with otherwise identical initial conditions.

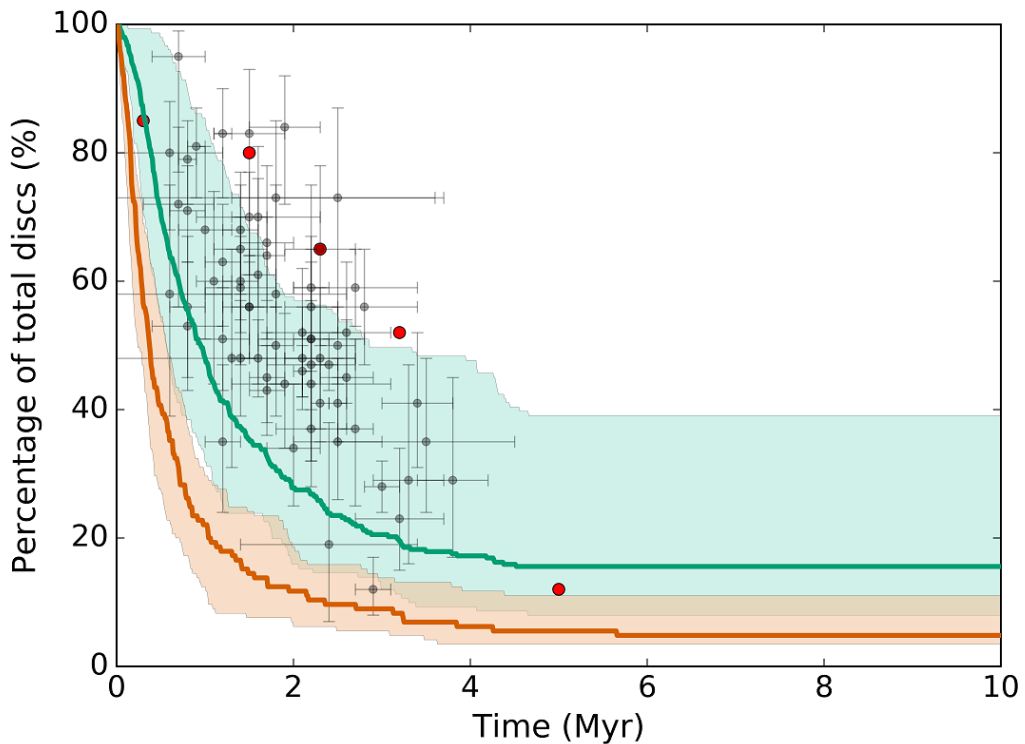


FIGURE 4.5: The median percentage of protoplanetary discs (100 AU) remaining with time for two $100 M_{\odot}$ clusters with initial densities of $100 M_{\odot} \text{ pc}^{-3}$ but different numbers of massive stars. The green line shows values for a cluster with 1 massive star ($> 15 M_{\odot}$) and the orange a cluster with 2 massive stars. The red data points are observational values from Haisch et al. (2001). The grey data points are from Richert et al. (2018) using ages from the stellar model in Siess et al. (2000). The coloured shaded regions show the complete range of values from the 20 runs for each set of the different clusters.

4.4 Discussion

The initial conditions of a star-forming region will affect the rate at which protoplanetary discs are photoevaporated due to the radiation from nearby massive

stars. The initial substructure and net bulk motion of a star-forming region impacts the rate of disc dispersal.

4.4.1 Changing the initial conditions of star-forming regions

In the low-density simulations, highly substructured ($D = 1.6$) regions disperse half of the protoplanetary discs within 1.51 Myr, more than twice as fast as smooth ($D = 3.0$) regions. In simulations with a Plummer sphere distribution, more than 30 per cent of discs remain at the end of the 10 Myr simulation, almost double that of discs within highly substructured clusters.

In moderately dense initial conditions ($100 M_{\odot} \text{ pc}^{-3}$), the difference in the fraction of discs that are photoevaporated between different initial spatial distributions decreases greatly, although regions with a Plummer sphere distribution retain more of their discs than regions with initial substructure. However, the average of all runs indicates that the amount of initial substructure has little effect on the survival rates of discs at these densities and fewer than 50 per cent of discs remain after 1 Myr.

The effect of changing the net bulk motion of the star-forming region has a similar impact on the rate of disc dispersal as the initial substructure has. For low density regions ($10 M_{\odot} \text{ pc}^{-3}$), the difference between the amount of discs surviving within a collapsing and an expanding star forming region is ~ 15 per cent, with the collapsing regions enabling more photoevaporation than in expanding regions. Again, approximately double the number of discs remain in expanding clusters compared to collapsing clusters. In moderately dense clusters it is similar, with ~ 6 per cent of discs surviving in highly substructured clusters, in comparison to 3 per cent surviving in cluster with a Plummer sphere distribution.

For low mass star-forming regions ($100 M_{\odot}$), disc dispersal rates are similar to those in higher mass regions. Whilst the UV field strength can vary due to different realisations of the IMF (Fatuzzo and Adams, 2008), these low mass regions show that the mere presence of a high mass star ($> 15 M_{\odot}$) will cause disc lifetimes to be shortened dramatically.

The simulations are set up to mimic the observations of star formation in filaments, where the pre-stellar cores have subvirial motion (Larson, 1981; Foster et al., 2015). The local velocity dispersion is therefore always subvirial to some degree, and because mass-loss due to photoevaporation is so fast (Eqns. 2.22 and 2.21), most of the photoevaporation occurs during the substructured phase of a star-forming region.

Previous studies investigating the effects of external photoevaporation on disc dispersal rates assumed smooth and centrally concentrated spatial distributions (Scally and Clarke, 2001; Adams et al., 2004, 2006; Winter et al., 2018a), replicating environments like the present-day conditions of the ONC. However, using the present-day spatial and kinematic distributions to model star clusters may not accurately replicate the dynamical history of the star-forming region from which the cluster formed (Parker et al., 2014b).

Furthermore, the photoevaporation prescriptions used are from Scally and Clarke (2001), rather than determining the photoevaporation rate from the EUV/FUV fluxes as a function of the flux in the ISM (the G_0 value, $1.6 \times 10^{-3} \text{ erg s}^{-1} \text{ cm}^{-2}$ Habing, 1968). In comparison with Scally and Clarke (2001), I find that discs are destroyed earlier in ONC-type regions because the initial densities are higher (in line with current observations, as discussed in Parker, 2014), and the star-forming regions are substructured (Cartwright and Whitworth, 2004).

An initially highly substructured star-forming region can become smooth and centrally concentrated within a few Myr due to a combination of violent and two body relaxation. Protoplanetary discs in these highly substructured environments will be photoevaporated at faster rates than discs within initially smooth regions. Even though they will both appear smooth within a few Myr, the percentage of discs remaining, and possibly the population of planets within the regions, will differ greatly.

The initial density of the cluster has the largest effect on the disc dispersal rate due to external photoevaporation. The ‘moderately-dense’ clusters reflect the likely initial densities of many star-forming regions (Parker, 2014). However, these ‘moderately-dense’ environments are found to be very destructive for protoplanetary discs and evaporate discs at rates faster than suggested by observations (compare the black points in Figs. 4.1 and 4.2 with the simulated data). My results suggest that protoplanetary discs (or at least their gas content) would always be significantly depleted in moderately dense ($100 M_{\odot} \text{ pc}^{-3}$) star-forming regions, if those regions contain massive stars.

Haisch et al. (2001) finds that the fraction of disc-hosting stars in young star-forming regions falls to 50 per cent after ~ 3 Myr whereas Richert et al. (2018) find that after only ~ 2 Myr half of the discs remain in their observed regions. In comparison, more than half of the discs in the simulations that are within dense environments are destroyed within ~ 1 Myr. One interesting data point in the Haisch et al. (2001) sample is the ONC. With an age of ~ 1 Myr, the centre of the ONC contains 4 massive stars and a density of $\sim 400 M_{\odot} \text{ pc}^{-3}$ (Hillenbrand and

Hartmann, 1998). Observations of this part of the ONC suggest that $\sim 80 - 85$ per cent of stars within the cluster are surrounded by bright ionization fronts, interpreted to be discs, with radii of ~ 1000 AU (Bally et al., 2000; Lada et al., 2000).

The age of the simulated regions, when 80 per cent of stars still possess a 100 AU disc with some mass, is 0.48 Myr – likely to be less than half the age of the ONC. This suggests that the massive stars within the ONC should have destroyed the majority of 100 AU discs. From similar arguments, Clarke (2007) concluded that the ‘discs’ in the ONC with radii >10 AU are likely to be merely ionisation fronts, containing little mass. The simulations with different initial disc radii show that the radius of the disc will greatly affect the rate at which it is photoevaporated (see also Clarke, 2007) due to the dependence on disc radius within the FUV and EUV photoevaporation prescriptions.

Recent surveys suggest that most stars in the Galactic field host planets, and many of these are gas or ice giants (Mayor et al., 2011). This implies that the majority of planet forming discs were able to survive a significant amount of time in their birth environment. The simulations suggest that this is only possible in low-density regions that contain no photoionising sources (i.e. massive stars). Therefore, (giant) planet formation must occur on very rapid timescales (<1 Myr), or stars that host giant planets must have formed in very benign environments.

Many observed protoplanetary discs are located in low-mass, low-density star-forming regions (Andrews et al., 2013; Ansdell et al., 2018) and would be unaffected by external photoevaporation. However, many star-forming regions are typically moderate-density ($\sim 100 M_{\odot} \text{ pc}^{-3}$) environments (Parker, 2014) and these results suggest that the majority of protoplanetary discs in star-forming regions with these densities do not survive for long enough periods of time to form giant planets.

4.4.2 Caveats

There are several caveats to the results, which I will discuss below.

The effects of external EUV radiation on protoplanetary discs can be reduced when thick winds are present, caused by FUV heating of the disc (Alexander et al., 2014). However, the majority of the disc mass loss occurs due to FUV radiation.

It is possible that the amount of photoevaporation from massive stars is being overestimated. However, recent research suggests that the prescriptions used

here are actually underestimating the amount of FUV radiation that discs receive (Facchini et al., 2016; Haworth et al., 2018b). As FUV is the dominant source of external photoevaporation, the protoplanetary discs in the simulations could dissipate on even shorter timescales.

Star formation is an inherently inefficient process, with typically only ~ 30 per cent of the mass of a giant molecular cloud converted into stars. Young star-forming regions are observed to contain a large amount of dust and gas, which could shield the proplyds from significant photoevaporation. At these early stages the stellar density within the substructure is highest, and is therefore when the largest percentage of stars are in closest proximity to the massive stars. However, hydrodynamical simulations of star-forming regions show that massive stars blow large (\sim pc-scale) cavities within the gas on short time scales (Dale et al., 2013), and so low-mass disc-hosting stars that would be affected by EUV/FUV radiation will likely reside in the cavities blown out by the massive stars. If the gas and dust could shield the disc, this would protect them for a very short period of time (Gorti et al., 2015). Whether this grace period would be long enough to allow gas-rich giant planets to form is uncertain.

Given that most star-forming regions have stellar densities above a few $M_{\odot} \text{ pc}^{-3}$ (Bressert et al., 2010), external photoevaporation will detrimentally affect protoplanetary discs in any star-forming region that contains massive stars. This implies that star-forming regions that do not contain massive stars are more likely to form giant planets, but it should be noted that massive stars appear necessary in order to deliver short-lived radioisotopes to the young Solar System (Lugaro et al., 2018). The number of massive stars in a star-forming region appears to only be limited by the mass of the star-forming cloud (Parker and Goodwin, 2007), but this also means that low-mass star forming regions ($< 10^4 M_{\odot}$) stochastically sample the IMF, meaning that the simulations cannot be described as ‘typical’ star-forming regions.

Quantifying disc dispersal is further complicated by how difficult it is to determine the ages of young stars, especially before 1 Myr (Siess et al., 2000). The stellar ages used in the simulations are from the Siess et al. (2000) model. However, models of pre-main sequence stellar evolution calculate different ages depending on the physics that is implemented. Of the three models presented in Richert et al. (2018) the ages from Siess et al. (2000) are used so that the lower end of cluster ages are being compared to the simulations. The average stellar age calculated for the clusters in Richert et al. (2018) is significantly shorter than in more recent models from Feiden (2016). By using these lower age limits, the

possible average life times of the discs within the observed clusters are more than halved.

Furthermore, recent work by [Bell et al. \(2013\)](#) suggests that the ages of pre-main sequence stars may be underestimated by up to a factor of two, meaning that the observed discs (e.g. [Haisch et al., 2001](#)) are also a factor of two older. This would make it even more surprising that discs would remain around low-mass stars, if those stars form in regions containing massive stars.

There is also the question of how quickly the photoionising massive stars form. In the competitive accretion models ([Bonnell et al., 2001](#)), massive stars gradually gain in mass over ~ 1 Myr ([Wang et al., 2010](#)), suggesting high-mass stars form later than low-mass stars ([Tan et al., 2014](#)), which would in turn decrease the amount of time low-mass stars spend near the photoionising sources ([Dale et al., 2012, 2014](#)). In the simulations all stars form simultaneously, and therefore the disc-hosting low-mass stars do not have this grace period, which would increase disc lifetimes.

The growth of planetesimals into planets can be greatly accelerated by the accretion of cm-scale pebbles (see Section 1.2.5). [Johansen and Lambrechts \(2017\)](#) show that once a $10^{-2} M_{\oplus}$ planetesimal has formed it can grow to Jupiter mass in 1 Myr when starting as far out as about 15 AU. An initial phase of accreting pebbles forms a $10 M_{\oplus}$ core in about 0.8 Myr, which then undergoes runaway gas accretion to reach Jupiter mass. Such processes potentially allow close-in giant planets to be formed even in the relatively hostile conditions that are considered here.

However, photoevaporation by the central star can cause large amounts of mass loss in the inner disc, potentially affecting giant planet formation ([Alexander et al., 2014](#)). Grain size also has a significant effect on disc dispersal rates. Mass loss occurs much more quickly when grain growth has occurred because the FUV radiation can penetrate deeper into the disc ([Facchini et al., 2016](#)).

Discs that can survive in moderately dense environments have small radii (10 – 50 AU). This is because of the disc radius dependency in the external photoevaporation prescriptions. Internal UV radiation can cause significant mass loss and erosion of the disc within short time scales (1 Myr, [Gorti and Hollenbach, 2008](#)). The timescale for internal disc dispersal is very short (10^5 yr), with a UV switch being triggered due to the slowing of accretion onto the inner 10 AU of the disc ([Clarke et al., 2001](#)), also calling into question the survivability of small discs.

The disc radii in these models are fixed, but in reality disc radii change with time, often in an inside-out fashion where the initial radius is small (and not as susceptible to photoevaporation) compared to later in the disc's life. Several different disc radii are included to help visualise what happens for different disc initial conditions, but the full viscous evolution cannot be modeled in the post-processing analysis.

In these simulations, the stellar IMF was kept constant across different realisations of the spatial and kinematic initial conditions of the star-forming regions. The reasons for this are two-fold. The first is to isolate the possible effects of stochastic dynamical evolution (Allison et al., 2010; Parker and Goodwin, 2012; Parker et al., 2014b), which could lead to different photoevaporation rates even if the ionising flux from massive stars were kept constant. The uncertainties shown by the shaded regions in Figs. 4.1, 4.2, and 4.5 show this stochasticity for the same initial conditions. Secondly, the photoevaporation prescriptions that are adopted (following Scally and Clarke, 2001) are actually quite insensitive to the mass of the most massive stars (but rather depend on whether the massive stars are present or not).

The majority of discs observed with ALMA have been located in low-mass, low-density star-forming regions. Current observations suggest that the majority of stars form in moderately dense ($\sim 100 M_{\odot} \text{ pc}^{-3}$) environments (Parker, 2014). However, the majority of protoplanetary discs in clusters with these densities do not survive for long enough periods of time to form planets, as planet formation is thought to take place over a few million years (Pollack et al., 1996). The fact that the majority of stars have planetary systems around them poses important questions as a result of the discrepancies that seemingly arise. This may indicate that the majority of stars form in low mass clusters where there are few to no high mass stars.

In these simulations, initial disc masses are adopted that are 10 per cent of the host star mass, which is likely to be a large overestimate. When looking at more realistic values (1 per cent), discs are destroyed on even shorter timescales (see Fig. 4.4). However, it should be noted that accretion and internal photoevaporation will have much larger effects on disc mass evolution for these lower mass discs.

4.5 Conclusions

I have calculated the mass loss due to external photoevaporation of protoplanetary discs in N -body simulations of the evolution of star-forming regions. A suite of simulations were run where the initial spatial structure, bulk motion and initial density of the regions were varied. I compared the simulations that more closely represent observed star-forming regions (subvirial, substructured) with those of primordially mass segregated, spherical clusters, similar to those used in previous studies of external photoevaporation.

The parameter that most affects rates of disc dispersal is the initial density of the star-forming region. The majority of protoplanetary discs within simulated regions that mimic the conditions in nearby star-forming regions are dispersed due to external photoevaporation within very short time scales. In moderately dense ($\sim 100 M_{\odot} \text{ pc}^{-3}$) star-forming regions which have moderate levels of substructure ($D = 2.0$) and are collapsing ($\alpha_{\text{vir}} = 0.3$), the time taken for half of 100 AU discs to dissipate is found to be significantly shorter (3 times less) than suggested in observational studies (Haisch et al., 2001). Lower density clusters ($\sim 10 M_{\odot} \text{ pc}^{-3}$) allow discs to survive long enough to match observations of disc lifetimes, although the half-life of 100 AU discs is still less than that of Haisch et al. (2001).

The initial spatial distribution of the star-forming region also affects the rate of protoplanetary disc dispersal due to external photoevaporation. The degree to which initial substructure affects disc dispersal rates depends on the initial density. In moderately dense ($\sim 100 M_{\odot} \text{ pc}^{-3}$) regions the effects are washed out, but in lower-density regions ($\sim 10 M_{\odot} \text{ pc}^{-3}$) it seems that the more fractal and clumpy a star-forming region is, the higher the rate of disc dispersal. This is due to violent relaxation and the rapid increase in density (sometimes up to an order of a magnitude) of the star forming region within a short amount of time. As most star forming regions appear to have a high degree of substructure, it is important for future studies of disc dispersal to take the initial conditions into consideration due to external photoevaporation in dense environments.

The virial ratio of the star forming region affects the rate of disc dispersal in a similar way to substructure. Regions that have a low initial density and are collapsing photoevaporate more discs on average than clusters which are expanding. The effects of varying the initial net bulk motion in moderately dense clusters is negligible.

The majority of observed stars in the Galactic field host planetary systems,

implying their protoplanetary discs survived long enough for formation to take place. There are three possible scenarios to resolve this apparent tension between observations and the simulations presented here:

i) The majority of planets may not form in moderately dense star-forming regions ($\sim 100 M_{\odot} \text{ pc}^{-3}$); rather, they would form in low density regions with no photoionising massive stars present. Many protoplanetary discs have been observed in these low-density ambient environments (Ansdell et al., 2018), but significant numbers of protoplanetary discs (or at least their remnants) have been observed in dense, hostile regions like the ONC (McCaughrean and O'dell, 1996).

ii) If some planets do form in dense, clustered environments containing massive stars (such as the ONC), then this suggests that giant planet formation must happen on very short time scales (less than 1 – 2 Myr), or be confined to discs with radii significantly smaller than the orbit of Neptune in our Solar System. Johansen and Lambrechts (2017) show that giant planet formation can occur on these timescales once large enough planetesimals have formed. However, internal photoevaporation processes can deplete the inner disc and set limits on the formation time of giant planets (Alexander et al., 2014).

iii) The current calculations of mass-loss in discs due to external photoevaporation severely overestimate the detrimental effects of EUV and FUV radiation. However, recent research (Facchini et al., 2016; Haworth et al., 2018b) suggests that photoevaporative mass-loss rates caused by FUV radiation may be underestimated, and the calculations used here also underestimated the effects as the adopted initial disc masses are conservatively high, and so it is unlikely that this can explain the results.

Chapter 5

UV background fields in clusters

In this Chapter I focus on how the initial spatial distribution of stars within star-forming regions affects the background UV radiation field. Massive stars ($\geq 15 M_{\odot}$) produce UV fields which, based on observations of nearby star-forming regions, appear to disperse protoplanetary discs. The initial spatial distribution of these stars, especially massive stars, may affect the amount of UV radiation that stars receive. I shall investigate whether varying the spatial profile of stars affects the strength of UV fields, and if differences persist for the duration of the 10 Myr simulation.

I show that the stars in the simulations of highly substructured star-forming regions, which are based on observations of young star-forming regions, are consistently subjected to less UV radiation than stars within smooth, spherical star-forming regions. Over the duration of the 10 Myr simulation, stars within highly substructured clusters receive less FUV (~ 40 per cent) and EUV (~ 45 per cent) flux. This difference remains even when UV radiation is delayed until 0.5 Myr in an attempt to mimic the effects of delaying the formation of massive stars. Massive stars ($\geq 15 M_{\odot}$), or O-type stars, produce the majority of UV radiation, however [Armitage \(2000\)](#) show that stars with masses $< 15 M_{\odot}$ still produce significant amounts of UV radiation. When comparing the contribution of B-type stars to the UV field against O-type stars, it is found that B-type stars produce ~ 4 – 5 per cent of the FUV flux. The amount of EUV radiation that B-type stars produce is inconsequential (< 0.2 per cent) in comparison to the amount produced by O-type stars. The FUV field strength produced by B-type stars is likely still high enough to affect protoplanetary discs.

5.1 Introduction

The presence of massive stars in star forming regions and the close proximity of stars to one another means that cluster environments produce FUV and EUV radiation fluxes that are thousands of times more intense than in the field (Armitage, 2000). Observations and models of protoplanetary discs that reside in nearby star-forming regions, such as the ONC, suggest that protoplanetary discs are being dispersed by the strong UV fields produced by massive stars. In star-forming regions, the UV radiation that protoplanetary discs receive from neighbouring massive stars often dominates the radiation provided by the central star (Adams, 2010).

There are a wide range of possible UV field strengths that can affect planet formation, depending on the IMF of the star-forming region, with the most extreme environments potentially being too hostile to form planetary systems such as the Solar System (see Chapter 4). The effects of the UV radiation field on protoplanetary discs will depend upon the number of cluster members, the mass of the most massive stars, and the UV flux, which is dependent on the position of other stars in relation to one another. Previous studies have shown that clusters of a given size display a large range of FUV fluxes, which may be in part due to incomplete sampling of the IMF, or due to the position of the stars in relation to one another (Adams et al., 2006; Fatuzzo and Adams, 2008).

Constraints can be placed on the birth environment of the Solar System based upon its architecture (Adams, 2010). The Solar System likely formed in the presence of a moderate radiation field, meaning that it could have formed within a low-mass cluster with one or two massive stars ($\geq 8 M_{\odot}$) present, or on the edges of a large cluster containing a few massive stars, such as the ONC. If the Solar System formed within a large ($\geq 1000 M_{\odot}$) star-forming region, the massive stars would need to reside at the centre, with the Solar System spending the majority of its time on the outer edges to avoid experiencing large UV radiation fields. For the Solar System to have formed within a large star-forming region and remained relatively unaffected, the massive stars must either form at the centre of the cluster (Bonnell and Davies, 1998; Zinnecker, 1982; Testi et al., 2000; Bonnell et al., 2001), or mass segregation must occur rapidly due to initial conditions within the cluster (Allison et al., 2009; Moeckel and Bonnell, 2009).

Previous studies have explored spherical, centrally concentrated stellar profiles (Adams et al., 2006). However, observations show that star-forming regions

are composed of filamentary structures (André et al., 2010), and that stars inherit this spatial substructure. As previously explained, the dynamical evolution depends on the initial density, virial ratio, and spatial distribution. Therefore, simulations that adopt initial conditions that do not reflect the conditions of young star-forming regions will dynamically evolve differently to simulations which do. The extent to which the initial spatial profile of a star-forming region changes the UV field is unknown, but if the distribution of massive stars in the star-forming region is random to begin with, rather than centrally concentrated, this may change the range of UV fluxes stars experience.

How the initial spatial distribution of stars changes the rate of photoevaporation of discs due to massive stars ($\geq 15 M_{\odot}$) in clusters with different initial conditions was examined in Chapter 4, using the prescriptions from Scally and Clarke (2001), developed by Störzer and Hollenbach (1999), and Hollenbach et al. (2000). However, UV radiation was limited to only the most massive stars ($\geq 15 M_{\odot}$), and mass loss due to FUV radiation only occurred when stars were within 0.3pc of a massive star, which is based on the size of the FUV-dominated ionization bubble within the star forming region $\theta^1\text{C Ori}$. Calculating the background UV field created by every cluster member will give a more comprehensive view of the amount of FUV and EUV flux that protoplanetary discs are receiving.

The time taken for the photoionising massive stars to form will also affect UV fields and rates at which protoplanetary discs are dispersed. In the competitive accretion models previously mentioned (see Section 1.3.4), massive stars do not form simultaneously along with low mass stars, but slowly accumulate mass over time (Bonnell et al., 2001). Simulations have shown that it can take ~ 1 Myr for massive stars to form (Wang et al., 2010), reducing the amount of time that protoplanetary discs spend in proximity to photoionising sources (Dale et al., 2012, 2014). Hydrodynamical simulations of star forming regions also show that massive stars are responsible for blowing giant cavities (\sim pc-scale), or ‘bubbles’, within the the gas on short time scales (Dale et al., 2013). This removal of gas between stars will expose protoplanetary discs to the radiation from the massive stars. In these simulations, all stars form simultaneously and therefore the disc-hosting low-mass stars do not have this grace period, which could increase disc lifetimes. However, if there is a delay in the formation of massive stars in comparison to low mass stars, this could lead to protoplanetary discs spending considerable amounts of time protected from potentially harmful radiation fields.

Massive stars are responsible for the vast majority of UV radiation within star-forming regions. However, O-type stars are rare, as are massive star-forming regions. Far more common are star-forming regions containing a few B-type stars, for example IC 348, a cluster with ~ 420 stars with an age of 2.3 Myr. Approximately 60 per cent of stars within IC 348 host protoplanetary discs (Haisch et al., 2001; Luhman et al., 2003). The most massive stars within IC 348 have masses of $\sim 5 M_{\odot}$ (Luhman et al., 2016). Fig. 2.6, from Armitage (2000) which shows stellar EUV and FUV luminosity with mass, shows that stars with masses $< 15 M_{\odot}$ still produce significant amounts of FUV radiation, and therefore star forming environments such as IC 348 may not be quiescent, and in fact host UV fields that are strong enough to photoevaporate protoplanetary discs.

In this Chapter I present work which calculates the UV fields for star-forming regions that have different initial spatial distributions. I compare the median UV fields for the three different initial stellar profiles, briefly examine the effects of delaying feedback, and investigate the amount of UV radiation that is produced by different stellar types.

5.2 Method

Following the methods explained in Chapter 2, the median $1000 M_{\odot}$ star-forming region was selected from the Monte Carlo sampling of the CMF and IMF (Maschberger, 2013), resulting in the star-forming regions used in Chapter 4. The star forming regions were created with stellar densities of $100 M_{\odot} \text{pc}^{-3}$ (Bressert et al., 2010), and are sub-virial ($\alpha_{vir} = 0.3$), which, based on observations of present-day star-forming regions and models, reflects the initial conditions of these regions (Peretto et al., 2006; Arzoumanian et al., 2011; Foster et al., 2015). The initial median density for all star-forming regions is kept the same, so that the only difference between simulations is the amount of initial substructure. Each realisation of the star-forming region is created with a varying amount of substructure using the box-fractal method from Goodwin and Whitworth (2004): $D = 1.6$ (highly sub-structured), $D = 2.0$ (moderately sub-structured), and $D = 3.0$ (smooth).

Each actualisation of the star-forming region was then evolved for 10 Myr using the kira integrator within the Starlab environment, as described in Chapter 2. No binary or multiple stellar systems were included in these simulations, although the potential implication of binaries shall be discussed in Section 5.4. Twenty realisations of the same initial conditions were run to gauge the amount

of stochasticity in the amount of FUV and EUV flux that stars are receiving. These runs are identical apart from the random number seed used to assign the positions and velocities.

The EUV and FUV luminosities were calculated as a function of mass using values from [Armitage \(2000\)](#). These values were then applied to the corresponding stars within the star-forming regions, and the cumulative EUV and FUV flux that every star receives from the entire cluster was calculated. The FUV fluxes are expressed in units of G_0 , where $G_0 = 1$ corresponds to $F_{FUV} = 1.6 \times 10^{-3} \text{ erg s}^{-1} \text{ cm}^{-2}$, which is the background value for the ISM ([Habing, 1968](#)).

As previously mentioned, the time taken for the photoionising massive stars to form will also affect UV fields and rates at which protoplanetary discs are dispersed. Therefore, UV radiation is switched off for the first 0.5 Myr of every simulation, to mimic the effect of delaying massive star formation. However, this is likely a conservative estimate, as massive stars have been shown to blow cavities within gas shortly after formation ([Dale et al., 2013](#)).

The majority of studies to date have considered only the radiation produced by massive ($\geq 15 M_\odot$), or O-type, stars as they individually produce the most significant amount of radiation due to their mass. However, the presence of O-type stars in star forming regions is rare; much more common are B-type stars (see Fig. 1.3.2). Stars with masses $< 15 M_\odot$ still produce large amounts of UV radiation, especially FUV (see Fig. 2.6). B-type stars are also more common, with the $\sim 1000 M_\odot$ cluster created for these calculations containing 5 O-type stars and 59 B-type stars.

To understand the total contribution from various mass ranges of stars, the UV radiation from every single star is considered. Stars are also split by mass into O-type ($\geq 15 M_\odot$) and B-type stars ($3 < M_* < 15 M_\odot$), and the amount of flux that each star receives from the rest of the cluster is recorded for each timestep. If a non-negligible portion of UV radiation comes from B-type stars, this has been neglected in most studies, and therefore should be considered. If the majority comes from O-type stars, then the only factor dictating disc lifetimes when considering external processes are massive stars.

5.3 Results

I focus on the specific $1000 M_{\odot}$ star-forming region from Chapter 4, which contains 5 massive stars ($M_* > 15M_{\odot}$); 43.2, 32.7, 25.7 and two $17 M_{\odot}$. The cluster also contains 59 stars ranging between 3 and $15 M_{\odot}$. I focus on the results for a cluster with an initial stellar density of $\sim 100 M_{\odot} \text{ pc}^{-3}$. A range of fractal dimensions for varying amounts of substructure are used: $D = 1.6$ (highly sub-structured), $D = 2.0$ (moderately sub-structured), and $D = 3.0$ (smooth).

I present the results from varying initial spatial distributions within star-forming regions, and show how the total UV flux that stars receive from the surrounding environment varied based on this substructure. In Section 5.3.2, the results for stars in a star-forming region where external UV radiation has been delayed by 0.5 Myr are presented. The difference in the amount of UV radiation produced by B-type ($3 \leq M_* < 15 M_{\odot}$) stars in comparison to O-type ($\geq 15 M_{\odot}$) stars is also examined in Section 5.3.3.

5.3.1 FUV and EUV fluxes

First the results from the simulations of the star-forming region are presented, where each simulation has a different initial spatial distribution; $D = 1.6, 2.0,$ and 3.0 . Table 5.1 shows the average \log_{10} values for FUV and EUV fluxes that the median star receives at several timesteps throughout the 10 Myr simulations.

Fig. 5.1 shows the average amount of FUV and EUV flux ($\text{erg s}^{-1} \text{ cm}^{-2}$) that every star receives from the surrounding environment across the 20 simulation runs. During the first time step, when the density is $\sim 100 M_{\odot} \text{ pc}^{-3}$, stars within highly substructured clusters ($D = 1.6$) receive ~ 21 per cent of the FUV flux that stars in clusters with initially smooth, spherical ($D = 3.0$) spatial distributions receive. The results are similar for EUV radiation, with the amount of EUV flux that stars in highly substructured receive being ~ 16 per cent of that which stars in smooth, spherical clusters receive.

The maximum amount of EUV and FUV flux that stars receive is at ~ 2 Myr for all different initial spatial distributions. The density of the cluster increases within the first few Myr, due to two-body relaxation, and because the cluster is initially collapsing ($\alpha_{vir} = 0.3$, sub-virial). By 10 Myr, stars within highly substructured clusters receive ~ 35 per cent less FUV flux and ~ 46 per cent less EUV flux than at 2 Myr. Stars within smooth, spherical clusters receive ~ 25 per cent less FUV flux and ~ 21 per cent less EUV flux at 10 Myr than at 2 Myr.

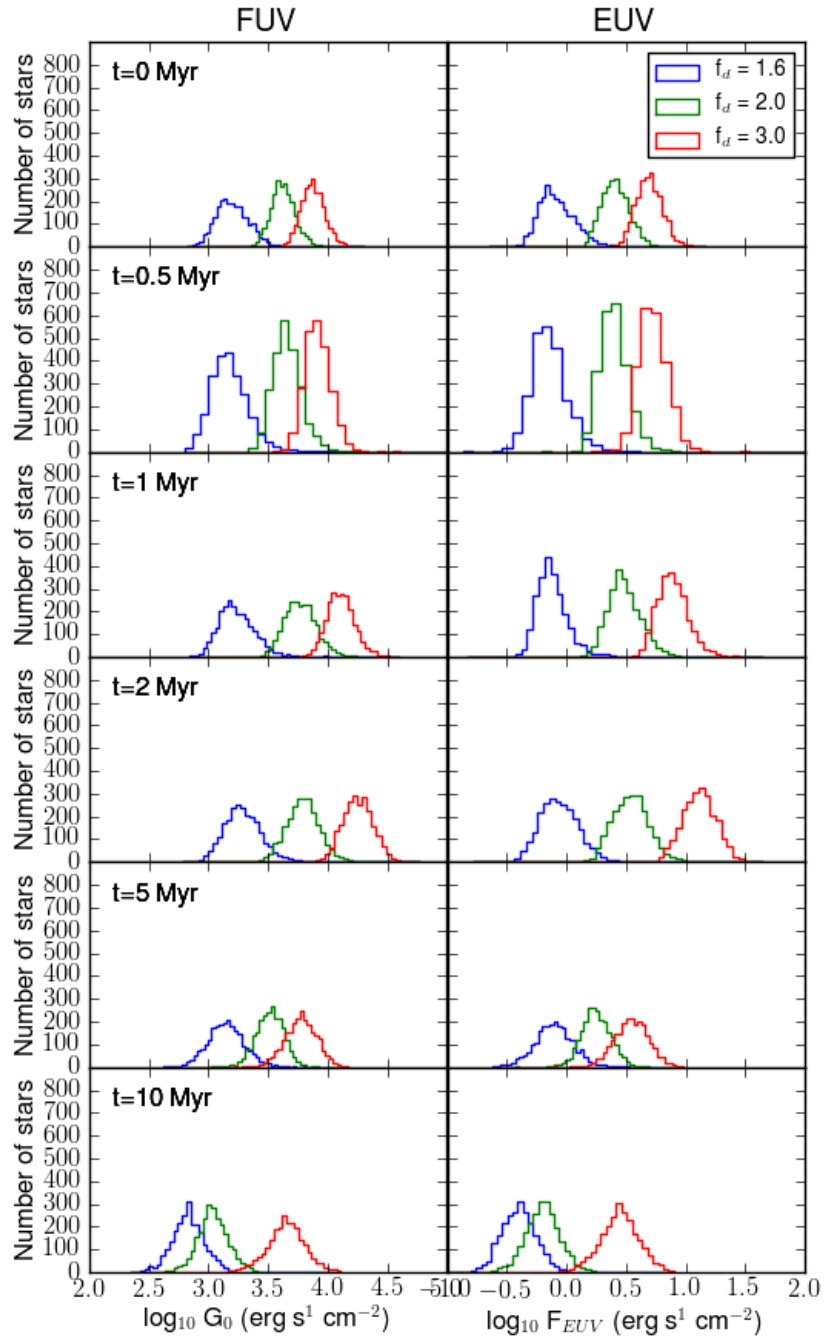


FIGURE 5.1: The average FUV and EUV radiation that stars receive within a $1000 M_{\odot}$ cluster, which has an initial density of $100 M_{\odot} \text{pc}^{-3}$ and is sub-virial ($\alpha_{vir} = 0.3$), for a selection of timesteps. Each coloured line represents a different fractal dimension.

TABLE 5.1: The average FUV and EUV fluxes that the median star receives at each timestep for stars within $1000 M_{\odot}$ star-forming regions; all have the same IMF, initial density ($\sim 100 M_{\odot}$), and virial ratio ($\alpha_{vir} = 0.3$, or sub-virial). The amount of substructure is varied from highly substructured ($D = 1.6$) to smooth and spherical ($D = 3.0$). The minimum and maximum FUV and EUV fluxes are also shown for each timestep.

UV radiation with time for B-type stars						
	FUV (G_0)			EUV ($ergs^{-1}cm^{-2}$)		
Time (Myr)	1.6	2.0	3.0	1.6	2.0	3.0
0	3.19	3.62	3.87	-0.10	0.40	0.69
0.5	3.16	3.65	3.90	-0.16	0.39	0.71
1	3.22	3.76	4.10	-0.14	0.47	0.88
2	3.27	3.79	4.25	-0.07	0.54	1.11
5	3.14	3.51	3.77	-0.11	0.24	0.54
10	2.82	3.03	3.65	-0.41	-0.20	0.44

Integrated over 10 Myr, the total amount of FUV flux that stars receive in highly substructured clusters in comparison to smooth, spherical clusters is ~ 40 per cent. Integrated over 10 Myr, the total amount of EUV flux that stars in highly substructured clusters receive over the entire 10 Myr is ~ 45 per cent that which stars in smooth, spherical clusters receive.

Stars within highly substructured clusters consistently receive less FUV and EUV flux than stars in smooth clusters. Fig 2.2 shows two spatial distributions of the stars within the $\sim 1000 M_{\odot}$ cluster. Fig 2.2(a) shows a highly substructured cluster with the same initial density as the smooth, spherical cluster in Fig 2.2(b). The ranges of separations between stars in panels (a) and (b) are similar, however, stars in panel (a) have a significantly larger average separation due to their clumpy distribution. This larger separation reduces the amount of flux received from all other stars within the cluster.

5.3.2 Feedback

To mimic the effects of delaying massive star formation due to competitive accretion, and thereby delaying the creation of cavities within the star-forming region which will expose stars to the UV radiation from all other cluster members, the

fluxes that stars receive from all other stars are only calculated from 0.5 Myr onwards. The same $1000 M_{\odot}$ cluster is used, along with the three different initial spatial substructures.

The amount of FUV flux that stars within highly substructured clusters receive within the first time step is ~ 15 per cent of that of stars in a smooth, spherical cluster receive. Integrated over 10 Myr, the total amount of radiation that stars in highly substructured clusters receive is ~ 46 per cent of what stars within smooth, spherical clusters receive. For EUV radiation it is similar, with stars in highly substructured clusters receiving ~ 10 per cent of the EUV flux during the first timestep at 0.5 Myr that stars in smooth, spherical clusters receive. Integrated over 10 Myr, the total amount of EUV flux that stars in highly substructured clusters receive is ~ 38 per cent that which stars in smooth, spherical clusters receive.

5.3.3 Mass of stars

Fig. 5.2 shows the average amount of FUV and EUV flux each star receives from all 20 runs of each simulation. The UV radiation received has been split by mass for O-type ($\geq 15 M_{\odot}$, see Table 5.2) and B-type ($3 \leq M_{*} < 15 M_{\odot}$, see Table 5.3) stars.

The percentage of FUV flux that stars within a highly substructured ($D = 1.6$) cluster receive from B-type stars in comparison to O-type stars is ~ 5 per cent for the first time-step. For smooth, spherical ($D = 3.0$) clusters, the initial difference is slightly larger, with ~ 4 per cent of FUV radiation coming from B-type stars in comparison to O-type. Stars receive very small amounts of EUV flux from B-type stars in comparison to O-type stars. FUV radiation is thought to be the primary driver behind the dispersal of protoplanetary discs due to external photoevaporation, with EUV radiation causing significant mass loss only when stars are within close proximity. The contribution of UV flux from B-type stars is likely still significant enough to affect protoplanetary discs, even though the amount of EUV radiation B-type stars produce is small.

Integrated over the 10 Myr simulation, the total amount of radiation that the median star receives from B-type stars in comparison to O-type stars in highly substructured clusters is ~ 4 per cent (see Table 5.4). The difference in smooth, spherical clusters is very similar, with stars receiving ~ 3.8 per cent of FUV radiation from B-type stars in comparison to O-type stars. The amount of EUV flux that stars receive from B-type stars in highly substructured clusters in comparison to O-type stars is ~ 0.001 per cent. In smooth, spherical clusters, the amount

TABLE 5.2: The median FUV and EUV fluxes produced by O-type stars ($M_* \geq 15 M_\odot$) at each timestep for stars within a $1000 M_\odot$ star-forming region, all have the same IMF, initial density ($\sim 100 M_\odot$), and virial ratio ($\alpha_{vir} = 0.3$, or sub-virial). The amount of substructure is varied from highly substructured ($D = 1.6$) to smooth and spherical ($D = 3.0$). The minimum and maximum FUV and EUV fluxes are also shown for each timestep.

UV radiation with time for O-type stars						
	FUV (G_0)			EUV ($ergs^{-1}cm^{-2}$)		
Time (Myr)	1.6	2.0	3.0	1.6	2.0	3.0
0	3.14	3.56	3.85	-2.82	0.39	0.70
0.5	3.05	3.58	3.87	-0.17	0.38	0.71
1	3.10	3.68	4.07	-0.15	0.47	0.88
2	3.19	3.75	4.23	-0.08	0.53	1.11
5	3.10	3.48	3.73	-0.11	0.24	0.54
10	2.78	2.99	3.62	-0.41	-0.20	0.44

of EUV flux that stars receive from B-type stars in comparison to O-type stars is ~ 0.1 per cent.

The B-type stars produce a background FUV field of $\sim 300 G_0$ in smooth, spherical clusters in the first timestep. For clusters which are initially highly substructured, the FUV field is $\sim 50 G_0$. [Haworth et al. \(2018a\)](#) show that clusters with FUV fields of ~ 10 – $100 G_0$ can cause 200 AU discs to disperse within 0.1–1 Myr, depending on disc properties such as surface density.

5.4 Discussion

These simulations are set up that represent observations of star-forming regions containing massive stars ([Larson, 1981](#); [Foster et al., 2015](#)). For stars within a $1000 M_\odot$ cluster with an initial density of $\sim 100 M_\odot pc^{-3}$ that are sub-virial ($\alpha_{vir} = 0.3$), the initial spatial substructure of the star-forming region will affect the amount of UV radiation that stars receive, and therefore will change the rates at which protoplanetary discs are photoevaporated.

Stars within highly substructured clusters consistently receive, on average, less UV radiation than stars within smooth, spherical clusters. This trend continues throughout the duration of the simulation, resulting in stars within substructured clusters receiving lower amounts of FUV and EUV radiation (~ 40 and ~ 46

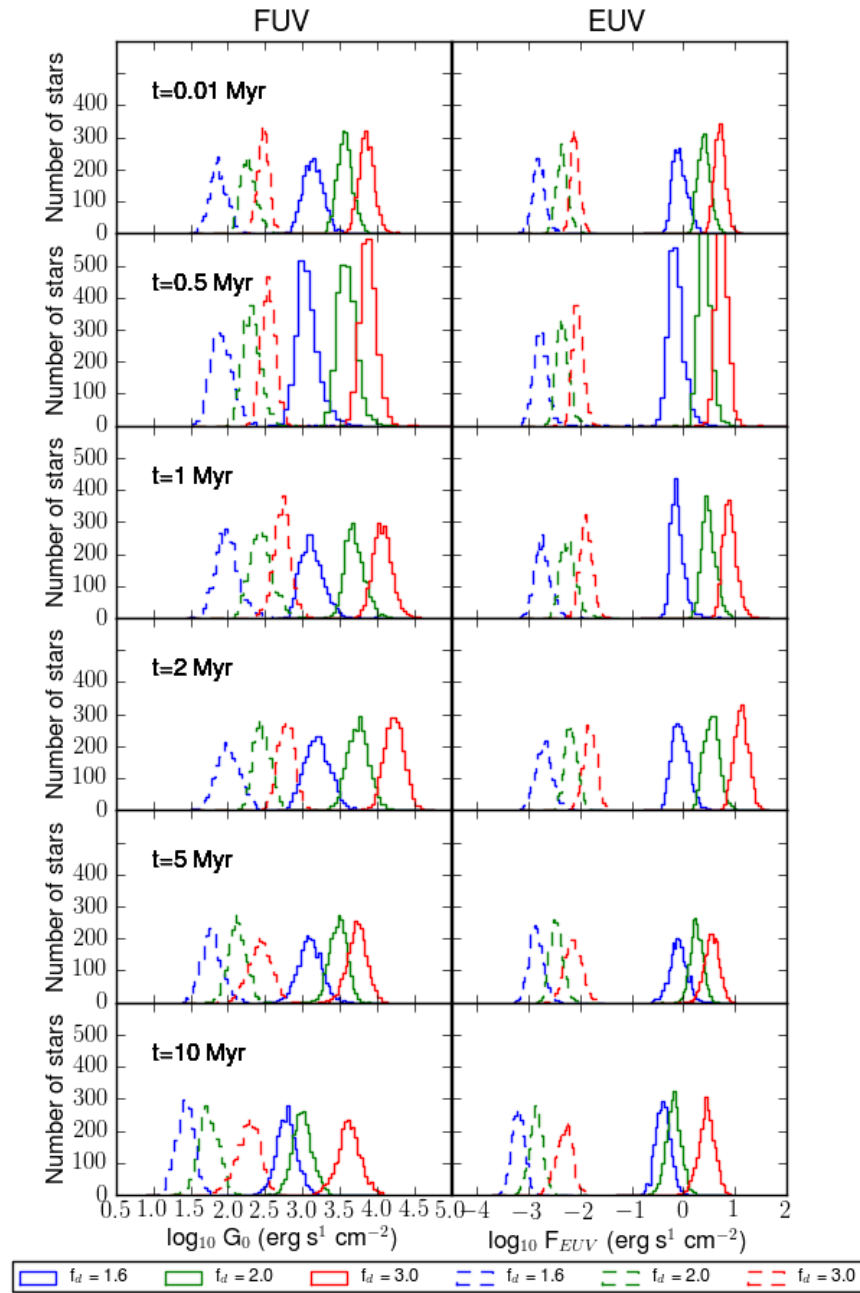


FIGURE 5.2: The average FUV and EUV flux that every single star receives from O-type (solid lines) and B-type stars (dashed lines) within the $1000 M_{\odot}$ cluster at each timestep. The radiation from stars has been delayed by 0.5 Myr to mimic the late formation of massive stars and subsequent delay in bubble formation. Each different coloured line represents an initial fractal dimension ($f_d = 1.6, 2.0, 3.0$).

TABLE 5.3: The median FUV and EUV fluxes produced by B-type stars ($3 \leq M_* < 15 M_\odot$) at each timestep for stars within a $1000 M_\odot$ star-forming region, all have the same IMF, initial density ($\sim 100 M_\odot$), and virial ratio ($\alpha_{vir} = 0.3$, or sub-virial). The amount of substructure is varied from highly substructured ($D = 1.6$) to smooth and spherical ($D = 3.0$).

UV radiation with time for B-type stars						
Time (Myr)	FUV (G_0)			EUV ($ergs^{-1}cm^{-2}$)		
	1.6	2.0	3.0	1.6	2.0	3.0
0	1.86	2.26	2.47	-2.82	-2.37	-2.12
0.5	1.90	2.31	2.54	-2.78	-2.36	-2.06
1	1.98	2.43	2.73	-2.75	-2.26	-1.91
2	1.99	2.45	2.78	-2.72	-2.20	-1.82
5	1.77	2.12	2.43	-2.87	-2.48	-2.16
10	1.43	1.73	2.27	-3.22	-2.87	-2.31

TABLE 5.4: The percentage of FUV and EUV flux that the median star receives from B-type stars in comparison to O-type stars, across all 20 runs of the three simulations of the $1000 M_\odot$ star-forming regions. The star-forming regions all have the same IMF, initial density ($\sim 100 M_\odot$), and virial ratio ($\alpha_{vir} = 0.3$, or sub-virial). The amount of substructure is varied from highly substructured ($D = 1.6$) to smooth and spherical ($D = 3.0$).

UV radiation from B-type stars in comparison to O-type stars						
Time (Myr)	FUV (%)			EUV (%)		
	$\alpha_{vir} = 1.6$	$\alpha_{vir} = 2.0$	$\alpha_{vir} = 3.0$	$\alpha_{vir} = 1.6$	$\alpha_{vir} = 2.0$	$\alpha_{vir} = 3.0$
0	5.25	5.01	4.17	0	0.17	0.15
0.5	5.50	4.42	3.68	0.18	0.16	0.14
1	5.44	4.68	3.83	0.19	0.17	0.14
2	4.64	4.22	3.71	0.16	0.15	0.13
5	4.21	3.85	3.68	0.15	0.14	0.13
10	4.08	3.89	3.79	0.14	0.14	0.14

per cent respectively) in comparison to their counterparts within smooth clusters, and therefore discs in highly substructured clusters may survive for longer periods of time. As the EUV mass loss rate scales as $\sqrt{F_{EUV}}$, a large decrease in the amount of F_{EUV} received does not reflect as large a decrease in the amount of mass loss that will occur. However, FUV mass loss does not have such a relationship. Therefore, if different spatial distributions do impact the rate at which protoplanetary discs are dispersed due to external photoevaporation, FUV radiation will have the largest impact.

However, this is contrary to the results found in Chapter 4, where protoplanetary discs within highly substructured regions were photoevaporated at faster rates than those in smooth, spherical clusters. Because the contribution of every single star is considered within this Chapter, rather than focusing specifically on the contribution of FUV and EUV radiation of O-type stars, the results have dramatically changed. When considering specifically O-type stars, and limiting the FUV radiation to a radius of 0.3pc, stars within highly substructured clusters have a greater chance of being within the sphere of influence of a massive star in comparison to stars within smooth clusters, by virtue of clustering. However, when the cumulative effect of the entire cluster is considered, the initial average separation of stars in highly substructured clusters is much greater than that of stars in smooth clusters (see Fig. 2.2).

Previous studies considering the effects of UV radiation fields on protoplanetary disc dispersal have focused on discs within clusters that reflect present day conditions of star-forming regions (Sclally and Clarke, 2001; Adams et al., 2004, 2006; Fatuzzo and Adams, 2008; Winter et al., 2018a). However, star-forming regions are observed to be initially substructured, and using present-day spatial and kinematic distributions to model star clusters will not accurately replicate the dynamical history of star-forming regions (Parker et al., 2014b), or the amount of UV radiation that protoplanetary discs receive over time. For models including FUV background fields, the initial substructure of the cluster will impact the amount of UV radiation that discs receive, and should be taken into consideration.

Mimicking the effects of delaying massive star formation and therefore delaying UV radiation until 0.5 Myr increases the difference in the total amount of FUV and EUV flux that stars receive, depending on their star-forming environment. Stars within highly substructured clusters receive in total ~ 46 per cent less FUV flux and ~ 38 per cent less EUV flux than stars within smooth, spherical clusters. Protoplanetary discs within highly substructured star-forming regions,

even with a delay in UV radiation, still therefore receive less than stars within smooth, spherical clusters.

Haworth et al. (2018a) show that for discs around low-mass stars, external photoevaporation can be effective down to small radii (<50 AU), for UV fields that are as weak as $10G_0$. When compared to the FUV fields discussed in Haworth et al. (2018a), clusters with background FUV fields of $100G_0$ can still significantly truncate protoplanetary discs and cause large amounts of mass loss. Protoplanetary discs with radii of 100–200 AU could be completely photoevaporated within 1 Myr, depending on the properties of the protoplanetary disc. Even at 10 Myr, the average amount of FUV flux that the median star receives within all clusters is greater than $100G_0$, a strong enough FUV field to cause large amounts of mass loss in protoplanetary discs due to photoevaporation.

As discussed in Section 1.3.8, external photoevaporation can be responsible for mass loss within protoplanetary discs. B-type stars within the simulated clusters presented here produce a background FUV field of $\sim 300 G_0$ in smooth, spherical clusters within the first timestep. For clusters which are initially highly substructured, the FUV field is $\sim 50 G_0$. Again, FUV fields with strengths this high are still significant enough to potentially disperse protoplanetary discs. However, over 10 times the number of B-type stars are required to produce ~ 5 per cent of UV radiation that O-type stars produce, and therefore protoplanetary discs within star-forming regions that contain only a few B-type stars may not be subjected to UV fields that are strong enough to cause large amounts of mass loss. As star-forming regions containing B-type stars are some of the most common in the solar neighbourhood, such as IC 348 (Haisch et al., 2001; Luhman et al., 2003), simulations replicating these conditions should be analysed.

All stars within the simulated star-forming region produced UV radiation, resulting in ~ 10 per cent of the radiation coming from stars with masses $<3 M_\odot$. Fig 2.6 shows that stars $\sim M_* > 2 M_\odot$ do not produce any UV radiation, therefore this is likely an overestimate. However, separating the masses of stars into O and B-type stars shows that the amount of UV flux that stars receive still greatly depends on the initial spatial distribution. In future work, the amount of UV radiation that low mass stars produce will be more realistically calculated.

To understand the extent to which the FUV fields within these clusters can affect protoplanetary discs, realistic models need to be applied, such as the FRIED models from Haworth et al. (2018a). By applying realistic protoplanetary disc models that account for changes within the disc with time, and the extent to which protoplanetary discs are dispersed in star-forming environments due to

different initial spatial distributions for stars can be examined.

Fatuzzo and Adams (2008) have shown that there is considerable variance in the UV field strength when randomly sampling the IMF. The one specific sampling of the IMF presented here shows that a star-forming region with similar number of massive stars to the ONC creates UV fields that are potentially strong enough to inhibit planet formation. Star-forming regions with a differing IMFs should also be considered in future, to see how the effects of substructure change depending on the number and mass range of massive stars. The mass and IMF of star-forming regions should also be varied, to see whether varying the initial substructure of a star-forming regions is consistently an important factor in determining the amount of UV radiation that stars receive.

Star-forming regions which are initially highly substructured can become smooth and centrally concentrated within a few Myr. Massive stars, due to two-body relaxation, can sink to the centre of clusters over time. The location of massive stars within the star-forming region will affect the amount of UV radiation that stars receive. It is also a common occurrence in simulations of dense star-forming regions that massive stars are ejected from the centre of the cluster when mass segregation occurs (Allison et al., 2010; Oh and Kroupa, 2016). These ejected massive stars may affect protoplanetary discs that are in the path of their trajectory, and therefore individual simulations where massive stars are ejected should be analysed.

5.5 Conclusions

The amount of UV radiation that stars receive has been calculated using the N -body simulations detailed in Chapter 2 of an evolving $1000 M_{\odot}$ star-forming region which has three different initial spatial distributions. Suites of simulations were run, using conditions that are observed in young star-forming regions.

i) The initial spatial distribution of stars greatly affects the amount of UV radiation that stars receive. Stars within initially highly substructured star-forming regions consistently receive less UV radiation than their counterparts within smooth star-forming regions, even after 10 Myr. The UV field increases during the first few Myr, due to two-body relaxation, which leads to an increase in density. After a few Myr, the density will decrease, and as the density decreases the UV field also decreases. However, the UV field strengths at 10 Myrs are still strong enough to potentially cause significant damage to protoplanetary discs. Stars

within highly substructured star-forming regions receive considerably less UV radiation than their counterparts in smooth clusters.

ii) Mimicking the effect of delaying massive star formation, and delaying UV radiation for 0.5 Myr, reduces the total amount of radiation that stars receive. Stars within substructured clusters still receive less than stars within smooth clusters, as the initial substructure has not yet been wiped out by two-body relaxation.

iii) The types of stars that produce UV radiation should be considered. Previous studies have mostly focused on O-type stars, however B-type stars outnumber O-type stars greatly. Due to the sheer number of B-type stars present, the UV field they produce is still large, and may still be able to disperse protoplanetary discs within short timescales.

Chapter 6

Conclusions

6.1 Main results

I have performed N -body simulations of star clusters with the aim of exploring initial conditions of star forming regions and how changing these affects various properties, with the primary aim of understanding how the birth environment of stars can impact planet formation.

6.1.1 Supernova enrichment of planetary systems in low-mass clusters

In Chapter 3, the effects of SN enrichment within low mass clusters ($\sim 100 M_{\odot}$) was investigated. Using clusters with one or two massive ($\geq 15 M_{\odot}$) stars, and a range of initial conditions, the number of unperturbed, enriched stars with masses similar to that of the Sun ($0.8 - 1.2 M_{\odot}$) was found. No initial set of conditions (virial ratio and fractal dimension) significantly increased the rate of enriched stars.

A default model, using realistic initial conditions of star forming regions ($\alpha_{\text{vir}} = 0.3$, $r_F = 1.0$ pc, $D = 1.6$) and which contained two massive stars, resulted in ~ 0.5 per cent of stars that were unperturbed becoming enriched, similar to the fraction of enriched G-dwarf stars found by [Parker et al. \(2014a\)](#). Due to the significant fraction of low-mass clusters containing massive stars, these could be viable birth environments for enriched planetary systems, and relax the constraints placed on the birth environment of the Solar System.

6.1.2 Rapid destruction of protoplanetary discs due to external photoevaporation

The mass loss of protoplanetary discs due to external photoevaporation in N -body simulations was calculated using the prescriptions from [Haisch et al. \(2001\)](#). N -body simulations of star forming regions with masses of 1000 and 100 M_{\odot} were evolved for 10 Myr. Initial conditions of the star forming regions were varied, such as the sub-structure ($f_d = 1.6, 2.0,$ and 3.0), virial ratio ($\alpha_{vir} = 0.3, 0.5,$ and 0.7), and density (10 and $100 M_{\odot} \text{pc}^{-3}$), to see how this affected the rate at which protoplanetary discs were photoevaporated by external UV radiation from massive stars. The parameter that most affected the rate at which discs dispersed was the initial density of the star forming region. Protoplanetary discs within simulated regions that mimic observed conditions of present-day star forming regions are dispersed due to external photoevaporation within very short time scales. These timescales are significantly shorter than what is suggested in observational studies ([Haisch et al., 2001](#)).

The initial spatial distribution and virial ratio of the star-forming region also affect the rates that discs are dispersed due to external photoevaporation. However, the degree to which these conditions affect disc dispersal rates depends on the initial density. Star-forming regions that are moderately dense ($\sim 100 M_{\odot} \text{pc}^{-3}$) experience little difference in disc dispersal rates when conditions are changed, whereas low-density ($\sim 10 M_{\odot} \text{pc}^{-3}$) regions do experience appreciable differences.

The rapid rate at which protoplanetary discs are being dispersed within these simulations makes planet formation difficult in such short timescales. However, planet-hosting stars seem universal, implying that protoplanetary discs in the majority of cases survive long enough to form planets. This presents us with three possible scenarios:

i) The majority of planets do not form in moderately dense star-forming regions ($\sim 100 M_{\odot} \text{pc}^{-3}$), and rather form in low-density clusters with no massive stars present.

ii) If some planets do form in dense, clustered environments containing massive stars (such as the ONC), then giant planet formation must happen on very short time scales (less than 1 – 2 Myr), or be confined to discs with very small radii (< 30 AU).

iii) The current calculations of mass-loss in discs due to external photoevaporation severely overestimate the detrimental effects of EUV and FUV radiation.

6.1.3 UV background fields in clusters

The amount of UV radiation that stars receive has been calculated using the same N -body simulations of an evolving $1000 M_{\odot}$ star-forming region which has three different initial spatial distributions. Suites of simulations were run, using conditions observed in young star-forming regions. These simulations are then compared to UV field values found by other studies (Fatuzzo and Adams, 2008; Haworth et al., 2018a).

The initial spatial distribution of stars greatly affects the amount of UV radiation that stars receive. Stars within highly substructured ($D = 1.6$) clusters receive less than 50 per cent of the radiation that stars within smooth clusters receive. Delaying UV radiation for 0.5 Myr reduces the total amount of radiation that stars receive, however stars within substructured clusters still receive less than stars within smooth clusters. B-type stars produce significant amounts of UV radiation (~ 5 per cent of that which O-type stars produce), potentially enough to damage protoplanetary discs within star-forming regions. To understand the full impact of varying the initial spatial distribution of stars, the IMF, mass, and density of the star-forming region should be varied within these simulations.

Chapter 7

Future work

The work in this thesis has explored how certain initial conditions of star-forming regions can affect planet formation. However, there are still many avenues of research that remain unexplored, and many improvements that can be made to the simulations presented here to achieve more realistic results.

Enrichment of protoplanetary discs within low-mass ($\sim 100 M_{\odot}$) clusters is feasible, however the range of distances that a protoplanetary disc is allowed to inhabit during the SN event is likely very conservative. [Lichtenberg et al. \(2016b\)](#) calculate the yield of ^{26}Al and ^{60}Fe from SN explosions and, using a simplistic disc profile, determine how much nuclear enrichment protoplanetary discs receive. They show that the likelihood of enrichment levels similar to or higher than that of the Solar System can vary considerably depending on the initial morphology of the cluster, and that the range of distances over which a protoplanetary disc can become enriched also varies. This is likely to relax the distances at which protoplanetary discs can be enriched. Applying these techniques to low-mass star-forming regions containing massive stars will give more realistic results, and may increase the percentage of enriched protoplanetary discs.

Planet formation is almost universal, therefore planet formation must be easily achieved. However, the rate at which protoplanetary discs are dispersed within these simulations is faster than the timescales on which giant planets can form. Much of the work simplifies processes which are far more complicated than presented here. Models which use realistic disc physics need to be combined with these simulations that more closely resemble observations of young star-forming regions to see if discs are being dispersed within these short timescales. [Haworth et al. \(2018a\)](#) present an open access grid of thousands of externally evaporating protoplanetary discs, with a range of protoplanetary disc radii (1– 400 AU), disc masses, UV field strength ($10\text{--}10^4 G_0$) and stellar masses ($0.05\text{--}1.9 M_{\odot}$). Using the UV field strengths calculated in Chapter 5, the FRIED protoplanetary disc mass

loss grid should be applied to each star. With these realistic values of disc mass loss, a better understanding of the rate at which protoplanetary discs are being dispersed within substructured clusters can be achieved.

Within the simulations in this thesis, binaries and multiple systems are not turned on, however the majority of stars are thought to form in multiple systems (Eggleton and Tokovinin, 2008; Goodwin, 2010), and therefore need be considered. The external effects of UV radiation from low-mass stars is minimal, however stars within binaries or multiples may be in close enough proximity that the radiation from the other star(s) needs to be considered. SeBa provides information for the evolution of binaries, taking into account the eccentricity of the binary and mass transfer between stars. Using models of binary evolution and seeding primordial binary and multiple star systems, the flux that protoplanetary discs receive and the truncation that may occur in tight binaries can be calculated. Considering protoplanetary discs within binary or multiple systems brings another set of difficulties. Protoplanetary discs can exist around each individual star within a binary, or around the entire system. With the existence of multiple discs within the stellar system, mass accretion from one to another may occur. The semi-major axis of the binaries, and whether this aligns with the protoplanetary discs also needs to be considered.

Bibliography

- S. J. Aarseth. *Gravitational N-Body Simulations*. October 2003.
- F. C. Adams. The Birth Environment of the Solar System. *ARA&A*, 48:47–85, September 2010. doi: 10.1146/annurev-astro-081309-130830.
- F. C. Adams and P. C. Myers. Modes of Multiple Star Formation. *ApJ*, 553:744–753, June 2001. doi: 10.1086/320941.
- F. C. Adams, D. Hollenbach, G. Laughlin, and U. Gorti. Photoevaporation of Circumstellar Disks Due to External Far-Ultraviolet Radiation in Stellar Aggregates. *ApJ*, 611:360–379, August 2004. doi: 10.1086/421989.
- F. C. Adams, E. M. Proszkow, M. Fatuzzo, and P. C. Myers. Early Evolution of Stellar Groups and Clusters: Environmental Effects on Forming Planetary Systems. *ApJ*, 641:504–525, April 2006. doi: 10.1086/500393.
- Fred C. Adams and Marco Fatuzzo. A Theory of the Initial Mass Function for Star Formation in Molecular Clouds. *ApJ*, 464:256, Jun 1996. doi: 10.1086/177318.
- J. C. Adams. Explanation of the observed irregularities in the motion of Uranus, on the hypothesis of disturbance by a more distant planet; with a determination of the mass, orbit, and position of the disturbing body. *MNRAS*, 7:149–152, November 1846. doi: 10.1093/mnras/7.9.149.
- E. Agol, J. Steffen, R. Sari, and W. Clarkson. On detecting terrestrial planets with timing of giant planet transits. *MNRAS*, 359:567–579, May 2005. doi: 10.1111/j.1365-2966.2005.08922.x.
- Eric Agol and Daniel C. Fabrycky. *Transit-Timing and Duration Variations for the Discovery and Characterization of Exoplanets*, page 7. 2018. doi: 10.1007/978-3-319-55333-7_7.
- R. Alexander, I. Pascucci, S. Andrews, P. Armitage, and L. Cieza. The Dispersal of Protoplanetary Disks. *Protostars and Planets VI*, pages 475–496, 2014. doi: 10.2458/azu_uapress_9780816531240-ch021.

- M. Ali-Dib, O. Mousis, J.-M. Petit, and J. I. Lunine. The Measured Compositions of Uranus and Neptune from their Formation on the CO Ice Line. *ApJ*, 793:9, September 2014. doi: 10.1088/0004-637X/793/1/9.
- R. L. Allen, G. M. Bernstein, and R. Malhotra. The Outer Edge of the Solar System. In *American Astronomical Society Meeting Abstracts*, volume 32 of *Bulletin of the American Astronomical Society*, page 1447, December 2000.
- R. J. Allison, S. P. Goodwin, R. J. Parker, R. de Grijs, S. F. Portegies Zwart, and M. B. N. Kouwenhoven. Dynamical Mass Segregation on a Very Short Timescale. *ApJ*, 700:L99–L103, August 2009. doi: 10.1088/0004-637X/700/2/L99.
- R. J. Allison, S. P. Goodwin, R. J. Parker, S. F. Portegies Zwart, and R. de Grijs. The early dynamical evolution of cool, clumpy star clusters. *MNRAS*, 407: 1098–1107, September 2010. doi: 10.1111/j.1365-2966.2010.16939.x.
- Y. Amelin, A. Kaltenbach, and C. H. Stirling. The U-Pb Systematics and Cooling Rate of Plutonic Angrite NWA 4590. In *Lunar and Planetary Science Conference*, volume 42 of *Lunar and Planetary Inst. Technical Report*, page 1682, March 2011.
- D. L. Anderson and R. L. Kovach. The composition of the terrestrial planets. *Earth and Planetary Science Letters*, 3:19–24, 1967. doi: 10.1016/0012-821X(67)90005-2.
- D. R. Anderson, C. Hellier, M. Gillon, A. H. M. J. Triaud, B. Smalley, L. Hebb, A. Collier Cameron, P. F. L. Maxted, D. Queloz, R. G. West, S. J. Bentley, B. Enoch, K. Horne, T. A. Lister, M. Mayor, N. R. Parley, F. Pepe, D. Pollacco, D. Ségransan, S. Udry, and D. M. Wilson. WASP-17b: An Ultra-Low Density Planet in a Probable Retrograde Orbit. *ApJ*, 709:159–167, January 2010. doi: 10.1088/0004-637X/709/1/159.
- P. André, A. Men'shchikov, S. Bontemps, V. Könyves, F. Motte, N. Schneider, P. Didelon, V. Minier, P. Saraceno, D. Ward-Thompson, J. di Francesco, G. White, S. Molinari, L. Testi, A. Abergel, M. Griffin, T. Henning, P. Royer, B. Merín, R. Vavrek, M. Attard, D. Arzoumanian, C. D. Wilson, P. Ade, H. Aussel, J.-P. Baluteau, M. Benedettini, J.-P. Bernard, J. A. D. L. Blommaert, L. Cambrésy, P. Cox, A. di Giorgio, P. Hargrave, M. Hennemann, M. Huang, J. Kirk, O. Krause, R. Launhardt, S. Leeks, J. Le Pennec, J. Z. Li, P. G. Martin, A. Maury, G. Olofsson, A. Omont, N. Peretto, S. Pezzuto, T. Prusti, H. Roussel, D. Russeil, M. Sauvage, B. Sibthorpe, A. Sicilia-Aguilar, L. Spinoglio, C. Waelkens,

- A. Woodcraft, and A. Zavagno. From filamentary clouds to prestellar cores to the stellar IMF: Initial highlights from the Herschel Gould Belt Survey. *A&A*, 518:L102, July 2010. doi: 10.1051/0004-6361/201014666.
- S. M. Andrews, K. A. Rosenfeld, A. L. Kraus, and D. J. Wilner. The Mass Dependence between Protoplanetary Disks and their Stellar Hosts. *ApJ*, 771:129, July 2013. doi: 10.1088/0004-637X/771/2/129.
- M. Ansdell, J. P. Williams, N. van der Marel, J. M. Carpenter, G. Guidi, M. Hogerheijde, G. S. Mathews, C. F. Manara, A. Miotello, A. Natta, I. Oliveira, M. Tazzari, L. Testi, E. F. van Dishoeck, and S. E. van Terwisga. ALMA Survey of Lupus Protoplanetary Disks. I. Dust and Gas Masses. *ApJ*, 828:46, September 2016. doi: 10.3847/0004-637X/828/1/46.
- M. Ansdell, J. P. Williams, C. F. Manara, A. Miotello, S. Facchini, N. van der Marel, L. Testi, and E. F. van Dishoeck. An ALMA Survey of Protoplanetary Disks in the σ Orionis Cluster. *AJ*, 153:240, May 2017. doi: 10.3847/1538-3881/aa69c0.
- M. Ansdell, J. P. Williams, L. Trapman, S. E. van Terwisga, S. Facchini, C. F. Manara, N. van der Marel, A. Miotello, M. Tazzari, M. Hogerheijde, G. Guidi, L. Testi, and E. F. van Dishoeck. ALMA Survey of Lupus Protoplanetary Disks II: Gas Disk Radii. *ArXiv e-prints*, March 2018.
- P. J. Armitage. Suppression of giant planet formation in stellar clusters. *A&A*, 362:968–972, October 2000.
- P. J. Armitage. *Astrophysics of Planet Formation*. 2010.
- P. J. Armitage and W. K. M. Rice. Planetary migration. *arXiv Astrophysics e-prints*, July 2005.
- D. Arzoumanian, P. André, P. Didelon, V. Könyves, N. Schneider, A. Men'shchikov, T. Soubie, A. Zavagno, S. Bontemps, J. di Francesco, M. Griffin, M. Hennemann, T. Hill, J. Kirk, P. Martin, V. Minier, S. Molinari, F. Motte, N. Peretto, S. Pezzuto, L. Spinoglio, D. Ward-Thompson, G. White, and C. D. Wilson. Characterizing interstellar filaments with Herschel in IC 5146. *A&A*, 529:L6, May 2011. doi: 10.1051/0004-6361/201116596.
- M. Asplund, N. Grevesse, A. J. Sauval, and P. Scott. The Chemical Composition of the Sun. *ARA&A*, 47:481–522, September 2009. doi: 10.1146/annurev.astro.46.060407.145222.

- S. K. Atreya, M. H. Wong, T. C. Owen, P. R. Mahaffy, H. B. Niemann, I. de Pater, P. Drossart, and T. Encrenaz. A comparison of the atmospheres of Jupiter and Saturn: deep atmospheric composition, cloud structure, vertical mixing, and origin. *Planet. Space Sci.*, 47:1243–1262, October 1999. doi: 10.1016/S0032-0633(99)00047-1.
- J. Baker, M. Bizzarro, N. Wittig, J. Connelly, and H. Haack. Early planetesimal melting from an age of 4.5662Gyr for differentiated meteorites. *Nature*, 436: 1127–1131, August 2005. doi: 10.1038/nature03882.
- J. Ballesteros-Paredes, R. S. Klessen, M.-M. Mac Low, and E. Vazquez-Semadeni. Molecular Cloud Turbulence and Star Formation. *Protostars and Planets V*, pages 63–80, 2007.
- J. Bally, C. R. O’Dell, and M. J. McCaughrean. Disks, Microjets, Windblown Bubbles, and Outflows in the Orion Nebula. *AJ*, 119:2919–2959, June 2000. doi: 10.1086/301385.
- S. Banerjee and P. Kroupa. Formation of Very Young Massive Clusters and Implications for Globular Clusters. In S. Stahler, editor, *The Birth of Star Clusters*, volume 424 of *Astrophysics and Space Science Library*, page 143, 2018. doi: 10.1007/978-3-319-22801-3_6.
- I. Baraffe, G. Chabrier, J. Fortney, and C. Sotin. Planetary Internal Structures. *Protostars and Planets VI*, pages 763–786, 2014. doi: 10.2458/azu_uapress_9780816531240-ch033.
- T. Barclay, J. F. Rowe, J. J. Lissauer, D. Huber, F. Fressin, S. B. Howell, S. T. Bryson, W. J. Chaplin, J.-M. Désert, E. D. Lopez, G. W. Marcy, F. Mullally, D. Ragozzine, G. Torres, E. R. Adams, E. Agol, D. Barrado, S. Basu, T. R. Bedding, L. A. Buchhave, D. Charbonneau, J. L. Christiansen, J. Christensen-Dalsgaard, D. Ciardi, W. D. Cochran, A. K. Dupree, Y. Elsworth, M. Everett, D. A. Fischer, E. B. Ford, J. J. Fortney, J. C. Geary, M. R. Haas, R. Handberg, S. Hekker, C. E. Henze, E. Horch, A. W. Howard, R. C. Hunter, H. Isaacson, J. M. Jenkins, C. Karoff, S. D. Kawaler, H. Kjeldsen, T. C. Klaus, D. W. Latham, J. Li, J. Lillo-Box, M. N. Lund, M. Lundkvist, T. S. Metcalfe, A. Miglio, R. L. Morris, E. V. Quintana, D. Stello, J. C. Smith, M. Still, and S. E. Thompson. A sub-Mercury-sized exoplanet. *Nature*, 494:452–454, February 2013. doi: 10.1038/nature11914.

- N. Bastian, B. Ercolano, M. Gieles, E. Rosolowsky, R. A. Scheepmaker, R. Gutermuth, and Y. Efremov. Hierarchical star formation in M33: fundamental properties of the star-forming regions. *MNRAS*, 379:1302–1312, August 2007. doi: 10.1111/j.1365-2966.2007.12064.x.
- N. Bastian, K. R. Covey, and M. R. Meyer. A Universal Stellar Initial Mass Function? A Critical Look at Variations. *ARA&A*, 48:339–389, September 2010. doi: 10.1146/annurev-astro-082708-101642.
- P. Battinelli, A. Brandimarti, and R. Capuzzo-Dolcetta. Integrated photometric properties of open clusters. *A&AS*, 104, May 1994.
- C. P. M. Bell, T. Naylor, N. J. Mayne, R. D. Jeffries, and S. P. Littlefair. Pre-main-sequence isochrones - II. Revising star and planet formation time-scales. *MNRAS*, 434:806–831, September 2013. doi: 10.1093/mnras/stt1075.
- W. Benz. Low Velocity Collisions and the Growth of Planetesimals. *Space Sci. Rev.*, 92:279–294, April 2000. doi: 10.1023/A:1005207631229.
- J. Binney and S. Tremaine. *Galactic Dynamics: Second Edition*. Princeton University Press, 2008.
- A. Blaauw. The O Associations in the Solar Neighborhood. *ARA&A*, 2:213, 1964. doi: 10.1146/annurev.aa.02.090164.001241.
- J. Blum and G. Wurm. Experiments on Sticking, Restructuring, and Fragmentation of Preplanetary Dust Aggregates. *Icarus*, 143:138–146, January 2000. doi: 10.1006/icar.1999.6234.
- P. Bodenheimer and J. B. Pollack. Calculations of the accretion and evolution of giant planets The effects of solid cores. *Icarus*, 67:391–408, September 1986. doi: 10.1016/0019-1035(86)90122-3.
- D. M. Boneberg, J. E. Dale, P. Girichidis, and B. Ercolano. Turbulence in giant molecular clouds: the effect of photoionization feedback. *MNRAS*, 447:1341–1352, February 2015. doi: 10.1093/mnras/stu2498.
- I. A. Bonnell and M. R. Bate. Binary systems and stellar mergers in massive star formation. *MNRAS*, 362:915–920, September 2005. doi: 10.1111/j.1365-2966.2005.09360.x.

- I. A. Bonnell and M. B. Davies. Mass segregation in young stellar clusters. *MNRAS*, 295:691, April 1998. doi: 10.1046/j.1365-8711.1998.01372.x.
- I. A. Bonnell, M. R. Bate, C. J. Clarke, and J. E. Pringle. Competitive accretion in embedded stellar clusters. *MNRAS*, 323:785–794, May 2001. doi: 10.1046/j.1365-8711.2001.04270.x.
- I. A. Bonnell, M. R. Bate, and S. G. Vine. The hierarchical formation of a stellar cluster. *MNRAS*, 343:413–418, August 2003. doi: 10.1046/j.1365-8711.2003.06687.x.
- A. P. Boss. Giant planet formation by gravitational instability. *Science*, 276:1836–1839, 1997. doi: 10.1126/science.276.5320.1836.
- R. Bourtembourg. Was Uranus Observed by Happarchus? *Journal for the History of Astronomy*, 44:377–388, November 2013. doi: 10.1177/002182861304400401.
- A. Bouvier, J. Blichert-Toft, F. Moynier, J. D. Vervoort, and F. Albarède. Pb–Pb dating constraints on the accretion and cooling history of chondrites. *Geochim. Cosmochim. Acta*, 71:1583–1604, March 2007. doi: 10.1016/j.gca.2006.12.005.
- W. Brandner, H. Zinnecker, J. M. Alcalá, F. Allard, E. Covino, S. Frink, R. Köhler, M. Kunkel, A. Moneti, and A. Schweitzer. Timescales of Disk Evolution and Planet Formation: HST, Adaptive Optics, and ISO Observations of Weak-Line and Post-T Tauri Stars. *AJ*, 120:950–962, August 2000. doi: 10.1086/301483.
- R. Brasser, M. J. Duncan, and H. F. Levison. Embedded star clusters and the formation of the Oort Cloud. *Icarus*, 184:59–82, September 2006. doi: 10.1016/j.icarus.2006.04.010.
- E. Bressert, N. Bastian, R. Gutermuth, S. T. Megeath, L. Allen, N. J. Evans, II, L. M. Rebull, J. Hatchell, D. Johnstone, T. L. Bourke, L. A. Cieza, P. M. Harvey, B. Merin, T. P. Ray, and N. F. H. Tothill. The spatial distribution of star formation in the solar neighbourhood: do all stars form in dense clusters? *MNRAS*, 409:L54–L58, November 2010. doi: 10.1111/j.1745-3933.2010.00946.x.
- M. E. Brown. The Compositions of Kuiper Belt Objects. *Annual Review of Earth and Planetary Sciences*, 40:467–494, May 2012. doi: 10.1146/annurev-earth-042711-105352.

- Michael E. Brown and Konstantin Batygin. Observational Constraints on the Orbit and Location of Planet Nine in the Outer Solar System. *ApJ*, 824:L23, June 2016. doi: 10.3847/2041-8205/824/2/L23.
- C. J. Burke, S. T. Bryson, F. Mullally, J. F. Rowe, J. L. Christiansen, S. E. Thompson, J. L. Coughlin, M. R. Haas, N. M. Batalha, D. A. Caldwell, J. M. Jenkins, M. Still, T. Barclay, W. J. Borucki, W. J. Chaplin, D. R. Ciardi, B. D. Clarke, W. D. Cochran, B.-O. Demory, G. A. Esquerdo, T. N. Gautier, III, R. L. Gilliland, F. R. Girouard, M. Havel, C. E. Henze, S. B. Howell, D. Huber, D. W. Latham, J. Li, R. C. Morehead, T. D. Morton, J. Pepper, E. Quintana, D. Ragozzine, S. E. Seader, Y. Shah, A. Shporer, P. Tenenbaum, J. D. Twicken, and A. Wolfgang. Planetary Candidates Observed by Kepler IV: Planet Sample from Q1-Q8 (22 Months). *ApJS*, 210:19, February 2014. doi: 10.1088/0067-0049/210/2/19.
- M. Busso, R. Gallino, and G. J. Wasserburg. Nucleosynthesis in Asymptotic Giant Branch Stars: Relevance for Galactic Enrichment and Solar System Formation. *ARA&A*, 37:239–309, 1999. doi: 10.1146/annurev.astro.37.1.239.
- M. Busso, R. Gallino, and G. J. Wasserburg. Short-Lived Nuclei in the Early Solar System: A Low Mass Stellar Source? *PASA*, 20:356–370, 2003. doi: 10.1071/AS03035.
- A. G. W. Cameron and J. W. Truran. The supernova trigger for formation of the solar system. *Icarus*, 30:447–461, March 1977. doi: 10.1016/0019-1035(77)90101-4.
- B. Campbell, G. A. H. Walker, and S. Yang. A search for substellar companions to solar-type stars. *ApJ*, 331:902–921, August 1988. doi: 10.1086/166608.
- A. Cartwright and A. P. Whitworth. The statistical analysis of star clusters. *MNRAS*, 348:589–598, February 2004. doi: 10.1111/j.1365-2966.2004.07360.x.
- A. Cassan, D. Kubas, J. P. Beaulieu, M. Dominik, K. Horne, J. Greenhill, J. Wambganss, J. Menzies, A. Williams, U. G. Jørgensen, A. Udalski, D. P. Bennett, M. D. Albrow, V. Batista, S. Brilliant, J. A. R. Caldwell, A. Cole, Ch. Coutures, K. H. Cook, S. Dieters, D. Dominis Prester, J. Donatowicz, P. Fouqué, K. Hill, N. Kains, S. Kane, J. B. Marquette, R. Martin, K. R. Pollard, K. C. Sahu, C. Vinter, D. Warren, B. Watson, M. Zub, T. Sumi, M. K. Szymański, M. Kubiak, R. Poleski, I. Soszynski, K. Ulaczyk, G. Pietrzyński, and Ł. Wyrzykowski. One or more bound planets per Milky Way star from microlensing observations. *Nature*, 481:167–169, January 2012. doi: 10.1038/nature10684.

- M. Cerviño, C. Román-Zúñiga, V. Luridiana, A. Bayo, N. Sánchez, and E. Pérez. Crucial aspects of the initial mass function. I. The statistical correlation between the total mass of an ensemble of stars and its most massive star. *A&A*, 553:A31, May 2013. doi: 10.1051/0004-6361/201219504.
- G. Chabrier. Galactic Stellar and Substellar Initial Mass Function. *PASP*, 115: 763–795, July 2003. doi: 10.1086/376392.
- T. C. Chamberlin. On a Possible Function of Disruptive Approach in the Formation of Meteorites, Comets, and NEBULAE. *ApJ*, 14:17, July 1901. doi: 10.1086/140831.
- D. Charbonneau, T. M. Brown, D. W. Latham, and M. Mayor. Detection of Planetary Transits Across a Sun-like Star. *ApJ*, 529:L45–L48, January 2000. doi: 10.1086/312457.
- R. A. Chevalier. Young Circumstellar Disks near Evolved Massive Stars and Supernovae. *ApJ*, 538:L151–L154, August 2000. doi: 10.1086/312814.
- P. C. Clark, R. S. Klessen, and I. A. Bonnell. Clump lifetimes and the initial mass function. *MNRAS*, 379:57–62, July 2007. doi: 10.1111/j.1365-2966.2007.11896.x.
- C. J. Clarke. The photoevaporation of discs around young stars in massive clusters. *MNRAS*, 376:1350–1356, April 2007. doi: 10.1111/j.1365-2966.2007.11547.x.
- C. J. Clarke and J. E. Pringle. Accretion disc response to a stellar fly-by. *MNRAS*, 261:190–202, March 1993. doi: 10.1093/mnras/261.1.190.
- C. J. Clarke, I. A. Bonnell, and L. A. Hillenbrand. The Formation of Stellar Clusters. *Protostars and Planets IV*, page 151, May 2000.
- C. J. Clarke, A. Gendrin, and M. Sotomayor. The dispersal of circumstellar discs: the role of the ultraviolet switch. *MNRAS*, 328:485–491, December 2001. doi: 10.1046/j.1365-8711.2001.04891.x.
- J. L. Coughlin, F. Mullally, S. E. Thompson, J. F. Rowe, C. J. Burke, D. W. Latham, N. M. Batalha, A. Ofir, B. L. Quarles, C. E. Henze, A. Wolfgang, D. A. Caldwell, S. T. Bryson, A. Shporer, J. Catanzarite, R. Akeson, T. Barclay, W. J. Borucki, T. S. Boyajian, J. R. Campbell, J. L. Christiansen, F. R. Girouard, M. R. Haas, S. B. Howell, D. Huber, J. M. Jenkins, J. Li, A. Patil-Sabale, E. V. Quintana,

- S. Ramirez, S. Seader, J. C. Smith, P. Tenenbaum, J. D. Twicken, and K. A. Zamudio. Planetary Candidates Observed by Kepler. VII. The First Fully Uniform Catalog Based on the Entire 48-month Data Set (Q1-Q17 DR24). *ApJS*, 224:12, May 2016. doi: 10.3847/0067-0049/224/1/12.
- P. A. Crowther. Near and mid infrared observations of ultracompact HII regions. In R. Cesaroni, M. Felli, E. Churchwell, and M. Walmsley, editors, *Massive Star Birth: A Crossroads of Astrophysics*, volume 227 of *IAU Symposium*, pages 389–396, 2005. doi: 10.1017/S1743921305004795.
- P. A. Crowther, D. J. Lennon, and N. R. Walborn. Physical parameters and wind properties of galactic early B supergiants. *A&A*, 446:279–293, January 2006. doi: 10.1051/0004-6361:20053685.
- P. A. Crowther, O. Schnurr, R. Hirschi, N. Yusof, R. J. Parker, S. P. Goodwin, and H. A. Kassim. The R136 star cluster hosts several stars whose individual masses greatly exceed the accepted $150M_{\text{solar}}$ stellar mass limit. *MNRAS*, 408:731–751, October 2010. doi: 10.1111/j.1365-2966.2010.17167.x.
- Patricia Curd. Anaxagoras. In Edward N. Zalta, editor, *The Stanford Encyclopedia of Philosophy*. Metaphysics Research Lab, Stanford University, winter 2015 edition, 2015.
- Fei Dai, Stefano Facchini, Cathie J. Clarke, and Thomas J. Haworth. A tidal encounter caught in the act: modelling a star-disc fly-by in the young RW Aurigae system. *MNRAS*, 449(2):1996–2009, May 2015. doi: 10.1093/mnras/stv403.
- J. E. Dale, B. Ercolano, and I. A. Bonnell. Ionizing feedback from massive stars in massive clusters - II. Disruption of bound clusters by photoionization. *MNRAS*, 424:377–392, July 2012. doi: 10.1111/j.1365-2966.2012.21205.x.
- J. E. Dale, B. Ercolano, and I. A. Bonnell. Ionizing feedback from massive stars in massive clusters - III. Disruption of partially unbound clouds. *MNRAS*, 430: 234–246, March 2013. doi: 10.1093/mnras/sts592.
- J. E. Dale, J. Ngoumou, B. Ercolano, and I. A. Bonnell. Before the first supernova: combined effects of H II regions and winds on molecular clouds. *MNRAS*, 442: 694–712, July 2014. doi: 10.1093/mnras/stu816.
- J. E. Dale, B. Ercolano, and I. A. Bonnell. Early evolution of embedded clusters. *MNRAS*, 451:987–1003, July 2015a. doi: 10.1093/mnras/stv913.

- J. E. Dale, T. J. Haworth, and E. Bressert. The dangers of being trigger-happy. *MNRAS*, 450:1199–1211, June 2015b. doi: 10.1093/mnras/stv396.
- R. de Grijs and P. Anders. How well do we know the age and mass distributions of the star cluster system in the Large Magellanic Cloud? *MNRAS*, 366:295–307, February 2006. doi: 10.1111/j.1365-2966.2005.09856.x.
- R. de Grijs, P. Anders, N. Bastian, R. Lynds, H. J. G. L. M. Lamers, and E. J. O’Neil. Star cluster formation and evolution in nearby starburst galaxies - II. Initial conditions. *MNRAS*, 343:1285–1300, August 2003. doi: 10.1046/j.1365-8711.2003.06777.x.
- W. J. de Wit, L. Testi, F. Palla, and H. Zinnecker. The origin of massive O-type field stars: II. Field O stars as runaways. *A&A*, 437:247–255, July 2005. doi: 10.1051/0004-6361:20042489.
- N. R. Deacon, J. E. Schlieder, and S. J. Murphy. A nearby young M dwarf with a wide, possibly planetary-mass companion. *MNRAS*, 457:3191–3199, April 2016. doi: 10.1093/mnras/stw172.
- W. Dehnen and J. I. Read. N-body simulations of gravitational dynamics. *European Physical Journal Plus*, 126:55, May 2011. doi: 10.1140/epjp/i2011-11055-3.
- M. L. Delitsky, D. A. Paige, M. A. Siegler, E. R. Harju, D. Schriver, R. E. Johnson, and P. Travnicek. Ices on Mercury: Chemistry of volatiles in permanently cold areas of Mercury’s north polar region. *Icarus*, 281:19–31, January 2017. doi: 10.1016/j.icarus.2016.08.006.
- S. J. Desch, L. Pan, and E. Scannapieco. Clumpy Supernova Ejecta Injection into Forming Planetary Systems. In *Workshop on Formation of the First Solids in the Solar System*, volume 1639 of *LPI Contributions*, page 9117, November 2011.
- S. E. Dodson-Robinson, D. Veras, E. B. Ford, and C. A. Beichman. The Formation Mechanism of Gas Giants on Wide Orbits. *ApJ*, 707:79–88, December 2009a. doi: 10.1088/0004-637X/707/1/79.
- S. E. Dodson-Robinson, K. Willacy, P. Bodenheimer, N. J. Turner, and C. A. Beichman. Ice lines, planetesimal composition and solid surface density in the solar nebula. *Icarus*, 200:672–693, April 2009b. doi: 10.1016/j.icarus.2008.11.023.
- L. Dones, P. R. Weissman, H. F. Levison, and M. J. Duncan. *Oort cloud formation and dynamics*, pages 153–174. 2004.

- G. Duchêne and A. Kraus. Stellar Multiplicity. *ARA&A*, 51:269–310, August 2013. doi: 10.1146/annurev-astro-081710-102602.
- M. Duncan, T. Quinn, and S. Tremaine. The formation and extent of the solar system comet cloud. *AJ*, 94:1330–1338, November 1987. doi: 10.1086/114571.
- G. Duvert, S. Guilloteau, F. Ménard, M. Simon, and A. Dutrey. A search for extended disks around weak-lined T Tauri stars. *A&A*, 355:165–170, March 2000.
- P. P. Eggleton and A. A. Tokovinin. A catalogue of multiplicity among bright stellar systems. *MNRAS*, 389:869–879, September 2008. doi: 10.1111/j.1365-2966.2008.13596.x.
- P. P. Eggleton, M. J. Fitchett, and C. A. Tout. The distribution of visual binaries with two bright components. *ApJ*, 347:998–1011, December 1989. doi: 10.1086/168190.
- J. A. Eisner, J. M. Bally, A. Ginsburg, and P. D. Sheehan. Protoplanetary Disks in the Orion OMC1 Region Imaged with ALMA. *ApJ*, 826:16, July 2016. doi: 10.3847/0004-637X/826/1/16.
- J. A. Eisner, H. G. Arce, N. P. Ballering, J. Bally, S. M. Andrews, R. D. Boyden, J. Di Francesco, M. Fang, D. Johnstone, J. S. Kim, R. K. Mann, B. Matthews, I. Pascucci, L. Ricci, P. D. Sheehan, and J. P. Williams. Protoplanetary Disk Properties in the Orion Nebula Cluster: Initial Results from Deep, High-resolution ALMA Observations. *ApJ*, 860:77, June 2018. doi: 10.3847/1538-4357/aac3e2.
- J. J. Eldridge. A new-age determination for γ^2 Velorum from binary stellar evolution models. *MNRAS*, 400:L20–L23, November 2009. doi: 10.1111/j.1745-3933.2009.00753.x.
- B. G. Elmegreen. Star Formation in a Crossing Time. *ApJ*, 530:277–281, February 2000a. doi: 10.1086/308361.
- B. G. Elmegreen. Modeling a High-Mass Turn-Down in the Stellar Initial Mass Function. *ApJ*, 539:342–351, August 2000b. doi: 10.1086/309204.
- B. G. Elmegreen. On the Similarity between Cluster and Galactic Stellar Initial Mass Functions. *ApJ*, 648:572–579, September 2006. doi: 10.1086/505785.

- B. G. Elmegreen and Y. N. Efremov. A Universal Formation Mechanism for Open and Globular Clusters in Turbulent Gas. *ApJ*, 480:235–245, May 1997. doi: 10.1086/303966.
- R. A. W. Elson, S. M. Fall, and K. C. Freeman. The structure of young star clusters in the Large Magellanic Cloud. *ApJ*, 323:54–78, December 1987. doi: 10.1086/165807.
- M. E. Esclançon, de Grandchamp, Canavaggia, Mineur, Barbier, W. Baade, H. Shapley, A. O. Leuschner, E. C. Bower, F. L. Whipple, and Meyer. Object Lowell Observatory. *IAU Circ.*, 268, April 1930.
- James Evans. *The History and Practice of Ancient Astronomy*. Oxford University Press, 1998.
- S. Facchini, C. J. Clarke, and T. G. Bisbas. External photoevaporation of protoplanetary discs in sparse stellar groups: the impact of dust growth. *MNRAS*, 457:3593–3610, April 2016. doi: 10.1093/mnras/stw240.
- M. Fatuzzo and F. C. Adams. UV Radiation Fields Produced by Young Embedded Star Clusters. *ApJ*, 675:1361–1374, March 2008. doi: 10.1086/527469.
- G. A. Feiden. Magnetic inhibition of convection and the fundamental properties of low-mass stars. III. A consistent 10 Myr age for the Upper Scorpius OB association. *A&A*, 593:A99, September 2016. doi: 10.1051/0004-6361/201527613.
- A. S. Font, I. G. McCarthy, D. Johnstone, and D. R. Ballantyne. Photoevaporation of Circumstellar Disks around Young Stars. *ApJ*, 607:890–903, June 2004. doi: 10.1086/383518.
- J. J. Fortney and N. Nettelmann. The Interior Structure, Composition, and Evolution of Giant Planets. *Space Sci. Rev.*, 152:423–447, May 2010. doi: 10.1007/s11214-009-9582-x.
- J. B. Foster, M. Cottaar, K. R. Covey, H. G. Arce, M. R. Meyer, D. L. Nidever, K. G. Stassun, J. C. Tan, S. D. Chojnowski, N. da Rio, K. M. Flaherty, L. Rebull, P. M. Frinchaboy, S. R. Majewski, M. Skrutskie, J. C. Wilson, and G. Zasowski. IN-SYNC. II. Virial Stars from Subvirial Cores - the Velocity Dispersion of Embedded Pre-main-sequence Stars in NGC 1333. *ApJ*, 799:136, February 2015. doi: 10.1088/0004-637X/799/2/136.

- C. Freissinet, D. P. Glavin, P. R. Mahaffy, K. E. Miller, J. L. Eigenbrode, R. E. Summons, A. E. Brunner, A. Buch, C. Szopa, P. D. Archer, Jr., H. B. Franz, S. K. Atreya, W. B. Brinckerhoff, M. Cabane, P. Coll, P. G. Conrad, D. J. Des Marais, J. P. Dworkin, A. G. Fairén, P. François, J. P. Grotzinger, S. Kashyap, I. L. ten Kate, L. A. Leshin, C. A. Malespin, M. G. Martin, J. F. Martin-Torres, A. C. McAdam, D. W. Ming, R. Navarro-González, A. A. Pavlov, B. D. Prats, S. W. Squyres, A. Steele, J. C. Stern, D. Y. Sumner, B. Sutter, M.-P. Zorzano, and MSL Science Team. Organic molecules in the Sheepbed Mudstone, Gale Crater, Mars. *Journal of Geophysical Research (Planets)*, 120:495–514, March 2015. doi: 10.1002/2014JE004737.
- M. Gieles, S. S. Larsen, N. Bastian, and I. T. Stein. The luminosity function of young star clusters: implications for the maximum mass and luminosity of clusters. *A&A*, 450:129–145, April 2006a. doi: 10.1051/0004-6361:20053589.
- M. Gieles, S. S. Larsen, R. A. Scheepmaker, N. Bastian, M. R. Haas, and H. J. G. L. M. Lamers. Observational evidence for a truncation of the star cluster initial mass function at the high mass end. *A&A*, 446:L9–L12, February 2006b. doi: 10.1051/0004-6361:200500224.
- D. R. Gies. The kinematical and binary properties of association and field O stars. *ApJS*, 64:545–563, July 1987. doi: 10.1086/191208.
- P. Girichidis, C. Federrath, R. Banerjee, and R. S. Klessen. Importance of the initial conditions for star formation - I. Cloud evolution and morphology. *MNRAS*, 413:2741–2759, June 2011. doi: 10.1111/j.1365-2966.2011.18348.x.
- P. Girichidis, C. Federrath, R. Allison, R. Banerjee, and R. S. Klessen. Importance of the initial conditions for star formation - III. Statistical properties of embedded protostellar clusters. *MNRAS*, 420:3264–3280, March 2012. doi: 10.1111/j.1365-2966.2011.20250.x.
- R. D. S. Gomes. On the origin of the Kuiper belt. *Celestial Mechanics and Dynamical Astronomy*, 104:39–51, June 2009. doi: 10.1007/s10569-009-9186-5.
- S. P. Goodwin. Binaries in star clusters and the origin of the field stellar population. *Philosophical Transactions of the Royal Society of London Series A*, 368:851–866, January 2010. doi: 10.1098/rsta.2009.0254.

- S. P. Goodwin and N. Bastian. Gas expulsion and the destruction of massive young clusters. *MNRAS*, 373:752–758, December 2006. doi: 10.1111/j.1365-2966.2006.11078.x.
- S. P. Goodwin and A. P. Whitworth. The dynamical evolution of fractal star clusters: The survival of substructure. *A&A*, 413:929–937, January 2004. doi: 10.1051/0004-6361:20031529.
- U. Gorti and D. Hollenbach. Line Emission from Gas in Optically Thick Dust Disks around Young Stars. *ApJ*, 683:287–303, August 2008. doi: 10.1086/589616.
- U. Gorti, C. P. Dullemond, and D. Hollenbach. Time Evolution of Viscous Circumstellar Disks due to Photoevaporation by Far-Ultraviolet, Extreme-Ultraviolet, and X-ray Radiation from the Central Star. *ApJ*, 705:1237–1251, November 2009. doi: 10.1088/0004-637X/705/2/1237.
- U. Gorti, D. Hollenbach, and C. P. Dullemond. The Impact of Dust Evolution and Photoevaporation on Disk Dispersal. *ApJ*, 804:29, May 2015. doi: 10.1088/0004-637X/804/1/29.
- D. A. Gouliermis, S. Hony, and R. S. Klessen. The complex distribution of recently formed stars. Bimodal stellar clustering in the star-forming region NGC 346. *MNRAS*, 439:3775–3789, April 2014. doi: 10.1093/mnras/stu228.
- M. Gounelle. The abundance of ^{26}Al -rich planetary systems in the Galaxy. *A&A*, 582:A26, October 2015. doi: 10.1051/0004-6361/201526174.
- M. Gounelle and G. Meynet. Solar system genealogy revealed by extinct short-lived radionuclides in meteorites. *A&A*, 545:A4, September 2012. doi: 10.1051/0004-6361/201219031.
- M. Gounelle, A. Meibom, P. Hennebelle, and S.-i. Inutsuka. Supernova Propagation and Cloud Enrichment: A New Model for the Origin of ^{60}Fe in the Early Solar System. *ApJ*, 694:L1–L5, March 2009. doi: 10.1088/0004-637X/694/1/L1.
- O. Gressel, R. P. Nelson, and N. J. Turner. Dead zones as safe havens for planetesimals: influence of disc mass and external magnetic field. *MNRAS*, 422:1140–1159, May 2012. doi: 10.1111/j.1365-2966.2012.20701.x.
- M. Gritschneder, D. N. C. Lin, S. D. Murray, Q.-Z. Yin, and M.-N. Gong. The Supernova Triggered Formation and Enrichment of Our Solar System. *ApJ*, 745:22, January 2012. doi: 10.1088/0004-637X/745/1/22.

- W. M. Grundy, R. P. Binzel, B. J. Buratti, J. C. Cook, D. P. Cruikshank, C. M. Dalle Ore, A. M. Earle, K. Ennico, C. J. A. Howett, A. W. Lunsford, C. B. Olkin, A. H. Parker, S. Philippe, S. Protopapa, E. Quirico, D. C. Reuter, B. Schmitt, K. N. Singer, A. J. Verbiscer, R. A. Beyer, M. W. Buie, A. F. Cheng, D. E. Jennings, I. R. Linscott, J. W. Parker, P. M. Schenk, J. R. Spencer, J. A. Stansberry, S. A. Stern, H. B. Throop, C. C. C. Tsang, H. A. Weaver, G. E. Weigle, and L. A. Young. Surface compositions across Pluto and Charon. *Science*, 351:aad9189, March 2016. doi: 10.1126/science.aad9189.
- R. A. Gutermuth, J. L. Pipher, S. T. Megeath, P. C. Myers, L. E. Allen, and T. S. Allen. A Correlation between Surface Densities of Young Stellar Objects and Gas in Eight Nearby Molecular Clouds. *ApJ*, 739:84, October 2011. doi: 10.1088/0004-637X/739/2/84.
- V. V. Gvaramadze and D. J. Bomans. Search for OB stars running away from young star clusters. I. NGC 6611. *A&A*, 490:1071–1077, November 2008. doi: 10.1051/0004-6361:200810411.
- H. J. Habing. The interstellar radiation density between 912 Å and 2400 Å. *Bull. Astron. Inst. Netherlands*, 19:421, January 1968.
- K. E. Haisch, Jr., E. A. Lada, and C. J. Lada. Disk Frequencies and Lifetimes in Young Clusters. *ApJ*, 553:L153–L156, June 2001. doi: 10.1086/320685.
- James Hannam. *The genesis of science*. 2011.
- P. Hartigan, L. Hartmann, S. J. Kenyon, S. E. Strom, and M. F. Skrutskie. Correlations of optical and infrared excesses in T Tauri stars. *ApJ*, 354:L25–L28, May 1990. doi: 10.1086/185714.
- L. Hartmann. *Accretion Processes in Star Formation: Second Edition*. Cambridge University Press, 2009.
- T. J. Haworth, C. J. Clarke, W. Rahman, A. J. Winter, and S. Facchini. The FRIED grid of mass-loss rates for externally irradiated protoplanetary discs. *MNRAS*, 481:452–466, November 2018a. doi: 10.1093/mnras/sty2323.
- T. J. Haworth, S. Facchini, C. J. Clarke, and S. Mohanty. Where can a Trappist-1 planetary system be produced? *MNRAS*, 475:5460–5473, April 2018b. doi: 10.1093/mnras/sty168.

- C. Hayashi. Structure of the Solar Nebula, Growth and Decay of Magnetic Fields and Effects of Magnetic and Turbulent Viscosities on the Nebula. *Progress of Theoretical Physics Supplement*, 70:35–53, 1981. doi: 10.1143/PTPS.70.35.
- D. C. Heggie and R. D. Mathieu. Standardised Units and Time Scales. In P. Hut and S. L. W. McMillan, editors, *The Use of Supercomputers in Stellar Dynamics*, volume 267 of *Lecture Notes in Physics*, Berlin Springer Verlag, page 233, 1986. doi: 10.1007/BFb0116419.
- R. Helled, P. Bodenheimer, M. Podolak, A. Boley, F. Meru, S. Nayakshin, J. J. Fortney, L. Mayer, Y. Alibert, and A. P. Boss. Giant Planet Formation, Evolution, and Internal Structure. *Protostars and Planets VI*, pages 643–665, 2014. doi: 10.2458/azu_uapress_9780816531240-ch028.
- P. Hennebelle and G. Chabrier. Analytical Theory for the Initial Mass Function: CO Clumps and Prestellar Cores. *ApJ*, 684:395–410, September 2008. doi: 10.1086/589916.
- W. Herschel and D. Watson. Account of a Comet. By Mr. Herschel, F. R. S.; Communicated by Dr. Watson, Jun. of Bath, F. R. S. *Philosophical Transactions of the Royal Society of London Series I*, 71:492–501, 1781.
- L. A. Hillenbrand. On the Stellar Population and Star-Forming History of the Orion Nebula Cluster. *AJ*, 113:1733–1768, May 1997. doi: 10.1086/118389.
- L. A. Hillenbrand and L. W. Hartmann. A Preliminary Study of the Orion Nebula Cluster Structure and Dynamics. *ApJ*, 492:540–553, January 1998. doi: 10.1086/305076.
- J. G. Hills. The effect of mass loss on the dynamical evolution of a stellar system - Analytic approximations. *ApJ*, 235:986–991, February 1980. doi: 10.1086/157703.
- J. G. Hills. Comet showers and the steady-state infall of comets from the Oort cloud. *AJ*, 86:1730–1740, November 1981. doi: 10.1086/113058.
- D. Hollenbach and F. C. Adams. Dispersal of Disks Around Young Stars: Constraints on Kuiper Belt Formation. In L. Caroff, L. J. Moon, D. Backman, and E. Praton, editors, *Debris Disks and the Formation of Planets*, volume 324 of *Astronomical Society of the Pacific Conference Series*, page 168, December 2004.

- D. Hollenbach, D. Johnstone, S. Lizano, and F. Shu. Photoevaporation of disks around massive stars and application to ultracompact H II regions. *ApJ*, 428: 654–669, June 1994. doi: 10.1086/174276.
- D. J. Hollenbach, H. W. Yorke, and D. Johnstone. Disk Dispersal around Young Stars. *Protostars and Planets IV*, page 401, May 2000.
- P. F. Hopkins. The stellar initial mass function, core mass function and the last-crossing distribution. *MNRAS*, 423:2037–2044, July 2012. doi: 10.1111/j.1365-2966.2012.20731.x.
- W. B. Hubbard and J. J. Macfarlane. Structure and evolution of Uranus and Neptune. *J. Geophys. Res.*, 85:225–234, January 1980. doi: 10.1029/JB085iB01p00225.
- D. A. Hunter, B. G. Elmegreen, T. J. Dupuy, and M. Mortonson. Cluster Mass Functions in the Large and Small Magellanic Clouds: Fading and Size-of-Sample Effects. *AJ*, 126:1836–1848, October 2003. doi: 10.1086/378056.
- J. R. Hurley, O. R. Pols, and C. A. Tout. Comprehensive analytic formulae for stellar evolution as a function of mass and metallicity. *MNRAS*, 315:543–569, July 2000. doi: 10.1046/j.1365-8711.2000.03426.x.
- S. Ida, T. Guillot, and A. Morbidelli. Accretion and Destruction of Planetesimals in Turbulent Disks. *ApJ*, 686:1292–1301, October 2008. doi: 10.1086/591903.
- B. Jacobsen, Q.-z. Yin, F. Moynier, Y. Amelin, A. N. Krot, K. Nagashima, I. D. Hutcheon, and H. Palme. ^{26}Al - ^{26}Mg and ^{207}Pb - ^{206}Pb systematics of Allende CAIs: Canonical solar initial $^{26}\text{Al}/^{27}\text{Al}$ ratio reinstated. *Earth and Planetary Science Letters*, 272:353–364, July 2008. doi: 10.1016/j.epsl.2008.05.003.
- J. H. Jeans. The Stability of a Spherical Nebula. *Philosophical Transactions of the Royal Society of London Series A*, 199:1–53, 1902. doi: 10.1098/rsta.1902.0012.
- J. H. Jeans. The Present Position of the Nebular Hypothesis. *JRASC*, 13:215, June 1919.
- R. D. Jeffries, R. J. Jackson, M. Cottaar, S. E. Koposov, A. C. Lanzafame, M. R. Meyer, L. Prisinzano, S. Randich, G. G. Sacco, E. Brugaletta, M. Caramazza, F. Damiani, E. Franciosini, A. Frasca, G. Gilmore, S. Feltzing, G. Micela, E. Alfaro, T. Bensby, E. Pancino, A. Recio-Blanco, P. de Laverny, J. Lewis, L. Magrini,

- L. Morbidelli, M. T. Costado, P. Jofré, A. Klutsch, K. Lind, and E. Maiorca. The Gaia-ESO Survey: Kinematic structure in the Gamma Velorum cluster. *A&A*, 563:A94, March 2014. doi: 10.1051/0004-6361/201323288.
- D. Jewitt and J. Luu. Discovery of the candidate Kuiper belt object 1992 QB1. *Nature*, 362:730–732, April 1993. doi: 10.1038/362730a0.
- A. Johansen and M. Lambrechts. Forming Planets via Pebble Accretion. *Annual Review of Earth and Planetary Sciences*, 45:359–387, August 2017. doi: 10.1146/annurev-earth-063016-020226.
- A. Johansen, J. Blum, H. Tanaka, C. Ormel, M. Bizzarro, and H. Rickman. The Multifaceted Planetary Formation Process. *Protostars and Planets VI*, pages 547–570, 2014. doi: 10.2458/azu_uapress_9780816531240-ch024.
- D. Johnstone, D. Hollenbach, and J. Bally. Photoevaporation of Disks and Clumps by Nearby Massive Stars: Application to Disk Destruction in the Orion Nebula. *ApJ*, 499:758–776, May 1998. doi: 10.1086/305658.
- J. H. Kastner and P. C. Myers. An observational estimate of the probability of encounters between mass-losing evolved stars and molecular clouds. *ApJ*, 421: 605–615, February 1994. doi: 10.1086/173676.
- S. J. Kenyon and B. C. Bromley. Stellar encounters as the origin of distant Solar System objects in highly eccentric orbits. *Nature*, 432:598–602, December 2004. doi: 10.1038/nature03136.
- S. J. Kenyon and L. Hartmann. Pre-Main-Sequence Evolution in the Taurus-Auriga Molecular Cloud. *ApJS*, 101:117, November 1995. doi: 10.1086/192235.
- M. Keppler, M. Benisty, A. Müller, T. Henning, R. van Boekel, F. Cantalloube, C. Ginski, R. G. van Holstein, A.-L. Maire, A. Pohl, M. Samland, H. Avenhaus, J.-L. Baudino, A. Boccaletti, J. de Boer, M. Bonnefoy, G. Chauvin, S. Desidera, M. Langlois, C. Lazzoni, G.-D. Marleau, C. Mordasini, N. Pawellek, T. Stolker, A. Vigan, A. Zurlo, T. Birnstiel, W. Brandner, M. Feldt, M. Flock, J. Girard, R. Gratton, J. Hagelberg, A. Isella, M. Janson, A. Juhasz, J. Kemmer, Q. Kral, A.-M. Lagrange, R. Launhardt, A. Matter, F. Ménard, J. Milli, P. Mollière, J. Olofsson, L. Pérez, P. Pinilla, C. Pinte, S. P. Quanz, T. Schmidt, S. Udry, Z. Wahhaj, J. P. Williams, E. Buenzli, M. Cudel, C. Dominik, R. Galicher, M. Kasper, J. Lannier, D. Mesa, D. Mouillet, S. Peretti, C. Perrot, G. Salter, E. Sissa, F. Wildi,

- L. Abe, J. Antichi, J.-C. Augereau, A. Baruffolo, P. Baudoz, A. Bazzon, J.-L. Beuzit, P. Blanchard, S. S. Brems, T. Buey, V. De Caprio, M. Carbillet, M. Carle, E. Cascone, A. Cheetham, R. Claudi, A. Costille, A. Delboulbé, K. Dohlen, D. Fantinel, P. Feautrier, T. Fusco, E. Giro, L. Gluck, C. Gry, N. Hubin, E. Hugot, M. Jaquet, D. Le Mignant, M. Llored, F. Madec, Y. Magnard, P. Martinez, D. Maurel, M. Meyer, O. Möller-Nilsson, T. Moulin, L. Mugnier, A. Origné, A. Pavlov, D. Perret, C. Petit, J. Pragt, P. Puget, P. Rabou, J. Ramos, F. Rigal, S. Rochat, R. Roelfsema, G. Rousset, A. Roux, B. Salasnich, J.-F. Sauvage, A. Sevin, C. Soenke, E. Stadler, M. Suarez, M. Turatto, and L. Weber. Discovery of a planetary-mass companion within the gap of the transition disk around PDS 70. *A&A*, 617:A44, September 2018. doi: 10.1051/0004-6361/201832957.
- I. R. King. The structure of star clusters. III. Some simple dynamical models. *AJ*, 71:64, February 1966. doi: 10.1086/109857.
- R. R. King, R. J. Parker, J. Patience, and S. P. Goodwin. Testing the universality of star formation - I. Multiplicity in nearby star-forming regions. *MNRAS*, 421: 2025–2042, April 2012. doi: 10.1111/j.1365-2966.2012.20437.x.
- T. Kleine, K. Mezger, C. Münker, H. Palme, and A. Bischoff. ^{182}Hf - ^{182}W isotope systematics of chondrites, eucrites, and martian meteorites: Chronology of core formation and early mantle differentiation in Vesta and Mars. *Geochim. Cosmochim. Acta*, 68:2935–2946, July 2004. doi: 10.1016/j.gca.2004.01.009.
- Q. M. Konopacky, J. Rameau, G. Duchêne, J. C. Filippazzo, P. A. Giorla Godfrey, C. Marois, E. L. Nielsen, L. Pueyo, R. R. Rafikov, E. L. Rice, J. J. Wang, S. M. Ammons, V. P. Bailey, T. S. Barman, J. Bulger, S. Bruzzone, J. K. Chilcote, T. Cotten, R. I. Dawson, R. J. De Rosa, R. Doyon, T. M. Esposito, M. P. Fitzgerald, K. B. Follette, S. Goodsell, J. R. Graham, A. Z. Greenbaum, P. Hibon, L.-W. Hung, P. Ingraham, P. Kalas, D. Lafrenière, J. E. Larkin, B. A. Macintosh, J. Maire, F. Marchis, M. S. Marley, B. C. Matthews, S. Metchev, M. A. Millar-Blanchaer, R. Oppenheimer, D. W. Palmer, J. Patience, M. D. Perrin, L. A. Poyneer, A. Rajan, F. T. Rantakyrö, D. Savransky, A. C. Schneider, A. Sivaramkrishnan, I. Song, R. Soummer, S. Thomas, J. K. Wallace, K. Ward-Duong, S. J. Wiktorowicz, and S. G. Wolff. Discovery of a Substellar Companion to the Nearby Debris Disk Host HR 2562. *ApJ*, 829:L4, September 2016. doi: 10.3847/2041-8205/829/1/L4.

- V. B. Kostov, P. R. McCullough, T. C. Hinse, Z. I. Tsvetanov, G. Hébrard, R. F. Díaz, M. Deleuil, and J. A. Valenti. A Gas Giant Circumbinary Planet Transiting the F Star Primary of the Eclipsing Binary Star KIC 4862625 and the Independent Discovery and Characterization of the Two Transiting Planets in the Kepler-47 System. *ApJ*, 770:52, Jun 2013. doi: 10.1088/0004-637X/770/1/52.
- M. B. N. Kouwenhoven and S. P. Goodwin. What does the IMF really tell us about star formation? In G. R. Bruzual and S. Charlot, editors, *Stellar Populations - Planning for the Next Decade*, volume 262 of *IAU Symposium*, pages 368–369, April 2010. doi: 10.1017/S1743921310003261.
- K. M. Kratter, R. A. Murray-Clay, and A. N. Youdin. The Runts of the Litter: Why Planets Formed Through Gravitational Instability Can Only Be Failed Binary Stars. *ApJ*, 710:1375–1386, February 2010. doi: 10.1088/0004-637X/710/2/1375.
- A. L. Kraus and M. J. Ireland. LkCa 15: A Young Exoplanet Caught at Formation? *ApJ*, 745:5, January 2012. doi: 10.1088/0004-637X/745/1/5.
- A. N. Krot, Y. Amelin, P. Bland, F. J. Ciesla, J. Connelly, A. M. Davis, G. R. Huss, I. D. Hutcheon, K. Makide, K. Nagashima, L. E. Nyquist, S. S. Russell, E. R. D. Scott, K. Thrane, H. Yurimoto, and Q.-Z. Yin. Origin and chronology of chondritic components: A review. *Geochim. Cosmochim. Acta*, 73:4963–4997, September 2009. doi: 10.1016/j.gca.2008.09.039.
- P. Kroupa. On the variation of the initial mass function. *MNRAS*, 322:231–246, April 2001. doi: 10.1046/j.1365-8711.2001.04022.x.
- P. Kroupa. Initial Conditions for Star Clusters. In S. J. Aarseth, C. A. Tout, and R. A. Mardling, editors, *The Cambridge N-Body Lectures*, volume 760 of *Lecture Notes in Physics*, Berlin Springer Verlag, page 181, 2008. doi: 10.1007/978-1-4020-8431-7_8.
- P. Kroupa. Star Cluster Formation and Some Implications for Gaia. In *Stellar Clusters Associations: A RIA Workshop on Gaia*, pages 17–27, 2011.
- J. M. D. Kruijssen, T. Maschberger, N. Moeckel, C. J. Clarke, N. Bastian, and I. A. Bonnell. The dynamical state of stellar structure in star-forming regions. *MNRAS*, 419:841–853, January 2012. doi: 10.1111/j.1365-2966.2011.19748.x.

- M. R. Krumholz, C. F. McKee, and R. I. Klein. The formation of stars by gravitational collapse rather than competitive accretion. *Nature*, 438:332–334, November 2005. doi: 10.1038/nature04280.
- Mark R. Krumholz. The big problems in star formation: The star formation rate, stellar clustering, and the initial mass function. *Phys. Rep.*, 539:49–134, Jun 2014. doi: 10.1016/j.physrep.2014.02.001.
- C. J. Lada. Star formation - From OB associations to protostars. In M. Peimbert and J. Jugaku, editors, *Star Forming Regions*, volume 115 of *IAU Symposium*, pages 1–17, 1987.
- C. J. Lada and E. A. Lada. Embedded Clusters in Molecular Clouds. *ARA&A*, 41: 57–115, 2003. doi: 10.1146/annurev.astro.41.011802.094844.
- C. J. Lada and B. A. Wilking. The nature of the embedded population in the Rho Ophiuchi dark cloud - Mid-infrared observations. *ApJ*, 287:610–621, December 1984. doi: 10.1086/162719.
- C. J. Lada, A. A. Muench, K. E. Haisch, Jr., E. A. Lada, J. F. Alves, E. V. Tollestrup, and S. P. Willner. Infrared L-Band Observations of the Trapezium Cluster: A Census of Circumstellar Disks and Candidate Protostars. *AJ*, 120:3162–3176, December 2000. doi: 10.1086/316848.
- R. B. Larson. Calculations of three-dimensional collapse and fragmentation. *MNRAS*, 184:69–85, July 1978. doi: 10.1093/mnras/184.1.69.
- R. B. Larson. Turbulence and star formation in molecular clouds. *MNRAS*, 194: 809–826, March 1981. doi: 10.1093/mnras/194.4.809.
- R. B. Larson. The physics of star formation. *Reports on Progress in Physics*, 66: 1651–1697, October 2003. doi: 10.1088/0034-4885/66/10/R03.
- T. Lee, D. A. Papanastassiou, and G. J. Wasserburg. Correction [to Demonstration of ^{26}Mg excess in Allende and evidence for ^{26}Al]. *Geophys. Res. Lett.*, 3:109–112, 1976. doi: 10.1029/GL003i002p00109.
- T. Lee, F. H. Shu, H. Shang, A. E. Glassgold, and K. E. Rehm. Protostellar Cosmic Rays and Extinct Radioactivities in Meteorites. *ApJ*, 506:898–912, October 1998. doi: 10.1086/306284.

- A. O. Leuschner. Preliminary Statistics on the Eccentricities of Comet Orbits. *PASP*, 19:67, April 1907. doi: 10.1086/121723.
- T. Lichtenberg, G. J. Golabek, T. V. Gerya, and M. R. Meyer. The effects of short-lived radionuclides and porosity on the early thermo-mechanical evolution of planetesimals. *Icarus*, 274:350–365, August 2016a. doi: 10.1016/j.icarus.2016.03.004.
- T. Lichtenberg, R. J. Parker, and M. R. Meyer. Isotopic enrichment of forming planetary systems from supernova pollution. *MNRAS*, 462:3979–3992, November 2016b. doi: 10.1093/mnras/stw1929.
- T. Lichtenberg, R. J. Parker, and M. R. Meyer. Isotopic enrichment of forming planetary systems from supernova pollution. *ArXiv e-prints*, August 2016c.
- J. J. Lissauer. Planet formation. *ARA&A*, 31:129–174, 1993. doi: 10.1146/annurev.aa.31.090193.001021.
- J. J. Lissauer and D. J. Stevenson. Formation of Giant Planets. *Protostars and Planets V*, pages 591–606, 2007.
- P. Lucey. Understanding the Lunar Surface and Space-Moon Interactions. *Reviews in Mineralogy and Geochemistry*, 60:83–219, January 2006. doi: 10.2138/rmg.2006.60.2.
- M. Lugaro, U. Ott, and Á. Kereszturi. Radioactive nuclei from cosmochronology to habitability. *Progress in Particle and Nuclear Physics*, 102:1–47, September 2018. doi: 10.1016/j.pnpnp.2018.05.002.
- K. L. Luhman, J. R. Stauffer, A. A. Muench, G. H. Rieke, E. A. Lada, J. Bouvier, and C. J. Lada. A Census of the Young Cluster IC 348. *ApJ*, 593:1093–1115, August 2003. doi: 10.1086/376594.
- K. L. Luhman, T. L. Esplin, and N. P. Loutrel. A Census of Young Stars and Brown Dwarfs in IC 348 and NGC 1333. *ApJ*, 827:52, August 2016. doi: 10.3847/0004-637X/827/1/52.
- J. X. Luu and D. C. Jewitt. Kuiper Belt Objects: Relics from the Accretion Disk of the Sun. *ARA&A*, 40:63–101, 2002. doi: 10.1146/annurev.astro.40.060401.093818.

- J. R. Lyons and E. D. Young. CO self-shielding as the origin of oxygen isotope anomalies in the early solar nebula. *Nature*, 435:317–320, May 2005. doi: 10.1038/nature03557.
- G. J. MacPherson, A. M. Davis, and E. K. Zinner. The distribution of aluminum-26 in the early Solar System - A reappraisal. *Meteoritics*, 30:365, July 1995.
- J. Makino and S. J. Aarseth. On a Hermite integrator with Ahmad-Cohen scheme for gravitational many-body problems. *PASJ*, 44:141–151, April 1992.
- E. E. Mamajek. Initial Conditions of Planet Formation: Lifetimes of Primordial Disks. In T. Usuda, M. Tamura, and M. Ishii, editors, *American Institute of Physics Conference Series*, volume 1158 of *American Institute of Physics Conference Series*, pages 3–10, August 2009. doi: 10.1063/1.3215910.
- C. F. Manara, A. Morbidelli, and T. Guillot. Why do protoplanetary disks appear not massive enough to form the known exoplanet population? *A&A*, 618:L3, October 2018. doi: 10.1051/0004-6361/201834076.
- K. K. Marhas, S. Amari, F. Gyngard, E. Zinner, and R. Gallino. Iron and Nickel Isotopic Ratios in Presolar SiC Grains. *ApJ*, 689:622–645, December 2008. doi: 10.1086/592599.
- C. Marois, B. Macintosh, T. Barman, B. Zuckerman, I. Song, J. Patience, D. Lafrenière, and R. Doyon. Direct Imaging of Multiple Planets Orbiting the Star HR 8799. *Science*, 322:1348, November 2008. doi: 10.1126/science.1166585.
- C. A. Martínez-Barbosa, A. G. A. Brown, T. Boekholt, S. Portegies Zwart, E. Antiche, and T. Antoja. The evolution of the Sun’s birth cluster and the search for the solar siblings with Gaia. *MNRAS*, 457:1062–1075, March 2016. doi: 10.1093/mnras/stw006.
- F. Martins, D. Schaerer, and D. J. Hillier. A new calibration of stellar parameters of Galactic O stars. *A&A*, 436:1049–1065, June 2005. doi: 10.1051/0004-6361:20042386.
- T. Maschberger. On the function describing the stellar initial mass function. *MNRAS*, 429:1725–1733, February 2013. doi: 10.1093/mnras/sts479.
- T. Maschberger and C. J. Clarke. Maximum stellar mass versus cluster membership number revisited. *MNRAS*, 391:711–717, December 2008. doi: 10.1111/j.1365-2966.2008.13903.x.

- C. D. Matzner and Y. Levin. Protostellar Disks: Formation, Fragmentation, and the Brown Dwarf Desert. *ApJ*, 628:817–831, August 2005. doi: 10.1086/430813.
- M. Mayor, M. Marmier, C. Lovis, S. Udry, D. Ségransan, F. Pepe, W. Benz, J. . Bertaux, F. Bouchy, X. Dumusque, G. Lo Curto, C. Mordasini, D. Queloz, and N. C. Santos. The HARPS search for southern extra-solar planets XXXIV. Occurrence, mass distribution and orbital properties of super-Earths and Neptune-mass planets. *ArXiv e-prints*, September 2011.
- M. J. McCaughrean and C. R. O’dell. Direct Imaging of Circumstellar Disks in the Orion Nebula. *AJ*, 111:1977, May 1996. doi: 10.1086/117934.
- Christopher F. McKee and Eve C. Ostriker. Theory of Star Formation. *Annual Review of Astronomy and Astrophysics*, 45:565–687, Sep 2007. doi: 10.1146/annurev.astro.45.051806.110602.
- G. E. Miller and J. M. Scalo. The initial mass function and stellar birthrate in the solar neighborhood. *ApJS*, 41:513–547, November 1979. doi: 10.1086/190629.
- N. Moeckel and I. A. Bonnell. Does subcluster merging accelerate mass segregation in local clusters? *MNRAS*, 400:657–664, December 2009. doi: 10.1111/j.1365-2966.2009.15499.x.
- A. Morbidelli, J. I. Lunine, D. P. O’Brien, S. N. Raymond, and K. J. Walsh. Building Terrestrial Planets. *Annual Review of Earth and Planetary Sciences*, 40:251–275, May 2012. doi: 10.1146/annurev-earth-042711-105319.
- Alessandro Morbidelli. Origin and Dynamical Evolution of Comets and their Reservoirs. *arXiv e-prints*, art. astro-ph/0512256, December 2005.
- F. R. Moulton. On the Evolution of the Solar System. *ApJ*, 22:165, October 1905. doi: 10.1086/141260.
- G. D. Mulders, F. J. Ciesla, M. Min, and I. Pascucci. The Snow Line in Viscous Disks around Low-mass Stars: Implications for Water Delivery to Terrestrial Planets in the Habitable Zone. *ApJ*, 807:9, July 2015. doi: 10.1088/0004-637X/807/1/9.
- Alexander J. Mustill, Sean N. Raymond, and Melvyn B. Davies. Is there an exoplanet in the Solar system? *MNRAS*, 460:L109–L113, July 2016. doi: 10.1093/mnrasl/slw075.

- S. Naoz, W. M. Farr, Y. Lithwick, F. A. Rasio, and J. Teyssandier. Hot Jupiters from secular planet-planet interactions. *Nature*, 473:187–189, May 2011. doi: 10.1038/nature10076.
- Arwen Nicholson and Duncan Forgan. Slingshot dynamics for self-replicating probes and the effect on exploration timescales. *International Journal of Astrobiology*, 12:337–344, Oct 2013. doi: 10.1017/S1473550413000244.
- R. A. Nicholson, J. Bland-Hawthorn, and K. Taylor. The structure and dynamics of the gaseous and stellar components in Centaurus A. *ApJ*, 387:503–521, March 1992. doi: 10.1086/171102.
- R. B. Nicholson and R. J. Parker. Supernova enrichment of planetary systems in low-mass star clusters. *MNRAS*, 464:4318–4324, February 2017. doi: 10.1093/mnras/stw2682.
- R. B. Nicholson, R. J. Parker, R. P. Church, M. B. Davies, N. M. Fearon, and S. R. J. Walton. Rapid destruction of protoplanetary discs due to external photoevaporation in star-forming regions. *MNRAS*, 485:4893–4905, June 2019. doi: 10.1093/mnras/stz606.
- H. B. Niemann, S. K. Atreya, G. R. Carignan, T. M. Donahue, J. A. Haberman, D. N. Harpold, R. E. Hartle, D. M. Hunten, W. T. Kasprzak, P. R. Mahaffy, T. C. Owen, and S. H. Way. The composition of the Jovian atmosphere as determined by the Galileo probe mass spectrometer. *J. Geophys. Res.*, 103:22831–22846, September 1998. doi: 10.1029/98JE01050.
- S. Oh and P. Kroupa. Dynamical ejections of massive stars from young star clusters under diverse initial conditions. *A&A*, 590:A107, May 2016. doi: 10.1051/0004-6361/201628233.
- C. Olczak, S. Pfalzner, and A. Eckart. Encounters in the ONC - observing imprints of star-disc interactions. *A&A*, 488:191–202, September 2008. doi: 10.1051/0004-6361:200809804.
- A. Önehag, A. Korn, B. Gustafsson, E. Stempels, and D. A. Vandenberg. M67-1194, an unusually Sun-like solar twin in M67. *A&A*, 528:A85, April 2011. doi: 10.1051/0004-6361/201015138.
- J. H. Oort. The structure of the cloud of comets surrounding the Solar System and a hypothesis concerning its origin. *Bull. Astron. Inst. Netherlands*, 11:91–110, January 1950.

- E. Opik. Meteorites and the Age of the Universe. *The Scientific Monthly*, 35:109, August 1932.
- N. Ouellette, S. J. Desch, and J. J. Hester. Interaction of Supernova Ejecta with Nearby Protoplanetary Disks. *ApJ*, 662:1268–1281, June 2007. doi: 10.1086/518102.
- J. E. Owen, B. Ercolano, and C. J. Clarke. Protoplanetary disc evolution and dispersal: the implications of X-ray photoevaporation. *MNRAS*, 412:13–25, March 2011. doi: 10.1111/j.1365-2966.2010.17818.x.
- R. J. Parker. Dynamics versus structure: breaking the density degeneracy in star formation. *MNRAS*, 445:4037–4044, December 2014. doi: 10.1093/mnras/stu2054.
- R. J. Parker and J. E. Dale. Did the Solar system form in a sequential triggered star formation event? *MNRAS*, 456:1066–1072, February 2016. doi: 10.1093/mnras/stv2765.
- R. J. Parker and S. P. Goodwin. Do O-stars form in isolation? *MNRAS*, 380:1271–1275, September 2007. doi: 10.1111/j.1365-2966.2007.12179.x.
- R. J. Parker and S. P. Goodwin. The same, but different: stochasticity in binary destruction. *MNRAS*, 424:272–281, July 2012. doi: 10.1111/j.1365-2966.2012.21190.x.
- R. J. Parker and M. R. Meyer. Characterizing the dynamical state of star clusters from snapshots of their spatial distributions. *MNRAS*, 427:637–650, November 2012. doi: 10.1111/j.1365-2966.2012.21851.x.
- R. J. Parker and S. P. Quanz. The effects of dynamical interactions on planets in young substructured star clusters. *MNRAS*, 419:2448–2458, January 2012. doi: 10.1111/j.1365-2966.2011.19911.x.
- R. J. Parker, R. P. Church, M. B. Davies, and M. R. Meyer. Supernova enrichment and dynamical histories of solar-type stars in clusters. *MNRAS*, 437:946–958, January 2014a. doi: 10.1093/mnras/stt1957.
- R. J. Parker, N. J. Wright, S. P. Goodwin, and M. R. Meyer. Dynamical evolution of star-forming regions. *MNRAS*, 438:620–638, February 2014b. doi: 10.1093/mnras/stt2231.

- R. J. Parker, T. Lichtenberg, and S. P. Quanz. Was Planet 9 captured in the Sun's natal star-forming region? *MNRAS*, 472:L75–L79, November 2017. doi: 10.1093/mnrasl/slx141.
- I. Pascucci, U. Gorti, D. Hollenbach, J. Najita, M. R. Meyer, J. M. Carpenter, L. A. Hillenbrand, G. J. Herczeg, D. L. Padgett, E. E. Mamajek, M. D. Silverstone, W. M. Schlingman, J. S. Kim, E. B. Stobie, J. Bouwman, S. Wolf, J. Rodmann, D. C. Hines, J. Lunine, and R. Malhotra. Formation and Evolution of Planetary Systems: Upper Limits to the Gas Mass in Disks around Sun-like Stars. *ApJ*, 651:1177–1193, November 2006. doi: 10.1086/507761.
- O. Pedersen and A. Jones. *A Survey of the Almagest*. 2011. doi: 10.1007/978-0-387-84826-6.
- N. Peretto, P. André, and A. Belloche. Probing the formation of intermediate- to high-mass stars in protoclusters. A detailed millimeter study of the NGC 2264 clumps. *A&A*, 445:979–998, January 2006. doi: 10.1051/0004-6361:20053324.
- S. Pfalzner, M. B. Davies, M. Gounelle, A. Johansen, C. Munker, P. Lacerda, S. Portegies Zwart, L. Testi, M. Tieloff, and D. Veras. The formation of the solar system. *Phys. Scr*, 90(6):068001, June 2015. doi: 10.1088/0031-8949/90/6/068001.
- S. Pfalzner, H. Kirk, A. Sills, J. S. Urquhart, J. Kauffmann, M. A. Kuhn, A. Bhandare, and K. M. Menten. Observational constraints on star cluster formation theory. I. The mass-radius relation. *A&A*, 586:A68, February 2016. doi: 10.1051/0004-6361/201527449.
- S. Pfalzner, A. Bhandare, K. Vincke, and P. Lacerda. Outer Solar System Possibly Shaped by a Stellar Fly-by. *ApJ*, 863:45, August 2018. doi: 10.3847/1538-4357/aad23c.
- R. J. Phillips, R. F. Raubertas, R. E. Arvidson, I. C. Sarkar, R. R. Herrick, N. Izenberg, and R. E. Grimm. Impact craters and Venus resurfacing history. *J. Geophys. Res.*, 97:15, October 1992. doi: 10.1029/92JE01696.
- G. Piazzzi. *Risultati delle osservazioni della nuova stella scoperta il di' 1. Gennaio all'Osservatorio Reale di Palermo*. 1801. doi: 10.3931/e-rara-8730.
- B. Pichardo, E. Moreno, C. Allen, L. R. Bedin, A. Bellini, and L. Pasquini. The Sun was Not Born in M67. *AJ*, 143:73, March 2012. doi: 10.1088/0004-6256/143/3/73.

- E. V. Pitjeva and N. P. Pitjev. Mass of the Kuiper belt. *Celestial Mechanics and Dynamical Astronomy*, 130:57, September 2018. doi: 10.1007/s10569-018-9853-5.
- H. C. Plummer. On the problem of distribution in globular star clusters. *MNRAS*, 71:460–470, March 1911. doi: 10.1093/mnras/71.5.460.
- J. B. Pollack, O. Hubickyj, P. Bodenheimer, J. J. Lissauer, M. Podolak, and Y. Greenzweig. Formation of the Giant Planets by Concurrent Accretion of Solids and Gas. *Icarus*, 124:62–85, November 1996. doi: 10.1006/icar.1996.0190.
- S. Portegies Zwart. The formation of solar-system analogs in young star clusters. *A&A*, 622:A69, February 2019. doi: 10.1051/0004-6361/201833974.
- S. F. Portegies Zwart. The Lost Siblings of the Sun. *ApJ*, 696:L13–L16, May 2009. doi: 10.1088/0004-637X/696/1/L13.
- S. F. Portegies Zwart. Stellar disc destruction by dynamical interactions in the Orion Trapezium star cluster. *MNRAS*, 457:313–319, March 2016. doi: 10.1093/mnras/stv2831.
- S. F. Portegies Zwart and F. Verbunt. Population synthesis of high-mass binaries. *A&A*, 309:179–196, May 1996.
- S. F. Portegies Zwart, J. Makino, S. L. W. McMillan, and P. Hut. Star cluster ecology. III. Runaway collisions in young compact star clusters. *A&A*, 348:117–126, August 1999.
- S. F. Portegies Zwart, S. L. W. McMillan, P. Hut, and J. Makino. Star cluster ecology - IV. Dissection of an open star cluster: photometry. *MNRAS*, 321:199–226, February 2001. doi: 10.1046/j.1365-8711.2001.03976.x.
- T. Preibisch and H. Zinnecker. Sequentially triggered star formation in OB associations. In B. G. Elmegreen and J. Palous, editors, *Triggered Star Formation in a Turbulent ISM*, volume 237 of *IAU Symposium*, pages 270–277, 2007. doi: 10.1017/S1743921307001597.
- J. E. Pringle. Accretion discs in astrophysics. *ARA&A*, 19:137–162, 1981. doi: 10.1146/annurev.aa.19.090181.001033.
- L. Prisinzano, F. Damiani, G. Micela, R. D. Jeffries, E. Franciosini, G. G. Sacco, A. Frasca, A. Klutsch, A. Lanzafame, E. J. Alfaro, K. Biazzo, R. Bonito,

- A. Bragaglia, M. Caramazza, A. Vallenari, G. Carraro, M. T. Costado, E. Flaccomio, P. Jofré, C. Lardo, L. Monaco, L. Morbidelli, N. Mowlavi, E. Pancino, S. Randich, and S. Zaggia. The Gaia-ESO Survey: membership and initial mass function of the γ Velorum cluster. *A&A*, 589:A70, May 2016. doi: 10.1051/0004-6361/201527875.
- D. Punzo, R. Capuzzo-Dolcetta, and S. Portegies Zwart. The secular evolution of the Kuiper belt after a close stellar encounter. *MNRAS*, 444:2808–2819, November 2014. doi: 10.1093/mnras/stu1650.
- S. P. Quanz, A. Amara, M. R. Meyer, J. H. Girard, M. A. Kenworthy, and M. Kasper. Confirmation and Characterization of the Protoplanet HD 100546 bDirect Evidence for Gas Giant Planet Formation at 50 AU. *ApJ*, 807:64, July 2015. doi: 10.1088/0004-637X/807/1/64.
- R. R. Rafikov. Can Giant Planets Form by Direct Gravitational Instability? *ApJ*, 621:L69–L72, March 2005. doi: 10.1086/428899.
- R. R. Rafikov. Constraint on the Giant Planet Production by Core Accretion. *ApJ*, 727:86, February 2011. doi: 10.1088/0004-637X/727/2/86.
- S. N. Raymond, E. Kokubo, A. Morbidelli, R. Morishima, and K. J. Walsh. Terrestrial Planet Formation at Home and Abroad. *Protostars and Planets VI*, pages 595–618, 2014. doi: 10.2458/azu_uapress_9780816531240-ch026.
- S. Refsdal. The gravitational lens effect. *MNRAS*, 128:295, 1964. doi: 10.1093/mnras/128.4.295.
- A. J. W. Richert, E. D. Feigelson, K. V. Getman, and M. A. Kuhn. No Evidence for Protoplanetary Disk Destruction By OB Stars in the MYStIX Sample. *ApJ*, 811: 10, September 2015. doi: 10.1088/0004-637X/811/1/10.
- A. J. W. Richert, K. V. Getman, E. D. Feigelson, M. A. Kuhn, P. S. Broos, M. S. Povich, M. R. Bate, and G. P. Garmire. Circumstellar disc lifetimes in numerous galactic young stellar clusters. *MNRAS*, 477:5191–5206, July 2018. doi: 10.1093/mnras/sty949.
- S. Richling and H. W. Yorke. Photoevaporation of protostellar disks. II. The importance of UV dust properties and ionizing flux. *A&A*, 327:317–324, November 1997.

- G. P. Rosotti, J. E. Dale, M. de Juan Ovelar, D. A. Hubber, J. M. D. Kruijssen, B. Ercolano, and S. Walch. Protoplanetary disc evolution affected by star-disc interactions in young stellar clusters. *MNRAS*, 441:2094–2110, July 2014. doi: 10.1093/mnras/stu679.
- M. N. Ross, G. Schubert, T. Spohn, and R. W. Gaskell. Internal structure of Io and the global distribution of its topography. *Icarus*, 85:309–325, June 1990. doi: 10.1016/0019-1035(90)90119-T.
- V. S. Safronov. *Evolution of the protoplanetary cloud and formation of the earth and planets*. 1972.
- E. E. Salpeter. The Luminosity Function and Stellar Evolution. *ApJ*, 121:161, January 1955. doi: 10.1086/145971.
- H. Sana, S. E. de Mink, A. de Koter, N. Langer, C. J. Evans, M. Gieles, E. Gosset, R. G. Izzard, J.-B. Le Bouquin, and F. R. N. Schneider. Binary Interaction Dominates the Evolution of Massive Stars. *Science*, 337:444, July 2012. doi: 10.1126/science.1223344.
- N. Sánchez and E. J. Alfaro. The Spatial Distribution of Stars in Open Clusters. *ApJ*, 696:2086–2093, May 2009. doi: 10.1088/0004-637X/696/2/2086.
- A. Scally and C. Clarke. Destruction of protoplanetary discs in the Orion Nebula Cluster. *MNRAS*, 325:449–456, August 2001. doi: 10.1046/j.1365-8711.2001.04274.x.
- A. Scally and C. Clarke. Primordial substructure in the Orion Nebula Cluster. *MNRAS*, 334:156–166, July 2002. doi: 10.1046/j.1365-8711.2002.05503.x.
- E. L. Schaller. Atmospheres and surfaces of small bodies and dwarf planets in the Kuiper Belt. In *European Physical Journal Web of Conferences*, volume 9 of *European Physical Journal Web of Conferences*, page 267, December 2010. doi: 10.1051/epjconf/201009021.
- S. Schmeja and R. S. Klessen. Evolving structures of star-forming clusters. *A&A*, 449:151–159, April 2006. doi: 10.1051/0004-6361:20054464.
- J. Schneider, C. Dedieu, P. Le Sidaner, R. Savalle, and I. Zolotukhin. Defining and cataloging exoplanets: the exoplanet.eu database. *A&A*, 532:A79, August 2011. doi: 10.1051/0004-6361/201116713.

- R. Schwarz, B. Funk, Á. Bzszó, and E. Pilat-Lohinger. Catalogue of Exoplanets in Multiple-Star-Systems. In *5th CHEOPS Science Workshop, held 24-26 July 2017 in Scholss Seggau, Austria., id.1*, page 1, July 2017.
- D. M. Segura-Cox, R. J. Harris, J. J. Tobin, L. W. Looney, Z.-Y. Li, C. Chandler, K. Kratter, M. M. Dunham, S. Sadavoy, L. Perez, and C. Melis. The VLA Nascent Disk and Multiplicity Survey: First Look at Resolved Candidate Disks around Class 0 and I Protostars in the Perseus Molecular Cloud. *ApJ*, 817:L14, February 2016. doi: 10.3847/2041-8205/817/2/L14.
- F. H. Shu, F. C. Adams, and S. Lizano. Star formation in molecular clouds - Observation and theory. *ARA&A*, 25:23–81, 1987. doi: 10.1146/annurev.aa.25.090187.000323.
- F. H. Shu, S. Lizano, S. P. Ruden, and J. Najita. Mass loss from rapidly rotating magnetic protostars. *ApJ*, 328:L19–L23, May 1988. doi: 10.1086/185152.
- F. H. Shu, H. Shang, M. Gounelle, A. E. Glassgold, and T. Lee. The Origin of Chondrules and Refractory Inclusions in Chondritic Meteorites. *ApJ*, 548:1029–1050, February 2001. doi: 10.1086/319018.
- L. Siess, E. Dufour, and M. Forestini. An internet server for pre-main sequence tracks of low- and intermediate-mass stars. *A&A*, 358:593–599, June 2000.
- Steinn Sigurdsson, Harvey B. Richer, Brad M. Hansen, Ingrid H. Stairs, and Stephen E. Thorsett. A Young White Dwarf Companion to Pulsar B1620-26: Evidence for Early Planet Formation. *Science*, 301:193–196, Jul 2003. doi: 10.1126/science.1086326.
- A. Sills, S. Rieder, J. Scora, J. McCloskey, and S. Jaffa. Dynamical evolution of stars and gas of young embedded stellar sub-clusters. *MNRAS*, 477:1903–1912, June 2018. doi: 10.1093/mnras/sty681.
- W. L. Slattery, W. Benz, and A. G. W. Cameron. Giant impacts on a primitive Uranus. *Icarus*, 99:167–174, September 1992. doi: 10.1016/0019-1035(92)90180-F.
- S. J. Smartt, M. Fraser, M. Crockett, J. Eldridge, J. Maund, and S. Mattila. Identification of progenitors of core collapse supernovae. In *Progenitors and Environments of Stellar Explosions*, page 8, June 2010.

- A. M. S. Smith, J. Cabrera, Sz Csizmadia, F. Dai, D. Gandolfi, T. Hirano, J. N. Winn, S. Albrecht, R. Alonso, G. Antoniciello, O. Barragán, H. Deeg, Ph Eigmüller, M. Endl, A. Erikson, M. Fridlund, A. Fukui, S. Grziwa, E. W. Guenther, A. P. Hatzes, D. Hidalgo, A. W. Howard, H. Isaacson, J. Korth, M. Kuzuhara, J. Livingston, N. Narita, D. Nespral, G. Nowak, E. Palle, M. Pätzold, C. M. Persson, E. Petigura, J. Prieto-Arranz, H. Rauer, I. Ribas, and V. Van Eylen. K2-137 b: an Earth-sized planet in a 4.3-h orbit around an M-dwarf. *MNRAS*, 474:5523–5533, Mar 2018. doi: 10.1093/mnras/stx2891.
- D. R. Soderblom, L. A. Hillenbrand, R. D. Jeffries, E. E. Mamajek, and T. Naylor. Ages of Young Stars. *Protostars and Planets VI*, pages 219–241, 2014. doi: 10.2458/azu_uapress_9780816531240-ch010.
- S. A. Stern, F. Bagenal, K. Ennico, G. R. Gladstone, W. M. Grundy, W. B. McKinnon, J. M. Moore, C. B. Olkin, J. R. Spencer, H. A. Weaver, L. A. Young, T. Aerdert, J. Andrews, M. Banks, B. Bauer, J. Bauman, O. S. Barnouin, P. Bedini, K. Beisser, R. A. Beyer, S. Bhaskaran, R. P. Binzel, E. Birath, M. Bird, D. J. Bogan, A. Bowman, V. J. Bray, M. Brozovic, C. Bryan, M. R. Buckley, M. W. Buie, B. J. Buratti, S. S. Bushman, A. Calloway, B. Carcich, A. F. Cheng, S. Conard, C. A. Conrad, J. C. Cook, D. P. Cruikshank, O. S. Custodio, C. M. Dalle Ore, C. Deboy, Z. J. B. Dischner, P. Dumont, A. M. Earle, H. A. Elliott, J. Ercol, C. M. Ernst, T. Finley, S. H. Flanigan, G. Fountain, M. J. Freeze, T. Greathouse, J. L. Green, Y. Guo, M. Hahn, D. P. Hamilton, S. A. Hamilton, J. Hanley, A. Harch, H. M. Hart, C. B. Hersman, A. Hill, M. E. Hill, D. P. Hinson, M. E. Holdridge, M. Horanyi, A. D. Howard, C. J. A. Howett, C. Jackman, R. A. Jacobson, D. E. Jennings, J. A. Kammer, H. K. Kang, D. E. Kaufmann, P. Kollmann, S. M. Krimigis, D. Kusnierkiewicz, T. R. Lauer, J. E. Lee, K. L. Lindstrom, I. R. Linscott, C. M. Lisse, A. W. Lunsford, V. A. Mallder, N. Martin, D. J. McComas, R. L. McNutt, D. Mehoke, T. Mehoke, E. D. Melin, M. Mutchler, D. Nelson, F. Nimmo, J. I. Nunez, A. Ocampo, W. M. Owen, M. Paetzold, B. Page, A. H. Parker, J. W. Parker, F. Pelletier, J. Peterson, N. Pinkine, M. Piquette, S. B. Porter, S. Protopapa, J. Redfern, H. J. Reitsema, D. C. Reuter, J. H. Roberts, S. J. Robbins, G. Rogers, D. Rose, K. Runyon, K. D. Retherford, M. G. Ryschkewitsch, P. Schenk, E. Schindhelm, B. Sepan, M. R. Showalter, K. N. Singer, M. Soluri, D. Stanbridge, A. J. Steffl, D. F. Strobel, T. Stryk, M. E. Summers, J. R. Szalay, M. Tapley, A. Taylor, H. Taylor, H. B. Throop, C. C. C. Tsang, G. L. Tyler, O. M. Umurhan, A. J. Verbiscer, M. H. Versteeg, M. Vincent, R. Webbert, S. Weidner, G. E. Weigle, O. L. White, K. Whittenburg, B. G. Williams, K. Williams,

- S. Williams, W. W. Woods, A. M. Zangari, and E. Zirnstein. The Pluto system: Initial results from its exploration by New Horizons. *Science*, 350:aad1815, October 2015. doi: 10.1126/science.aad1815.
- A. Sternberg, T. L. Hoffmann, and A. W. A. Pauldrach. Ionizing Photon Emission Rates from O- and Early B-Type Stars and Clusters. *ApJ*, 599:1333–1343, December 2003. doi: 10.1086/379506.
- H. Störzer and D. Hollenbach. Photodissociation Region Models of Photoevaporating Circumstellar Disks and Application to the Proplyds in Orion. *ApJ*, 515: 669–684, April 1999. doi: 10.1086/307055.
- T. Sumi, K. Kamiya, D. P. Bennett, I. A. Bond, F. Abe, C. S. Botzler, A. Fukui, K. Furusawa, J. B. Hearnshaw, Y. Itow, P. M. Kilmartin, A. Korpela, W. Lin, C. H. Ling, K. Masuda, Y. Matsubara, N. Miyake, M. Motomura, Y. Muraki, M. Nagaya, S. Nakamura, K. Ohnishi, T. Okumura, Y. C. Perrott, N. Rattenbury, To. Saito, T. Sako, D. J. Sullivan, W. L. Sweatman, P. J. Tristram, A. Udalski, M. K. Szymański, M. Kubiak, G. Pietrzyński, R. Poleski, I. Soszyński, Ł. Wyrzykowski, K. Ulaczyk, and Microlensing Observations in Astrophysics (MOA) Collaboration. Unbound or distant planetary mass population detected by gravitational microlensing. *Nature*, 473(7347):349–352, May 2011. doi: 10.1038/nature10092.
- J. C. Tan, M. T. Beltrán, P. Caselli, F. Fontani, A. Fuente, M. R. Krumholz, C. F. McKee, and A. Stolte. Massive Star Formation. *Protostars and Planets VI*, pages 149–172, 2014. doi: 10.2458/azu_uapress_9780816531240-ch007.
- L. Testi, A. I. Sargent, L. Olmi, and J. S. Onello. Star Formation in Clusters: Early Subclustering in the Serpens Core. *ApJ*, 540:L53–L56, September 2000. doi: 10.1086/312858.
- S. E. Thompson, J. L. Coughlin, K. Hoffman, F. Mullally, J. L. Christiansen, C. J. Burke, S. Bryson, N. Batalha, M. R. Haas, J. Catanzarite, J. F. Rowe, G. Barntsen, D. A. Caldwell, B. D. Clarke, J. M. Jenkins, J. Li, D. W. Latham, J. J. Lissauer, S. Mathur, R. L. Morris, S. E. Seader, J. C. Smith, T. C. Klaus, J. D. Twicken, J. E. Van Cleve, B. Wohler, R. Akeson, D. R. Ciardi, W. D. Cochran, C. E. Henze, S. B. Howell, D. Huber, A. Prša, S. V. Ramírez, T. D. Morton, T. Barclay, J. R. Campbell, W. J. Chaplin, D. Charbonneau, J. Christensen-Dalsgaard, J. L. Dotson, L. Doyle, E. W. Dunham, A. K. Dupree, E. B. Ford, J. C. Geary, F. R. Girouard, H. Isaacson, H. Kjeldsen, E. V. Quintana, D. Ragozzine, M. Shabram,

- A. Shporer, V. Silva Aguirre, J. H. Steffen, M. Still, P. Tenenbaum, W. F. Welsh, A. Wolfgang, K. A. Zamudio, D. G. Koch, and W. J. Borucki. Planetary Candidates Observed by Kepler. VIII. A Fully Automated Catalog with Measured Completeness and Reliability Based on Data Release 25. *ApJS*, 235:38, April 2018. doi: 10.3847/1538-4365/aab4f9.
- K. Thrane, M. Bizzarro, and J. A. Baker. Extremely Brief Formation Interval for Refractory Inclusions and Uniform Distribution of ^{26}Al in the Early Solar System. *ApJ*, 646:L159–L162, August 2006. doi: 10.1086/506910.
- G. Tobie, O. Grasset, J. I. Lunine, A. Mocquet, and C. Sotin. Titan’s internal structure inferred from a coupled thermal-orbital model. *Icarus*, 175:496–502, June 2005. doi: 10.1016/j.icarus.2004.12.007.
- J. E. Tohline. The Origin of Binary Stars. *ARA&A*, 40:349–385, 2002. doi: 10.1146/annurev.astro.40.060401.093810.
- J. M. Trigo-Rodríguez, D. A. García-Hernández, M. Lugaro, A. I. Karakas, M. van Raai, P. García Lario, and A. Manchado. The role of massive AGB stars in the early solar system composition. *Meteoritics and Planetary Science*, 44:627–641, July 2009. doi: 10.1111/j.1945-5100.2009.tb00758.x.
- H. C. Urey. The Cosmic Abundances of Potassium, Uranium, and Thorium and the Heat Balances of the Earth, the Moon, and Mars. *Proceedings of the National Academy of Science*, 41:127–144, March 1955. doi: 10.1073/pnas.41.3.127.
- W. D. Vacca, C. D. Garmany, and J. M. Shull. The Lyman-Continuum Fluxes and Stellar Parameters of O and Early B-Type Stars. *ApJ*, 460:914, April 1996. doi: 10.1086/177020.
- A. van Maanen. Two Faint Stars with Large Proper Motion. *PASP*, 29:258, December 1917. doi: 10.1086/122654.
- J. Villeneuve, M. Chaussidon, and G. Libourel. Homogeneous Distribution of ^{26}Al in the Solar System from the Mg Isotopic Composition of Chondrules. *Science*, 325:985, August 2009. doi: 10.1126/science.1173907.
- K. Vincke, A. Breslau, and S. Pflanzner. Strong effect of the cluster environment on the size of protoplanetary discs? *A&A*, 577:A115, May 2015. doi: 10.1051/0004-6361/201425552.

- P. Wang, Z.-Y. Li, T. Abel, and F. Nakamura. Outflow Feedback Regulated Massive Star Formation in Parsec-Scale Cluster-Forming Clumps. *ApJ*, 709:27–41, January 2010. doi: 10.1088/0004-637X/709/1/27.
- G. J. Wasserburg, M. Busso, R. Gallino, and C. M. Raiteri. Asymptotic Giant Branch stars as a source of short-lived radioactive nuclei in the solar nebula. *ApJ*, 424:412–428, March 1994. doi: 10.1086/173899.
- G. J. Wasserburg, M. Busso, R. Gallino, and K. M. Nollett. Short-lived nuclei in the early Solar System: Possible AGB sources. *Nuclear Physics A*, 777:5–69, October 2006. doi: 10.1016/j.nuclphysa.2005.07.015.
- S. J. Weidenschilling. The distribution of mass in the planetary system and solar nebula. *Ap&SS*, 51:153–158, September 1977. doi: 10.1007/BF00642464.
- C. Weidner and P. Kroupa. The maximum stellar mass, star-cluster formation and composite stellar populations. *MNRAS*, 365:1333–1347, February 2006. doi: 10.1111/j.1365-2966.2005.09824.x.
- C. Weidner, P. Kroupa, and J. Pflamm-Altenburg. The m_{max} - M_{cl} relation, the IMF and IGIMF: probabilistically sampled functions. *MNRAS*, 434:84–101, September 2013. doi: 10.1093/mnras/stt1002.
- P. R. Weissman. The Oort Cloud. In T. Rettig and J. M. Hahn, editors, *Completing the Inventory of the Solar System*, volume 107 of *Astronomical Society of the Pacific Conference Series*, pages 265–288, 1996.
- M. A. Wieczorek. The Constitution and Structure of the Lunar Interior. *Reviews in Mineralogy and Geochemistry*, 60:221–364, January 2006. doi: 10.2138/rmg.2006.60.3.
- J. P. Williams and L. A. Cieza. Protoplanetary Disks and Their Evolution. *ARA&A*, 49:67–117, September 2011. doi: 10.1146/annurev-astro-081710-102548.
- J. P. Williams and E. Gaidos. On the Likelihood of Supernova Enrichment of Protoplanetary Disks. *ApJ*, 663:L33–L36, July 2007. doi: 10.1086/519972.
- J. N. Winn and D. C. Fabrycky. The Occurrence and Architecture of Exoplanetary Systems. *ARA&A*, 53:409–447, August 2015. doi: 10.1146/annurev-astro-082214-122246.

- A. J. Winter, C. J. Clarke, G. Rosotti, J. Ih, S. Facchini, and T. J. Haworth. Protoplanetary disc truncation mechanisms in stellar clusters: comparing external photoevaporation and tidal encounters. *MNRAS*, 478:2700–2722, August 2018a. doi: 10.1093/mnras/sty984.
- A. J. Winter, C. J. Clarke, G. Rosotti, J. Ih, S. Facchini, and T. J. Haworth. Protoplanetary disc truncation mechanisms in stellar clusters: comparing external photoevaporation and tidal encounters. *ArXiv e-prints*, March 2018b.
- A. J. Winter, C. J. Clarke, and G. P. Rosotti. External photoevaporation of protoplanetary discs in Cygnus OB2: linking discs to star formation dynamical history. *MNRAS*, 485:1489–1507, May 2019. doi: 10.1093/mnras/stz473.
- A. Wolszczan and D. A. Frail. A planetary system around the millisecond pulsar PSR1257 + 12. *Nature*, 355:145–147, January 1992. doi: 10.1038/355145a0.
- M. M. Woolfson. The Solar - Origin and Evolution. *QJRAS*, 34, March 1993.
- S. E. Woosley and A. Heger. Nucleosynthesis and remnants in massive stars of solar metallicity. *Phys. Rep.*, 442:269–283, April 2007. doi: 10.1016/j.physrep.2007.02.009.
- B. A. Wootton and R. J. Parker. Enlarging habitable zones around binary stars in hostile environments. *MNRAS*, 485:L48–L52, May 2019. doi: 10.1093/mnrasl/sly238.
- N. J. Wright, R. J. Parker, S. P. Goodwin, and J. J. Drake. Constraints on massive star formation: Cygnus OB2 was always an association. *MNRAS*, 438:639–646, February 2014. doi: 10.1093/mnras/stt2232.
- H.-W. Yen, P. M. Koch, S. Takakuwa, R. Krasnopolsky, N. Ohashi, and Y. Aso. Signs of Early-stage Disk Growth Revealed with ALMA. *ApJ*, 834:178, January 2017. doi: 10.3847/1538-4357/834/2/178.
- H. W. Yorke and S. Richling. The Effects of Winds and Photoionization on the Evolution of Protostellar Disks. In W. J. Henney, J. Franco, and M. Martos, editors, *Revista Mexicana de Astronomia y Astrofisica Conference Series*, volume 12 of *Revista Mexicana de Astronomia y Astrofisica Conference Series*, pages 92–92, February 2002.
- Q. Zhang and S. M. Fall. The Mass Function of Young Star Clusters in the “Antennae” Galaxies. *ApJ*, 527:L81–L84, December 1999. doi: 10.1086/312412.

- H. Zinnecker. Prediction of the protostellar mass spectrum in the Orion near-infrared cluster. *Annals of the New York Academy of Sciences*, 395:226–235, October 1982. doi: 10.1111/j.1749-6632.1982.tb43399.x.
- H. Zinnecker and H. W. Yorke. Toward Understanding Massive Star Formation. *ARA&A*, 45:481–563, September 2007. doi: 10.1146/annurev.astro.44.051905.092549.
- B. Zuckerman. Recognition of the First Observational Evidence of an Extrasolar Planetary System. In P. Dufour, P. Bergeron, and G. Fontaine, editors, *19th European Workshop on White Dwarfs*, volume 493 of *Astronomical Society of the Pacific Conference Series*, page 291, June 2015.
- B. Zuckerman, T. Forveille, and J. H. Kastner. Inhibition of giant-planet formation by rapid gas depletion around young stars. *Nature*, 373:494–496, February 1995. doi: 10.1038/373494a0.